

# E-6600E and E-6600B Heat Exchanger Metallurgical Analysis

April 2, 2010 Tesoro Refinery Incident

Anacortes, Washington

**U.S. CHEMICAL SAFETY AND HAZARD INVESTIGATION BOARD**

## Table of Contents

Introduction .....	1
Executive Summary.....	2
Background .....	3
General Findings .....	8
Sample Locations .....	8
Composition.....	10
Mechanical Testing .....	12
Fractography and Deformation Measurements .....	20
Metallography.....	23
Discussion.....	30
Appendix I: BETA Laboratory Reports.....	34
1 BETA Lab No-M10198 Receipt Inspection (E-6600E).....	34
2 BETA Lab No-M10198 LS3 Bottom (E-6600E) .....	35
3 BETA Lab No-M10198 CS4-02(E-6600E).....	39
4 BETA Lab No-M10198 LS2-CS3 Tee Indications (E-6600E), August 13, 2010.....	42
5 BETA Lab No-M10198 CS4-01/LS3 Bottom(E-6600E), August 25,2010 .....	45
6 BETA Lab No-M10198- Mechanical Property Testing (E-6600E), August 27, 2010 .....	48
7 BETA Lab No-M10198 CS4-01/LS3 Bottom, Rev. 1 (E-6600E), September 20, 2010 .....	50
8 BETA Lab No-M10198 LS3 Top (E-6600E), September 20, 2010.....	52
9 BETA Lab No-M10198 LS3 Fractography and 19 M-5 Mount (E-6600E), September 23, 2010.....	56
10 Beta Lab No-M10198 LS2 and LS2-CS2 Tee (E-6600E), October 13, 2010.....	58
11 BETA Lab No-M10198 E-6600E Heat Exchanger E, Summary of Results and Part 17 Mounts Evaluation (E-6600E), February 3 2011.....	60
12 BETA Lab No-M10198, Rev 1 - Tesoro E-6600E, Summary of the Results, March 7, 2011.....	60
13 Beta Laboratory Report No. M10329, E-6600B, Parts 1B, 2B, and 3B, December 27, 2010 .....	67
14 Beta Laboratory Report No. M10329-B, E-E-6600B, Parts 1B, 4B, and 5B, March 8, 2011 .....	71
Appendix II: Additional reports for review. ....	74
Spectrum Inspection Engineering report, May 20 2010.....	74
Spectrum Inspection Engineering report, June 24 2010.....	74

## Introduction

BETA Laboratory, located in Mayfield Village, Ohio, conducted metallurgical testing of the E-6600 B/E heat exchangers through an agreement between Tesoro, the Washington Division of Occupational Safety and Health, and the U.S. Chemical Safety and Hazard Investigation Board (CSB). BETA Laboratory compiled a series of reports on the failed heat exchanger (E-6600E) and the exemplar heat exchanger (E-6600B) that was removed from service following the accident at Tesoro. In **Table 1**, the 14 reports created by BETA Laboratory are listed.

The CSB contracted the National Institute of Standards and Technology (NIST) to perform analysis of the Beta Laboratory reports and to prepare a report stating a professional opinion of the failure mechanism that caused the rupture of the E-6600E heat exchanger. This report identifies the primary E-6600E heat exchanger failure mechanism and analyzes the extent to which available evidence supports, or excludes, other potential failure mechanisms.

This review first presents a brief executive summary, and then provides a short background of the basic details of the accident, which is followed by general findings. The appendix provides details of each report that was reviewed.

Series #	BETA Report Title	Report Date
1	BETA Lab No-M10198 Receipt Inspection (E-6600E)	July 29, 2010
2	BETA Lab No-M10198 LS3 Bottom (E-6600E)	July 30, 2010
3	BETA Lab No-M10198 CS4-02(E-6600E)	August 5, 2010
4	BETA Lab No-M10198 LS2-CS3 Tee Indications (E-6600E)	August 13, 2010
5	BETA Lab No-M10198 CS4-01/LS3 Bottom(E-6600E)	August 25,2010
6	BETA Lab No-M10198- Mechanical Property Testing (E-6600E)	August 27, 2010
7	BETA Lab No-M10198 CS4-01/LS3 Bottom, Rev. 1 (E-6600E)	September 20, 2010
8	BETA Lab No-M10198 LS3 Top (E-6600E)	September 20, 2010
9	BETA Lab No-M10198 LS3 Bottom Fractography and 19 M-5 Mount (E-6600E)	September 23, 2010
10	Beta Lab No-M10198 LS2 and LS2-CS2 Tee (E-6600E)	October 13, 2010
11	BETA Lab No-M10198 E-6600E Heat Exchanger E, Summary of Results and Part 17 Mounts Evaluation (E-6600E)	February 3 2011
12	BETA Lab No-M10198, Rev 1 - Tesoro E-6600E, Summary of the Results	March 7, 2011
13	Beta Laboratory Report No. M10329, E-6600B, Parts 1B, 2B, and 3B,	December 27, 2010
14	Beta Laboratory Report No. M10329-B, E-E-6600B, Parts 1B, 4B, and 5B,	March 8, 2011

Table 1. BETA Laboratory Reports listed and assigned numbers in this review according to the date that they were written.

## Executive Summary

The metallurgical damage that resulted in the failure of the E-6600E heat exchanger was likely due to High Temperature Hydrogen Attack (HTHA). Other possible mechanisms, or an atypical HTHA mechanism, may have also contributed to the initiation of the underbead cracking in the welds. The damage documented in the shells of the E-6600E and E-6600B heat exchangers would, with a reasonable degree of engineering certainty, be expected to eventually result in the failure of the heat exchangers.

The damage documented for the heat exchanger that failed (E-6600E) is extensive. Damage is evident in the base metal, but only in regions adjacent to welds. The most characteristic damage is within the heat affected zones (HAZ) and along fusion boundaries in the welds. Because the fracture paths followed the narrow, damaged regions along welds, much of the damage in these regions was incorporated into the fracture surfaces during the failure (as these damaged regions linked-up to form the macro-fracture). In addition, new damage was produced during the fracture event, so that, in some cases, the pre-existing damage is obscured. Fortunately, damage is well documented in regions of the E-6600B heat exchanger that did not catastrophically fracture during the failure. Damage morphologies in the E-6600B heat exchanger were shown to be similar to the damage morphologies observed along the catastrophic fracture paths of the E-6600E heat exchanger. Much of the damage documented is consistent with HTHA.

Classical HTHA may not completely explain the damage morphologies observed, and it is suspected that alternate hydrogen-assisted cracking mechanisms and/or a lesser-understood lower temperature mechanism of HTHA are responsible for some damage. For example, hydrogen-induced cold cracking of the weld HAZs at ambient temperature could have occurred following the fabrication of the heat exchangers and served as initiation sites for further damage, or hydrogen-assisted cracking could have conceivably accumulated over the life of the heat exchangers during cool downs for cleanouts. The main factor driving this speculation is the underbead cracking found in the heat exchangers. This underbead crack morphology is indicative of hydrogen-induced cold cracking and may have occurred at ambient conditions followed by further HTHA of those regions during service, resulting in an “atypical” HTHA crack morphology. Heating and cooling cycles (expansion and contraction) and other mechanical loads also could have conceivably contributed to crack growth in the damaged regions, particularly near the dissimilar metal cladding. However, the existing evidence does not indicate that cyclic stresses contributed to the growth of cracks.

The damage from HTHA appears to be the principal metallurgical cause of the cracking documented in the heat exchangers. The damage documented for the exemplar heat exchanger (E-6600B) would be expected to eventually result in a failure exhibiting a similar configuration to the failure that occurred in the E-6600E heat exchanger, based on the extent and location of the damage documented.

## Background

Friday morning, April 2, 2010: A heat exchanger in the Naphtha Hydrotreater Unit at the Tesoro Refinery in Anacortes, Washington failed, resulting in a fire that fatally injured seven refinery workers. The refinery workers were in the process of returning the E-6600 A/B/C heat exchangers to operation after being down for maintenance. The E-6600E heat exchanger that failed is part of a system of six heat exchangers, shown in **Figure 1**. The system is made up of three sets of heat exchangers, where each set is a pair of heat exchangers that are designed and manufactured to be basically identical. In this system, the heat exchanger that failed is identified as E-6600E. Heat exchanger E-6600B is the other part of the pair. These heat exchangers are manufactured from ASTM SA-515 Grade 70 steel, with the highest temperature section of each heat exchanger clad with stainless steel. The E-6600B exchanger did not fail in the accident. It was removed from service to serve as an exemplar vessel for the investigation.

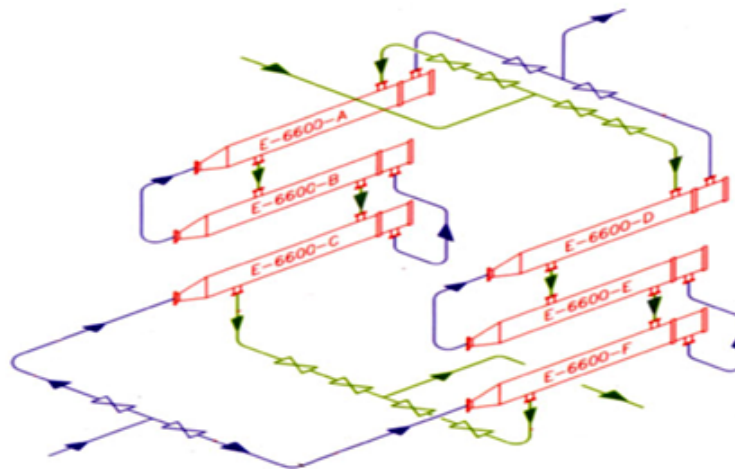


**Figure 1:** The heat exchanger that failed (E-6600-E) is between two other heat exchangers in the stack, and paired in the system with heat exchanger E-6600-B. In the photograph, the E-6600-E heat exchanger is in the front middle position and E-6600-B is not visible. In this series of heat exchangers, naphtha (a light fraction of crude oil) and hydrogen (effluent) are cooled following a reaction in which sulfur and nitrogen are removed from the naphtha by mixing it with hydrogen at a temperature of 630-700 °F and pressure of 600 psi. Flow into the shells comes in from the reaction process on the top (green). Naphtha and hydrogen are fed into the tubes (from bottom, in blue) to cool the reactor product and pre-heat the reactor charge. The top, middle, and bottom heat exchangers are pairs in the system that experience very similar conditions during processing. The highest temperature portion of the 6600-E and B heat exchangers is near the nozzle-shaped end. Inlet temperatures to 6600-A and D are estimated to be near 715 °F and outlet temperatures from 6600-C and F are expected to be near 300 °F (under ideal operating conditions).

The general definition for HTHA in API 941<sup>1</sup> states that “high temperature hydrogen can attack steels in two ways: a) surface decarburization and b) internal decarburization and fissuring.” API 941 explains, “Internal decarburization and fissuring are caused by hydrogen permeating the steel and reacting with carbon to form methane. The methane formed cannot diffuse out of the steel and typically accumulates at grain boundaries. This results in high localized stresses which lead to the formation of fissures, cracks, or blisters in the steel.” This definition of HTHA is quite specific, and particular types of damage and associated changes in the microstructure of the steel are expected to be present when the mechanism is operational.

The steel used for fabrication of the Tesoro exchangers would be considered a “carbon steel” for interpretation of its resistance to HTHA with the Nelson Diagram shown in **Figure 2**. The diagram

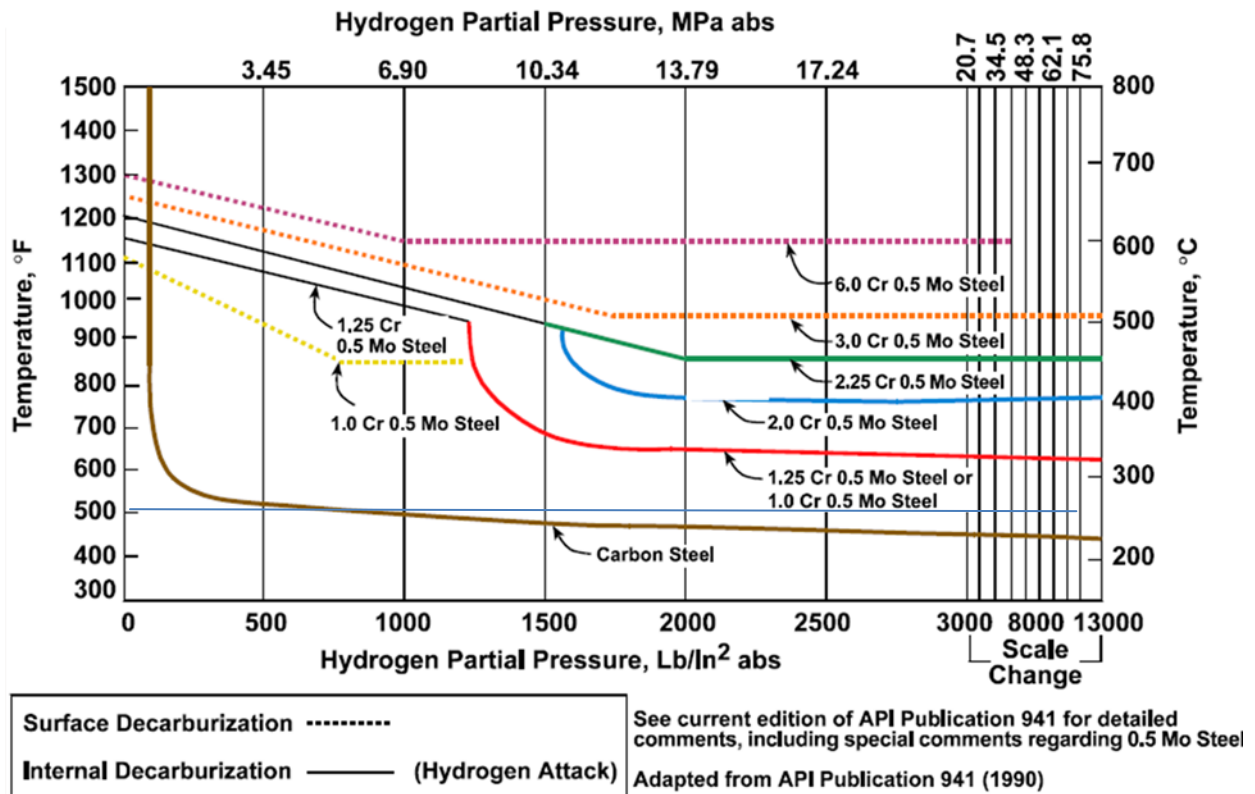


**Figure 2:** A Nelson Diagram that was adapted from API Publication 941, 1990.

indicates the hydrogen partial pressures and temperatures below which various materials are not expected to exhibit susceptibility to HTHA. The low carbon steels, which contain very little alloying additions of Cr and Mo, are most susceptible to HTHA. Cr-rich and Mo-rich carbides are inherently more stable than iron carbides, and resist dissolution of the carbon with hydrogen to form methane. Therefore, the alloys containing Cr and Mo resist HTHA at higher temperatures and hydrogen pressures. For carbon steel, this Nelson Diagram estimates that at approximately 520 °F and 500 psi partial pressure of hydrogen the steel can be susceptible to HTHA, and as the partial pressure of hydrogen

<sup>1</sup> Steels for Hydrogen Service at Elevated Temperatures and Pressures In Petroleum Refineries and Petrochemical Plants, API recommended practice 941, seventh edition, August 2008

increases the temperature for susceptibility to HTHA decreases (slightly). The original design calculations for the heat exchangers indicated an expected maximum shell-side inlet temperature of 504 °F and maximum hydrogen partial pressure of 291 psia based on reactor end-of-run conditions.

**Figure 3** shows an example of HTHA damage incurred in a C-0.5Mo steel. Note that the HTHA produced fissuring (small cracks) exclusively along the boundaries between different grains of the ferrite phase (ferrite phase is white, and grain boundaries separate the ferrite phase into polygonal shapes (grains)). These fissures then linked together to form a microcrack. Eventually, such damage will result in significant ductility loss and reduced load bearing capacity of a material. The damage typically occurs at grain boundaries or at the interface between the ferrite and pearlite phases as shown in **Figure 4**. The critical point in the initiation of the HTHA hydrogen damage is the formation of a bubble of high-pressure methane gas – a pressure that can be several orders of magnitude higher than the hydrogen partial pressure. This pressure can greatly exceed the yield strength of the steel material. As many

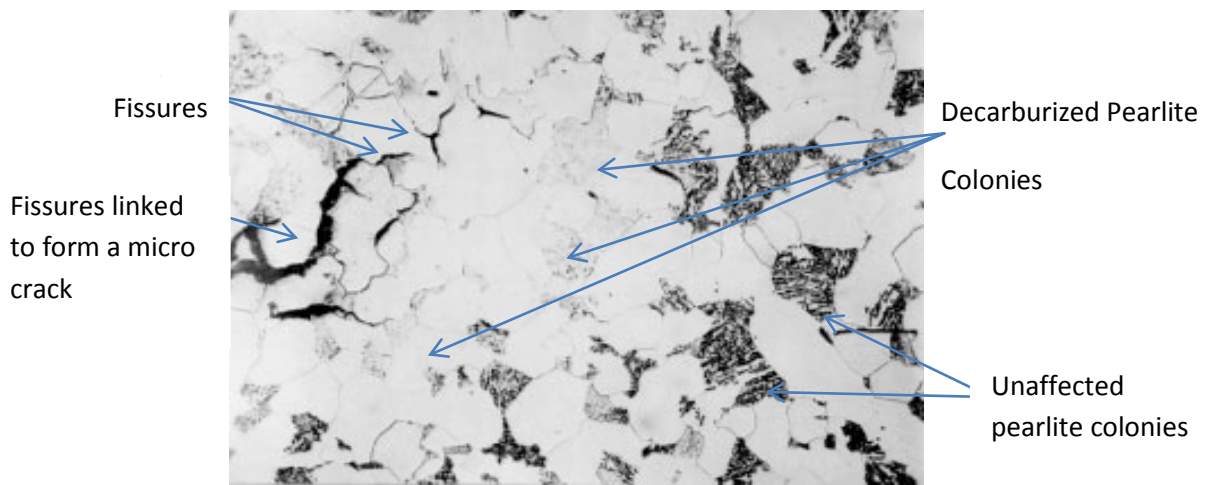


**Figure 3:** An example used in API Recommended Practice 941 (2008) for HTHA in a C-0.5Mo steel (520X, nital). The pearlite colonies, which consist of alternate layers of carbide and ferrite, are in the process of being decarburized, causing the pearlite structure to disappear because the dark carbide phase dissolves – leaving just white ferrite matrix. This dissolved carbon is needed to combine with hydrogen to form methane, which results in fissures (or blisters) in the microstructure.

bubbles form along a grain boundary, they will eventually link. The density and growth of the methane bubbles is limited by the available carbon when HTHA occurs at low temperature. This is why the most extensive HTHA damage is typically observed near the colonies of pearlite (pearlite is an alternating “lamellar” structure of ferrite and iron carbide plates.)

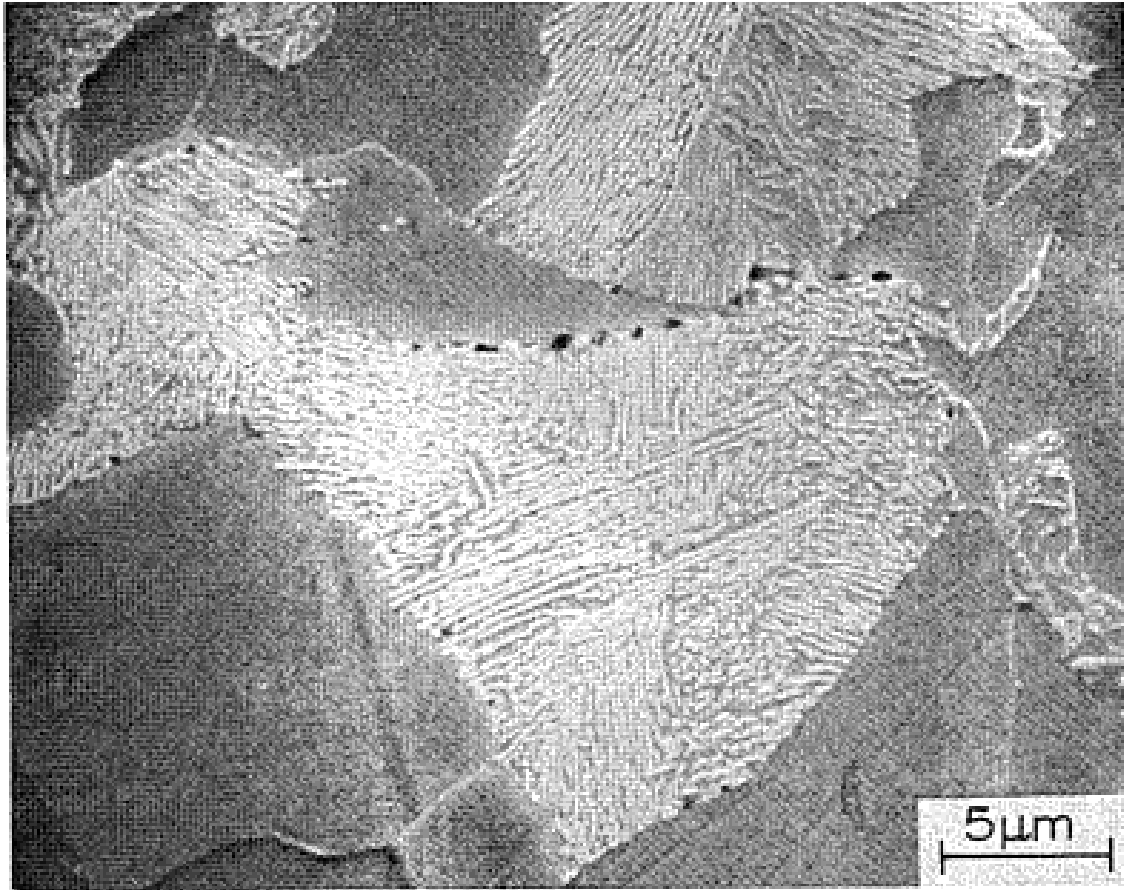


**Figure 4:** Typical methane bubble damage to the HAZ of carbon steel (Fe- 0.3C) after 88 Hr, 450° C,  $P_H = 6.5$  MPa. The bubbles form at the interface between the pearlite phase (whiter region) and the ferrite phase (dark here). Pearlite is a lamellar structure of iron carbides (white) and ferrite (dark). Carbides from the pearlite and isolated carbides at grain boundaries are dissolved to combine with hydrogen to form the bubbles. From R.Pishko, M.G. McKimpson, and P.G. Shewmon, Metall Trans, 1979, 10A, 887-894.

Fabrication of heat exchanger vessels requires the use of welding processes, which can alter the material's susceptibility to HTHA. The heat of welding significantly alters the metallurgical structure from that of the base metal, and the filler metal used during welding often has a different composition (e.g., lower carbon content) than that of the base metal. **Figure 5** shows a multipass weld cross-section typical of the Tesoro E-6600 heat exchangers and the regions within that weld that are metallurgically distinct. The weld metal represents the region containing a composite mixture of base metal and filler metal that solidified from the molten state during the welding process. The heat-affected zone (HAZ) is a region where the metal being joined was heated sufficiently by the welding process to cause metallurgical changes, but not enough to melt the material. The coarse-grained HAZ region is where sufficiently high temperatures are encountered such that significant grain growth occurs. This region typically contains the metallurgical structure with the highest hardness in carbon steel welds. Note also that in multipass welds, the previous weld passes are reheated. This can cause further metallurgical changes to the previous welds and their HAZs (e.g., the reheated weld metal), and are greatly simplified in the figure.

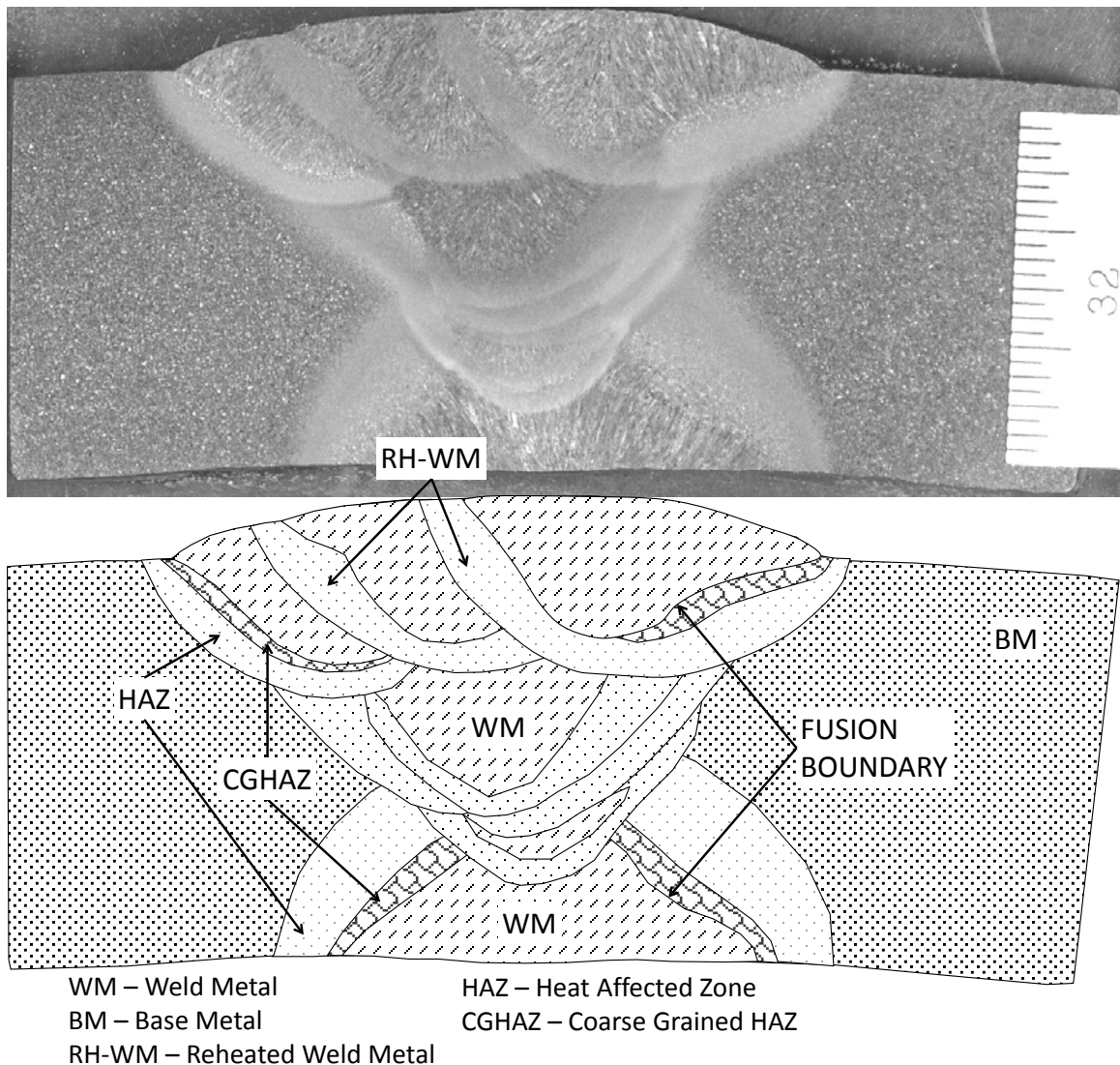


**Figure 5:** A cross section of a multipass weld typical of the Tesoro E-6600 heat exchangers and schematic defining terms associated with the weld.

## General Findings

This section is organized to serve as a summary of the data presented in the BETA Laboratory reports and to provide perspective for the comments and conclusions presented in this report. It begins with a short description of the sample and flaw locations on the heat exchanger that failed (E-6600E) and the exemplar heat exchanger (E-6600B). The mechanical test results and fracture path evaluations (measurements) are then presented. It concludes with a discussion of the metallographic data collected on the damage observed in the microstructures of the heat exchangers.

## Sample Locations

Inspection reports from Spectrum Inspection documented the condition of the E-6600E heat exchanger that failed at the Tesoro Anacortes Refinery (April 2, 2010), and the E-6600B heat exchanger (paired with E-6600E in the system). The inspections identified flaws in several weld seams and fractured

regions of the exchanger. Spectrum Inspection recommended a number of sample regions for removal and further evaluation (Figures 6 and 7).

*Principle sample locations in the E-6600E Heat Exchanger*

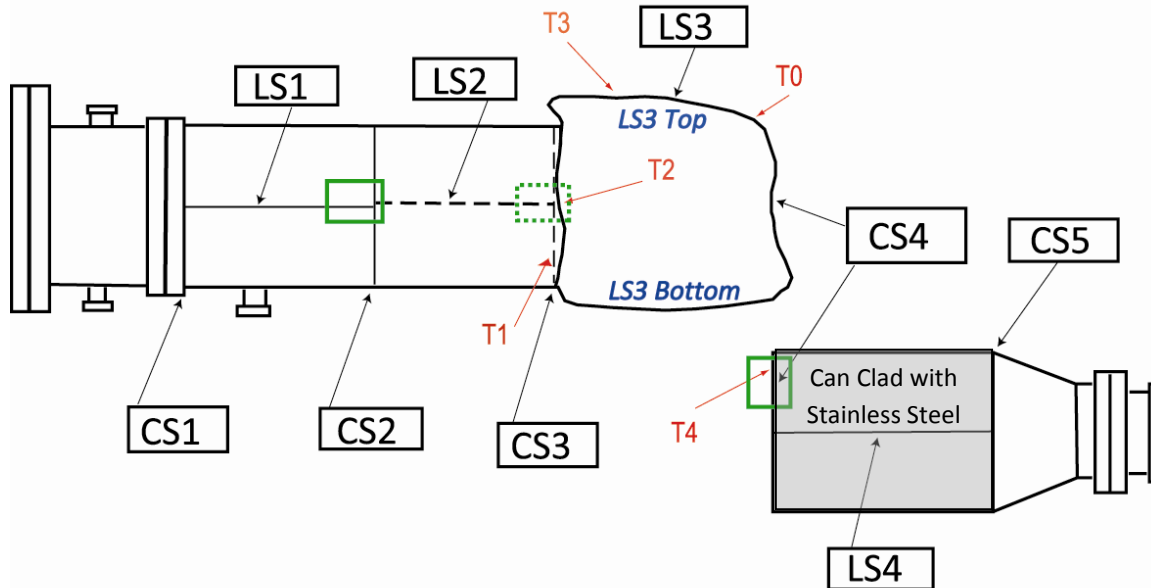


**Figure 6:** The E-6600E Heat Exchanger that failed is diagrammed here to show the identification labels (in black) for welds used in this review and the regions where cracks were identified by the Spectrum Inspection using ultrasonic techniques (labeled in red). The green boxes indicate some of the locations from which samples were removed (dotted green line indicates sample taken from back side of shell, away from fracture regions). The entire fracture regions labeled LS3 top and bottom were also removed for sampling and evaluation, as well as the CS4 fracture regions. For the welds, L represents longitudinal seam weld and C represents circumferential seam weld. From left to right there are four sections to the heat exchangers, referred to as CANs, and the welds change designations according to the section(s) they are associated with.

Spectrum Inspection detected cracking in five regions of the E-6600E (5/20/2010) heat exchanger. These regions were recommended for removal and further evaluation. The regions were identified as follows:

- TO, fractured LS3 weld had cracks on both sides (top and bottom) near CS4
- T1, cracking at CS3 (back side, dotted line) not too far from LS3 bottom section
- T2, at intersection of LS2 and CS3 (back side, dotted lines)
- T3, transverse crack along fracture of LS3 top section
- T4, cracks along CS4

During evaluation of this failed heat exchanger a number of samples were removed for evaluation, following the recommendation made in the Spectrum report. For example, the entire fracture along the LS3 weld (top and bottom) was removed, and these samples (top and bottom portions of the fracture) contain portions of the CS3 and CS4 fracture regions. A large sample region was also removed from the back side of the heat exchanger (on the side opposite from the fracture along the LS3 weld). This sample includes the intersection of the LS2 and CS3 welds.

### Principle sample locations in the E-6600B exemplar Heat Exchanger

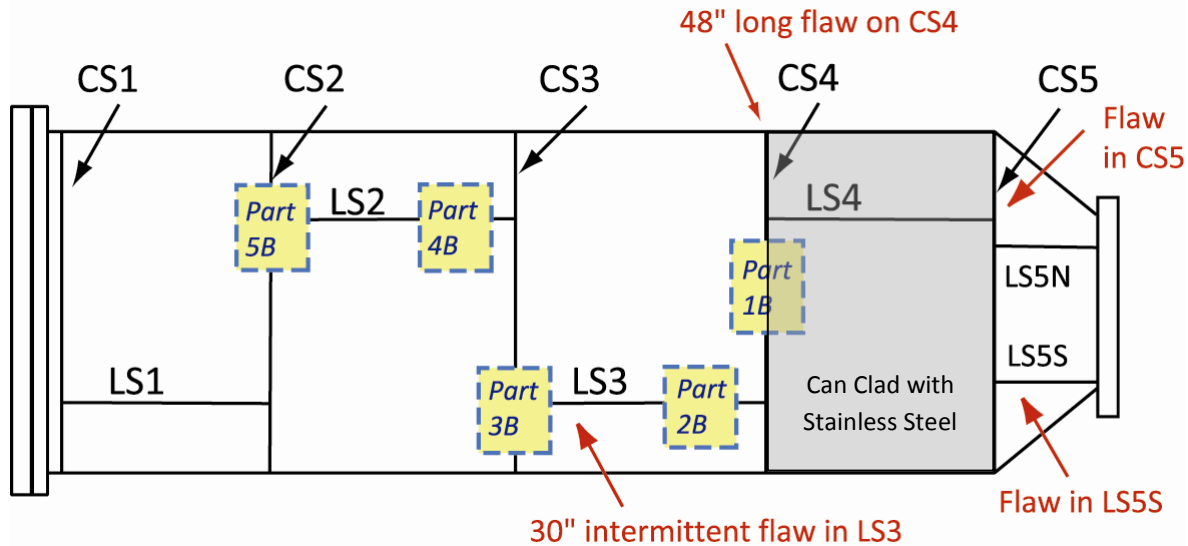


**Figure 7:** The schematic of the E-6600B exemplar heat exchanger shows weld identifications, flaw locations from the Spectrum Inspection report, and sample positions for specimens evaluated by BETA Laboratories. The positions shown for the welds are approximated for informative and semantic purposes, so differences shown for weld positions in E-6600E in Figure 3 and those shown here for E-6600B are not meaningful.

The Spectrum Inspection report identified a large crack in the E-6600B shell during the Phased Array inspections of the heat exchanger. The crack intersected the ID surface along the CS4 weld, at the edge of the stainless steel cladding. This crack was approximately 0.3 inches deep and 48 inches long (over 50 % of the weld length). Wet Fluorescent Magnetic Particle (WFMT) inspection of the ID surface by Spectrum Inspection confirmed the presence of this crack. Other evidence of flaws<sup>2</sup> was indicated in the Spectrum Inspection report on the E-6600B heat exchanger for the LS3 weld (30-inch-long intermittent mid-thickness flaw), the CS5 weld, and the LS5S weld.

Samples were taken from the exemplar heat exchanger from a number of locations. Parts 1B to 5B are the large sections removed from the shell of the heat exchanger, from which smaller samples for mechanical testing and metallography were taken.

### Composition

BETA Laboratory measured the chemical composition of the failed exchanger in various locations. **Table 1** compiles the chemistry of base metal and various weld deposits in the E-6600E heat exchanger. The steel used for fabrication of the Tesoro heat exchangers would be considered a “carbon steel” for interpretation of its resistance to HTHA with the Nelson Diagram shown in **Figure 2**. Note that some Cr and Mo were alloyed in the CAN materials, which may provide a slightly higher resistance to HTHA than a material not containing those elements; however, the Cr and Mo alloying content is still quite low.

<sup>2</sup> The Spectrum E-6600B report refers to these flaws as “Lack of Fusion” due to their proximity to welds. However, subsequent metallurgical analysis indicates that these areas were cracks caused by HTHA.

Table 1: Chemical composition of base metal and weld from the E-6600E heat exchanger.

Sample	C	Si	P	S	Mn	Ni	Cr	Mo	V	Cu	Co	Al
Base Metal												
CAN1	0.28	0.24	0.01	0.024	0.62	0.12	0.13	0.03	<0.001	0.18	0.01	0.005
CAN2	0.26	0.23	0.008	0.019	0.59	0.12	0.12	0.02	<0.001	0.18	0.01	0.01
CAN3	0.26	0.23	0.008	0.021	0.60	0.12	0.13	0.02	<0.001	0.18	0.01	0.01
CAN4	0.285	0.25	0.008	0.031	0.65	0.11	0.10	0.03	<0.001	0.13	0.01	0.005
SA-515 Grade 70	0.31 *	0.13– 0.45	0.035 *	0.035 *	1.30	NS	NS	NS	NS	NS	NS	NS
Clad												
CAN4 Clad	0.067	0.61	0.016	0.012	1.67	13.02	17.37	2.3	0.06	0.14	0.32	0.002
SA 240 Type 316 S331600	0.08 *	0.75 *	0.045 *	0.030 *	2.00 *	10.00– 14.00	16.00– 18.00	2.00– 3.00	NS	NS	NS	NS
Welds												
LS1												
LS2 OD crown	0.09	0.49	0.011	0.021	1.12	0.07	0.08	0.02	0.001	0.04	0.01	0.005
LS2 ID	0.13	0.54	0.011	0.018	1.15	0.05	0.07	0.01	0.002	0.14	0.01	0.010
LS3 OD crown	0.10	0.50	0.011	0.019	1.12	0.06	0.08	0.01	0.001	0.14	0.01	0.005
LS3 ID	0.16	0.37	0.010	0.021	1.04	0.08	0.09	0.02	0.001	0.14	0.01	0.005
LS4 OD 19W	0.07	0.53	0.011	0.021	1.13	0.06	0.07	0.01	0.001	0.13	0.01	0.006
CS1												
CS2 OD crown 17	0.08	0.57	0.011	0.017	1.16	0.05	0.07	0.01	0.002	0.15	0.01	0.007
CS2 ID 17	0.11	0.57	0.015	0.021	1.22	0.06	0.10	0.01	0.002	0.23	0.01	0.007
CS3 OD crown	0.06	0.57	0.011	0.018	1.14	0.05	0.06	0.01	0.002	0.15	0.01	0.005
CS3 ID	0.09	0.64	0.017	0.022	1.31	0.05	0.09	0.01	0.002	0.24	0.01	0.005
CS4 OD crown 19W	0.08	0.63	0.011	0.020	1.07	0.06	0.07	0.02	0.001	0.13	0.001	0.005
CS5												
Clad Welds												
LS4 ID 19W	0.03	0.78	0.014	0.019	0.89	13.27	19.05	2.92	0.05	0.07	0.08	ND
CS4 ID 19W	0.05	0.69	0.14	0.16	1.18	12.37	19.42	2.80	0.03	0.05	0.05	ND
SFA5.1 (E7016, E7018)	NS	0.75*	NS	NS	1.60*	0.30*	0.20*	0.30*	0.08*	NS	NS	NS
SFA5.17 (EM11K)	0.07– 0.15	0.65– 0.85	0.030*	0.025*	1.00– 1.50	NS	NS	NS		0.35	NS	NS
SFA5.17 (EL12)	0.04– 0.14	0.10*	0.030*	0.030*	0.25– 0.60	NS	NS	NS		0.35	NS	NS
SFA5.17 (EM12K)	0.05– 0.15	0.10– 0.35	0.030*	0.030*	0.80– 1.25	NS	NS	NS		0.35	NS	NS

\*max

Hardenability in the HAZ is an important variable to consider, particularly when welds will not be heat treated post-welding. The estimate of hardenability is a predictor of sensitivity to hydrogen-induced cracking of weldments, and it often calculated as carbon equivalency (CE). The American Welding Society carbon equivalency formula is as follows:

$$CE_{AWS} = C + \frac{(Mn + Si)}{6} + \frac{(Cr + Mo + V)}{5} + \frac{(Ni + Cu)}{15} \quad eq. 1.$$

The CE values of CANs 1, 2, 3, and 4 calculated with this formula are 0.476, 0.445, 0.449, and 0.477, respectively. These carbon equivalent values ( $\geq 0.45$ ) indicate that the weld HAZ region would have a moderate susceptibility to hydrogen-induced cracking (Zone II on the AWS hydrogen cracking prevention method, which generally requires hardness control or hydrogen control during welding).

Current structural welding standards require low hydrogen welding procedures for fabrication of these materials, and low hydrogen procedures may have been used during fabrication of the heat exchangers in the early 1970s. However, even if low hydrogen procedures were used and fabrication was completed successfully (no cracking as the welds cooled), the HAZ regions would remain moderately susceptible to hydrogen-induced cracking. So, if the HAZ regions did become hydrogen charged during the operations of the heat exchangers and the heat exchangers were cooled rapidly enough to retain the hydrogen, cold cracking could occur. Hydrogen-induced cracking of welds typically occurs in the coarse grained HAZ at weld toes, and is often referred to as “toe cracking” and “underbead cracking”.<sup>3</sup>

### *Mechanical Testing*

Macro and micro hardness, Charpy impact toughness, tensile properties, and bend failure locations were determined for selected regions of the E-6600E and E-6600B heat exchangers.

#### *Hardness Testing*

Hardness values were generally higher in the failed heat exchanger (E-6600E) compared with the exemplar (E-6600B), and in both exchangers the hardness values near CAN4 tended to be lower than those near CAN1. This variance is shown in **Table 2** and **Figure 8**. **Table 2** summarizes macro hardness values measured in each of the CAN base metals. **Figure 8** shows averaged microhardness values (converted from the Vickers scale to the Rockwell B scale) for different regions of both vessels including CAN, HAZ, and weld metal (WM) locations. In general, the CAN4 material tends to be softest, with increasing hardness towards CAN2. The CAN4 end was the hotter end of the exchanger and may have experienced a slight hardness reduction during service due to tempering or stress relief effects (that might have occurred at the vessel operating temperature). However, the heat from the fire during the accident, and the various subsequent cooling rates of the steel that might have resulted from extinguishing of the fire, could have significantly affected the hardness of the heat exchangers. This is particularly true for regions where the shell burst during the failure. If the E-6600E exchanger reached peak temperatures over approximately 730 °C (1350 °F), metallurgical transformations would be expected that could significantly alter hardness upon cooling.

EXCHANGER LOCATION	E-6600E	E-6600B
CAN 1	83	83
CAN 2	83	83
CAN 3	83	77
CAN 4	80	74

**Figure 8** summarizes average microhardness values provided in two Beta reports (Reports 12 and 13b). The bar chart shows average hardness values, and the error bars show both the minimum and maximum hardness values for each of the traversed regions. Microhardness was determined with Vickers indentations and was converted to the Rockwell B scale by Beta. Several trends are apparent from this figure. In general, *average* micro hardness was higher on the “cold” end of both exchangers (CAN 2) and decreased towards the “hot” end (CAN 4) in the various regions. This is consistent with macro hardness values in **Table 2**. Hardness in CAN 1 was similar or slightly lower than that found in CAN 2. Peak hardness values tended to be highest in CANs 3 and 4, and their associated welds. Also, peak hardness values were most often observed in the HAZ region directly adjacent to the weld fusion boundaries, which is a typical observation in welds of steels with these compositions. Whether the decreased

<sup>3</sup> N. Bailey, et. al., *Welding Steels Without Hydrogen Cracking*, Woodhead Publishing, Cambridge, 2004

hardness associated with CAN3 and CAN4 is due to service conditions or is a result of the accident was not clear from the available data.

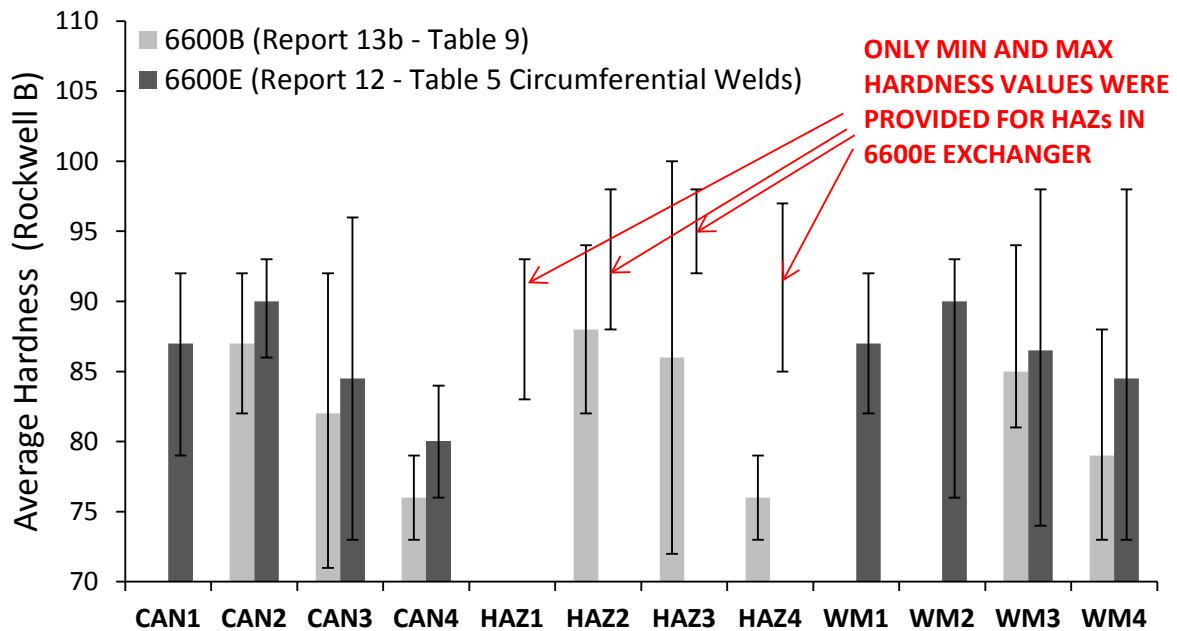


**Figure 8:** Average hardness values (converted from Vickers 500 g) in different regions of E-6600B and E-6600E exchangers. Minimum and maximum hardness values in each of the regions are indicated with the error bars.

Several examples of microhardness traverses across welded regions were shown in the Beta reports. The first type of weld hardness traverse characterizes the hardness of the girth welds joining the exchanger CANs together, as shown in **Figure 9**. These traverses completely cross from one side of a butt weld to the other, beginning and ending in the base metal. These hardness traverses typically show that the weld metal and base metal regions exhibit similar hardness levels. This is a result of the weld filler metal properties being matched to the base metal properties. The traverses also show a characteristic increase in hardness that peaks in the HAZ immediately adjacent to the fusion boundary. This increased hardness is a result of a metallurgical transformation to martensite that occurs during the welding process and is expected in welds of materials like the SA-515 steel. In general, damage to the heat exchangers tended to occur in the regions with the highest hardness, i.e., the coarse-grained HAZ.

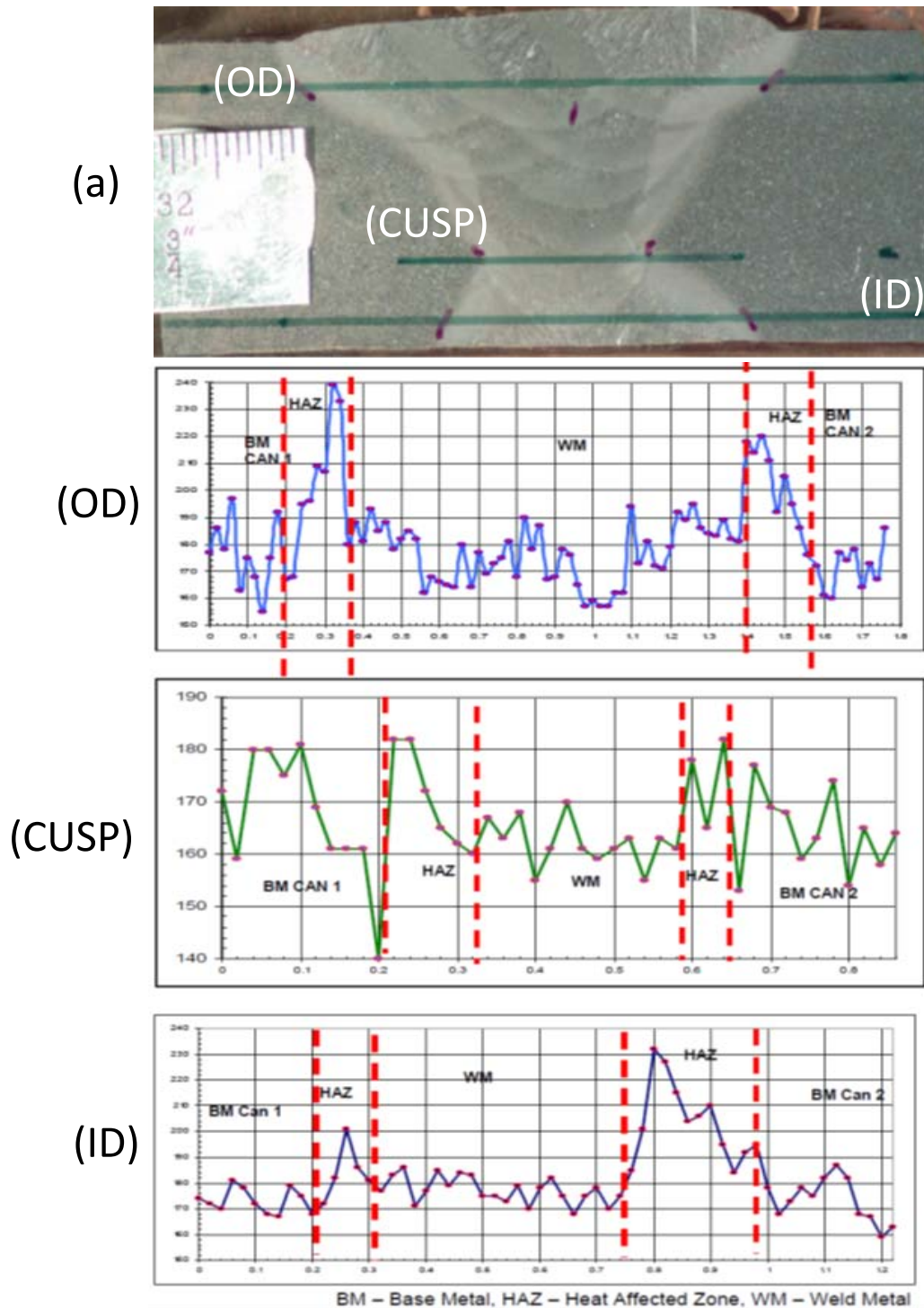


**Figure 9:** Example microhardness data collected from a cross section of the CS2 weld (CS2-A mount) on E-6600E. The green lines on the cross section in (a) indicate the location of the three hardness traces shown below it. The hardness across the OD line shows the HAZ regions of the three cap weld passes to be harder than the base metal or weld metal surrounding them (220 to 240 HV500). The base metal regions range from approximately 160 to 180 HV500, and weld metal regions have similar hardness.

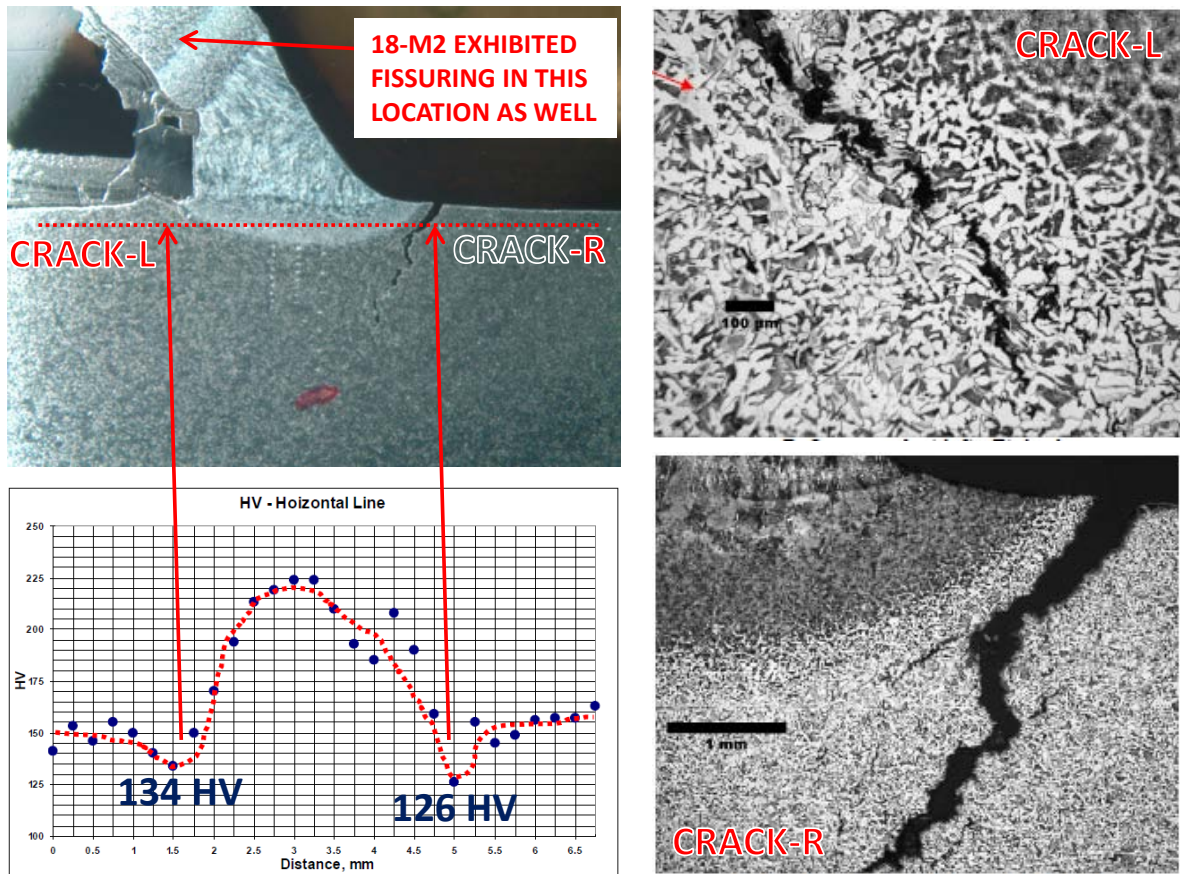


**Figure 10:** Example microhardness data collected from a cross section of the CS4 weld region (18-M1 mount) on E-6600E. Note that significant softening appears in the microhardness traverse just outside the HAZ regions of the fillet weld where fissuring is present.

Several other microhardness traverses were taken at the fillet welds where angle iron was joined to the ID of the exchangers. The hardness traverses like the one shown in **Figure 10** (Beta Report 5, Figures 10, 12, and 29) passed through only base metal and HAZ regions (not through the weld metal). This type of hardness trace showed a decrease in hardness *in the base metal* near the boundary between the base metal and the HAZ at the welded angle iron on the ID of the E-6600E exchanger. These plots of microhardness typically show significant softening adjacent to both sides of the fillet weld HAZ *in the base metal*. Extensive fissuring is present in both regions that exhibited the softening. The decarburization process occurring in the vicinity of these fissures is expected to form a softer ferritic structure than the ferrite-pearlite structure in the as-received condition of this base metal. Note in the microhardness traverse shown in **Figure 10** that the material in the vicinity of the fissures was softened by approximately 10 % and 20 % from the surrounding base metal near the left and right sides of the fillet weld, respectively. These mechanical data confirm observations of decarburization associated with fissures in the microstructure of the steel.

The fusion line cracking (underbead cracking) occurs in the vicinity of the peak hardness values shown in microhardness traverses of the first type (**Figure 9**). The HTHA that occurs in the second type of hardness traverse (**Figure 10**) is different in that it occurs in the base metal just outside the HAZ. The differences in the toe crack and underbead crack morphologies likely reflect influences of higher stress and higher microstructural susceptibility, respectively.

Drawing conclusions from absolute values of the hardness data should be done with caution, since discrepancies in hardness trends between the E-6600E and E-6600B vessels were observed. The fire following the failure of the heat exchanger likely influenced hardness of the E-6600E vessel to some degree. However, it is clear that hardness tends to be higher on the cold end and lower on the hot end of the exchangers.

**Impact Testing**

The impact properties of the heat exchangers are shown in **Figure 11**. The ductile-to-brittle-transition of the base material occurs at over 60 °F, likely closer to 100 °F (as indicated by the 50 % fracture appearance shear plot for this data, not shown here). This high transition temperature (above room temperature) at which brittle behavior can occur is expected for this coarse-grained carbon steel, as indicated by the literature data for a SA-515 Grade 70 steel shown in **Figure 12**. **Figure 12** also contains a plot of data points from the heat exchanger materials (approximate median values from **Figure 11**) for comparison. Note that the Charpy impact toughness of the exchanger material is within the typical scatter range shown in **Figure 11**, if not slightly better.

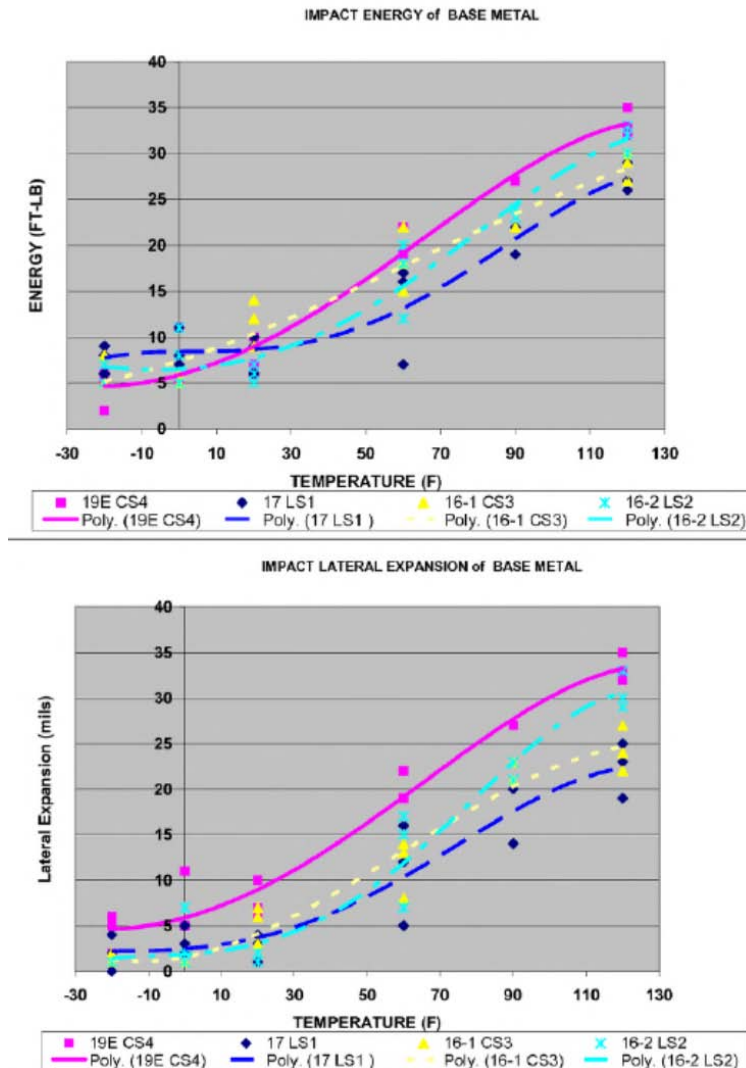


**Figure 11:** Impact energy and lateral expansion for the base metal samples.

It is difficult to conclude from the data in **Figure 11** what a fully developed transition curve (S-curve) for the base metal data looks like and what the upper shelf (top of S-curve) impact toughness for the steel is. However, it is expected that the Charpy impact toughness at a service temperature above 110 °F is at least 25 ft-lbf.

A transition curve was not developed for the weld metal, but tests at 0 °F show all weld metals had an impact toughness of 30 ft-lbf or greater (with lateral expansions of 0.020 to 0.030 inches). This compares with an impact toughness of 5 to 10 ft-lbf for the base metals tested at 0 °F. It is common and desirable for weld metal deposits to have better impact toughness than their associated base metals. The impact toughness of the HAZ, where fracture predominantly occurred in the heat exchangers was not tested. However, HAZ impact properties for multi-pass welds in pearlitic carbon steels are not expected to be lower than base metal properties.

At service temperatures expected for the heat exchangers, the Charpy impact toughness is not a critical design element (fully ductile). At room temperature, however, brittle fracture can occur in the presence of flaws. So, once a heat exchanger has developed flaws in service (such as cracks), brittle behavior at the lower temperatures associated with shut-down and start-up cycles could increase the chance of a brittle fracture event. However, the E-6600E failure occurred in ductile mode, and therefore brittle behavior did not play a role in the failure.

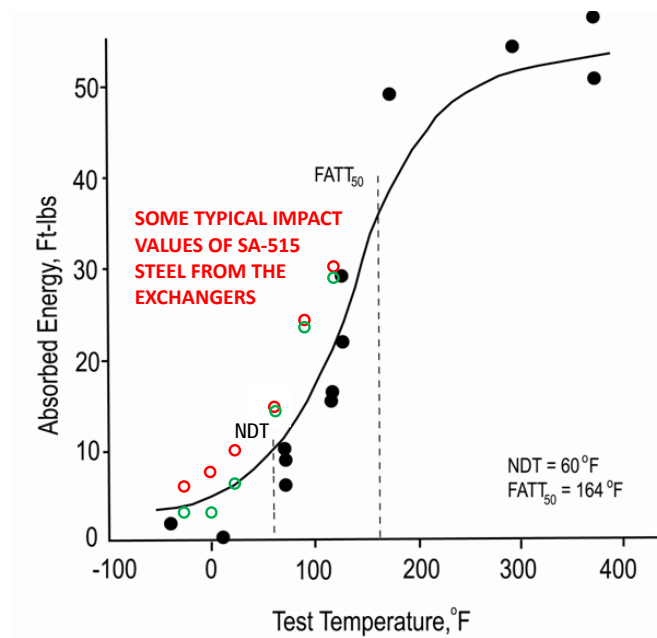


**Figure 12:** Charpy data showing transition example curve for SA-515 Grade 70 steel. The fracture area transition temperature indicated by the 50 % shear (FATT<sub>50</sub>) for this example is 164 °F and the nil ductility temperature is 60 °F. (Re-plotted data from Metallurgical failures in fossil fired boilers, D. N. French , Technology and Eng., John Wiley and Sons 1993 .)

### Bend Testing

Bend tests of the CS2, LS2, and LS1 welds (from E-6600E) passed ASME acceptance criteria for qualifying welders and welding procedures (no open discontinuities), whereas the seam weld specimens (CS3) failed the test criteria. As shown in **Figure 13**, the CS3 specimens formed cracks during the bend test. The cracks initiated near the toe of the root passes in both welds, but it is not clear from the

photographs what type of flaw initiated the cracking. The specimens from LS2 and CS3 are from the region of the heat exchanger where damage was identified in the Spectrum Inspection report (LS2/CS3 Tee region). The LS1 and CS2 specimens are from a region of the heat exchanger where no damage was identified by Spectrum Inspection (LS1/CS2 Tee region).

While these bend tests provide a good indication of weld ductility, use of these particular acceptance criteria suggests the tests were performed to determine if defects in the welds were caused by a welder or welding procedure. For this failure, the test is useful to help determine whether the defects associated with the welds were induced during fabrication of the exchanger or developed during service of the heat exchanger. In this case, no evidence was shown that would indicate that the flaws that initiated cracks in the bend bars were due to lack of fusion flaws in the welds. Evaluation of the fracture surfaces with SEM may have provided more insight into the cause of these fractures, but it is assumed that these cracks initiated at damage in the weld regions that developed during service of the heat exchangers (discussed in the metallographic section).

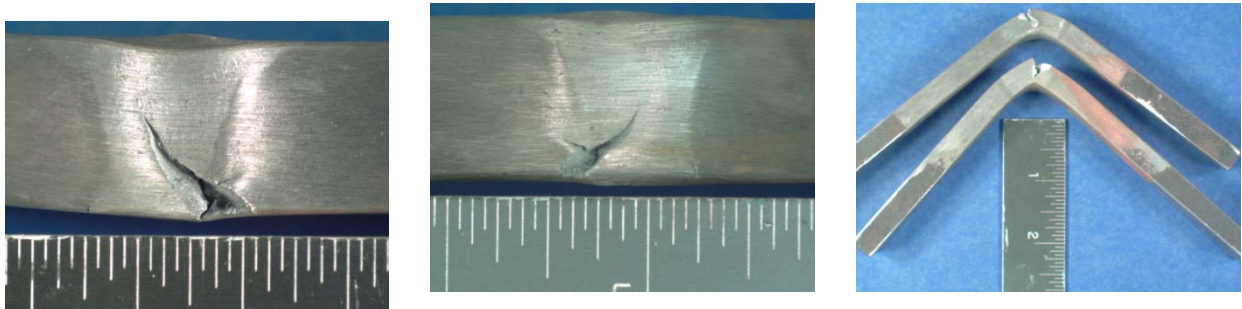


**Figure 13:** Showing two bend specimens that cracked during testing. It is difficult to clearly see the weld position in the figures, but it appears that the failures of both specimens initiated near or at the toe of the root pass in the welds (ID). Both fractures then propagated into the weld metal, where the stress of the bend bar is expected to be highest.

#### *Tensile Testing*

Tensile testing results for the base metal (**Table 3a**) on the E-6600E heat exchanger show that tensile strength, yield strength, elongation, and area reduction met or exceeded minimum values for the SA515 Grade 70. Yield strength of all weld metal deposits tested (**Table 3a**) exceeded base metal yield strength, whereas tensile strengths were typically similar between weld metal and base metal. This matching of tensile strengths and overmatching of yield strengths is a typical design approach and correlates well with the hardness testing. The LS2 and CS3 welds exhibited low values of elongation (indicated in **Table 3a**), which are likely a result of pre-existing cracks being present in the test specimens. It was indicated that the failures were ductile in nature, although this was not documented with fractography of failed specimens in the reports. In general, welds had significantly less ductility than base metal.

Only a limited comparison can be made between the E-6600E and E-6600B exchangers, since weld specimens from CW4 provide the only tensile data taken for the E-6600B heat exchanger. The results show (**Table 3b**) that yield strength values and elongation are below minimums for the base metal. It is unclear why the sample that failed in the base material had low tensile strength without showing fractography of the specimen fractures. However, again it is suspected that the effective cross sectional area of the specimen was lower than the measured area due to the presence of preexisting flaws in the

specimen. In the sample that failed in the HAZ region, flaws induced by HTHA likely resulted in reduction in the properties measured. The fracture locations in the weld specimens were in the same regions where extensive HTHA was shown in metallographic analysis.

Table 3(a): Tensile data for round base metal (BM) and weld metal (WM) specimens from the E-6600E exchanger.								
Sample	Tensile Strength, ksi		Yield Strength, ksi		Elongation (%)		Area Reduction (%)	
	BM	Weld	BM	Weld	BM	Weld	BM	Weld
LS1 A	77	77.5	42.6	55.5	51	20	51	-
LS1 B	76.5	78.5	41.9	55.5	52	22	52	-
LS2 A	72.5	68.5	41	56.5	55	7.5	55	-
LS2 B	72	74.5	38.9	55	54	15	54	-
CS2 A	-	76	-	47.1	-	29	-	-
CS2 B	-	76	-	42	-	29	-	-
CS3 A	75.5	66.5	45.2	58.5	52	12	52	-
CS3 B	75	65.5	45.7	58	52	12	52	-
CS4 A	74	-	42.4	-	49	-	49	-
CS4 B	73.5	-	41.6	-	52	-	52	-
Table 3(b): Tensile data for the rectangular CW4 welded joint specimens in E-6600B exchanger.								
CW4 <sup>1</sup>	-	-	40	-	-	-	-	-
CW4 <sup>1</sup>	-	-	44	-	-	-	-	-
CW4 <sup>2</sup>	63	-	35.3	-	11 <sup>3</sup>	-	-	-
CW4 <sup>2</sup>	56.5	-	34.5	-	9.5 <sup>3</sup>	-	-	-
SA-515 Grade 70	70 to 90	-	38 min	-	17 min	-	21 min	-
1. CW4 Full thickness specimen 2. CW4 Reduced thickness specimen from ID 3. Failures were in the base metal/HAZ								

Fire exposure is expected to affect strength much like it would hardness due to metallurgical changes in the steel. Therefore, the postmortem strength determined via tensile testing may not accurately represent the strength prior to the failure.

### Fractography and Deformation Measurements

E-6600E – PART 14 LS3 bottom with some CS3 & CS4

#### Fractographs

A few examples of fracture surface morphologies from the burst region along the LS3 weld are shown in **Figure 14** for general discussion. The fracture surfaces were exposed to fire and fire-fighting actions, so many features of the fracture surfaces are obscured. General morphologies of the fracture profiles do show that fracture paths followed the welds very closely in some regions. On some fracture surfaces, the contours of several weld passes are clearly recognizable.

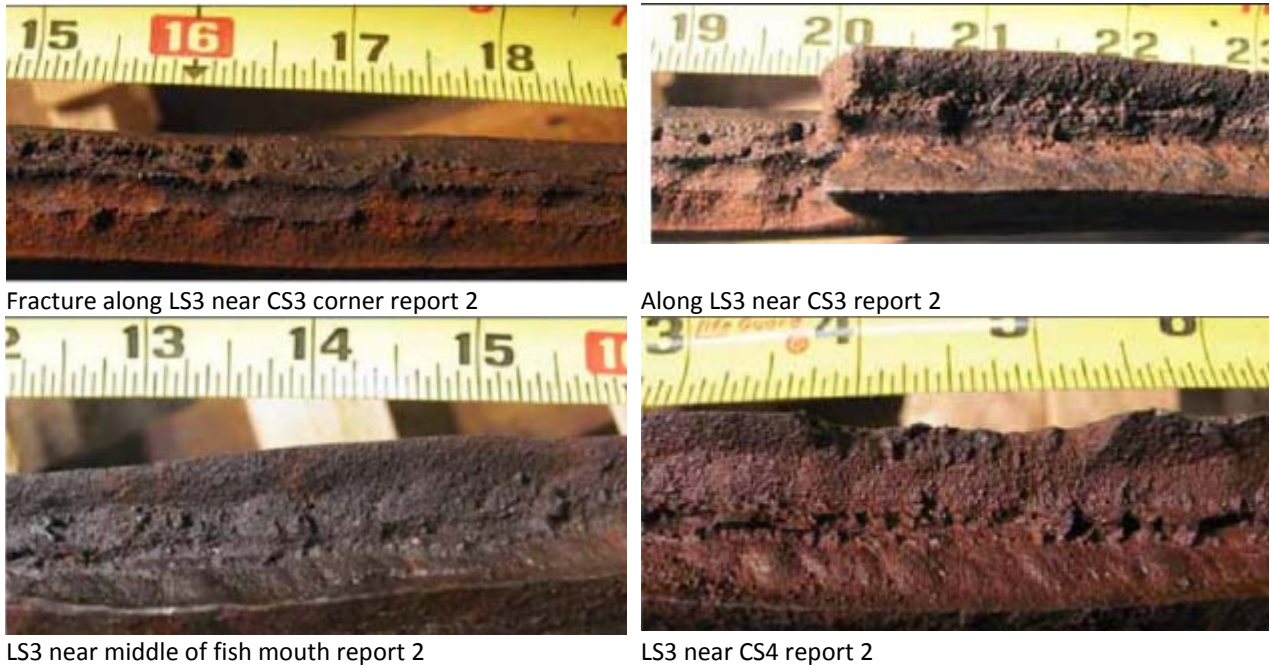


**Figure 14:** Fractography from Beta Laboratory reports 2 and 3.

Examination of the fractures during a visit to Beta laboratories on May 23, 2012 did not show any clear evidence of pre-existing cracks on the ID surface of the E-6600E heat exchanger. The fracture surface profile at the ID surface tends to extend into the shell thickness on oblique paths that are likely closely associated with the weld configuration (consistent with pre-existing HAZ damage). Detailed fracture surface evaluations would be needed to determine if pre-existing surface cracks were present in the E-6600E heat exchanger, as they are in the E-6600B heat exchanger. Due to extensive fire damage to the fractured regions, detailed fracture surface evaluation was not pursued.

The general point taken from the fractures is that the catastrophic failure event occurred in a ductile mode. This point is evident in the general texture of the fracture surfaces, and is also shown by the plastic thinning of the shell thickness measured adjacent to the fractured surfaces.

#### **WALL THICKNESS**

Wall thickness data were taken along the fractures in the E-6600E heat exchanger using calipers. The measurements were taken at a fixed distance from the fracture surface (2 inches). Wall thinning is assumed to be caused by plastic flow of the steel during fracture, transverse to the fracture direction. In regions with significant surface cracks or internal flaws, the thinning associated with the fracture would be low, as stresses would be accommodated by opening of the flaws, rather than plastic deformation. More thinning would be expected in regions with no flaws.

Reviewing the data in **Table 4 and 5** differences are not too apparent, but changes in these data are on the order of 5 to 10 % (as shown in **Figures 15 and 16**). The largest change in a continuous region is associated with the section of the fracture along the CS3 weld that is near the bottom fracture of LS3. Here, the thickness changes from 0.787 inches to 0.841 inches ( $\Delta$  % change of 6.4 %), and it is assumed that the thickness would return to the 0.86 inch thickness shown for other regions (or more). The

nominal thickness of the non-deformed steel was not given with these data for comparison, but the nominal design thickness for the E-6600E and B heat exchangers was 0.876 inch.

Considering the data for the fracture along the LS3 weld, the least thinning occurs between UT locations 55 to 75. This likely indicates that this region had more pre-existing damage than other regions along the LS3 weld (although local weld geometries, etc. could also influence these measurements). The increased thinning shown for the CS3 region may have to do with the fracture path turning to follow the CW3 and CW4 welds (fracture path may diverge from weld region into more ductile base metal region to make this turn).

**TABLE 4  
WALL THICKNESS MEASUREMENTS LS3 FRACTURE**

Location Number from UT reading	2 inch from fracture (inch)	Location Number from UT reading	2 inch from fracture (inch)	Location Number from UT reading	2 inch from fracture (inch)	Location Number from UT reading	2 inch from fracture (inch)
0		22	0.847	44	0.857	66	0.861
2	0.839	24	0.857	46	0.850	68	0.864
4	0.841	26	0.852	48	0.860	70	0.858
6	0.829	28	0.853	50	0.858	72	0.859
8	0.837	30	0.850	52	0.860	74	0.863
10	0.848	32	0.855	54	0.864	76	0.861
12	0.852	34	0.858	56	0.862	78	0.837
14	0.851	36	0.857	58	0.863	80	0.831
16	0.850	38	0.854	60	0.866	82	0.852
18	0.848	40	0.853	62	0.866	84	0.852
20	0.848	42	0.853	64	0.861		

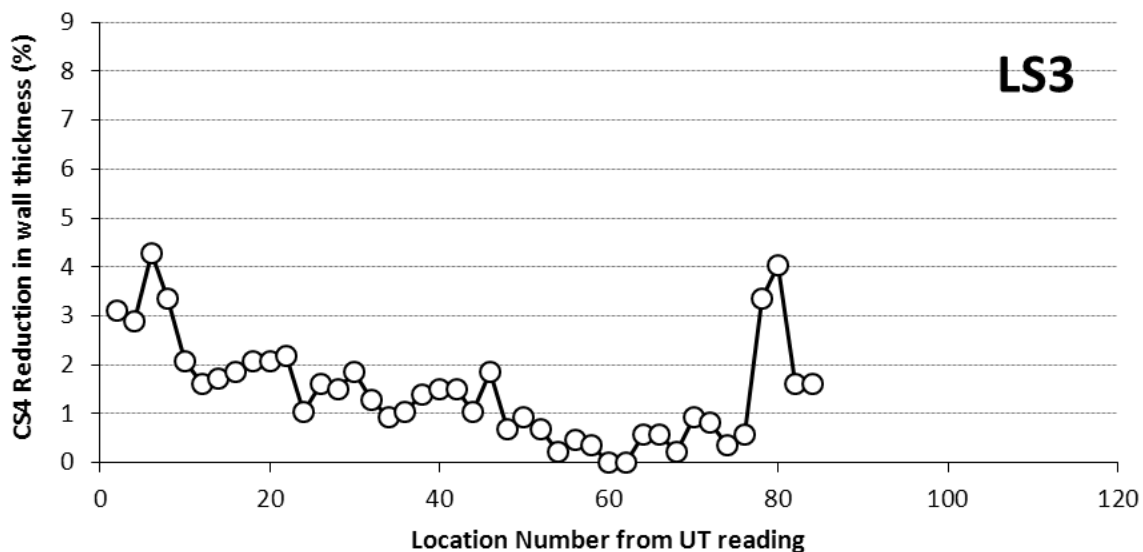


**Figure 15:** The thinning associated with the fracture along the LS3 weld is shown as percent change, with respect to the thickest region measured for the UT reading positions :  $\% \text{ Change} = \frac{(\text{thickest position} - \text{position})}{\text{thickest position}} \times 100$ . The zero UT location is near the CW3 and other end near CW4.

**TABLE 5**  
**WALL THICKNESS MEASUREMENTS FOR ADJOINING CS3 and CS4 FRACTURES**

CS3		CS4	
Location Number from UT reading*	2 inch from fracture (inch)	Location Number from UT reading*	2 inch from fracture (inch)
0	NM	0	NM
2	NM	2	0.846
4	NM	4	0.848
6	NM	6	0.856
8	0.787	8	0.862
10	0.798	10	0.852
12	0.827		
14	0.830		
16	0.841		

NM= not measurable because fracture is closer than 2 inches  
 \* marked in the field by others

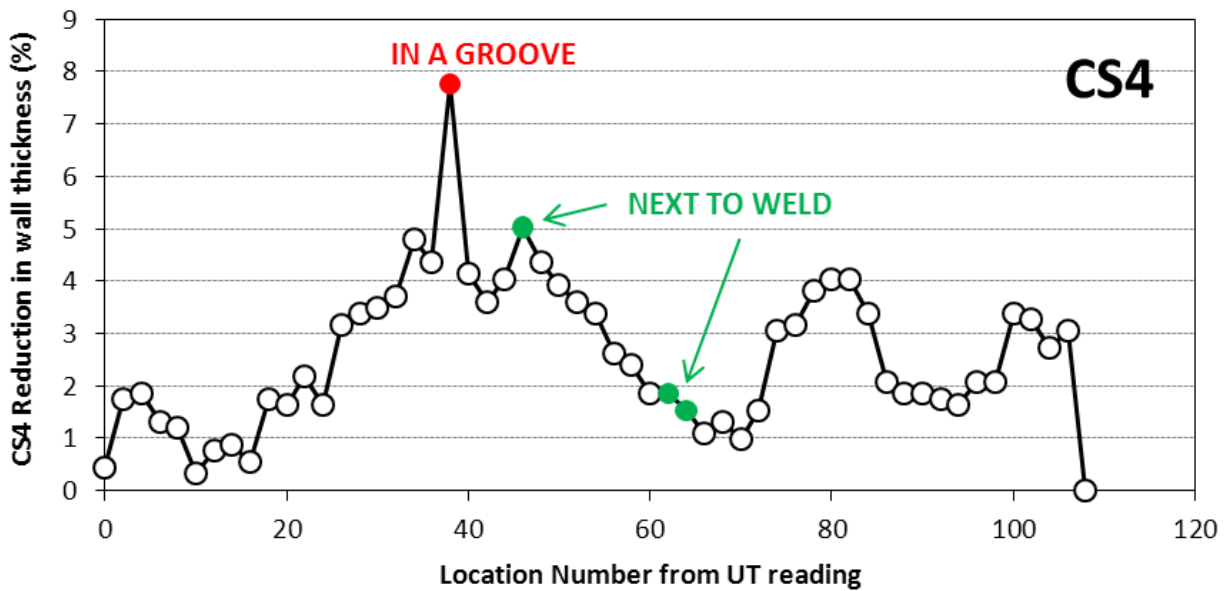


**Figure 16:** The thinning associated with the fracture along the CS4 weld is shown as percent change, with respect to the thickest region measured for the UT reading positions: % Change = [(thickest position – position)/ thickest position]\*100. The UT positions are around the circumference of the shell, so position 0 and position 108 are adjacent position. Position 0 is on top of the shell (12 O'clock) at the nozzle. The LS3 and LS4 welds intersect the fracture along CS3 near the 26 and 86 UT positions. The meaning of “next to weld” was not clear, but it is assumed that it means the thinning measurement position along the fracture was close to the CS3 weld in these locations.

Thinning measurements along the fracture path of the CW4 weld show that UT positions from about 0 to 25, 60 to 70, and 85 to 100 had less thinning than other positions along the fracture. The least thinning occurred near the top of the shell (UT near 0). This position was identified to have multiple large cracks in the Spectrum Inspection report (region T4). Reductions in thinning likely indicate regions with pre-existing macrocracks or a higher density of HTHA damage (relative to other regions along the failure path).

### *Metallography*

The damage documented on the samples removed from the E-6600E heat exchanger was typically near to the inside surface of the shell of the heat exchanger. Damage was characteristically concentrated near the fusion lines of welds in the heat exchanger, like the damage shown in **Figure 17**. In this particular example, a macroscopic crack near the toe of the weld (on the right side) is shown and a micro crack (on the left side of the weld) is also shown. The microcracking follows the contour of the weld along a path very near to the fusion line in the coarse grain heat affected zone (HAZ). The “fusion line” cracking morphology is sometimes referred to as “underbead cracking,” and it appears to follow intergranular paths in the microstructure. The toe cracks and the underbead cracking are both characteristic damage morphologies for the heat exchangers.

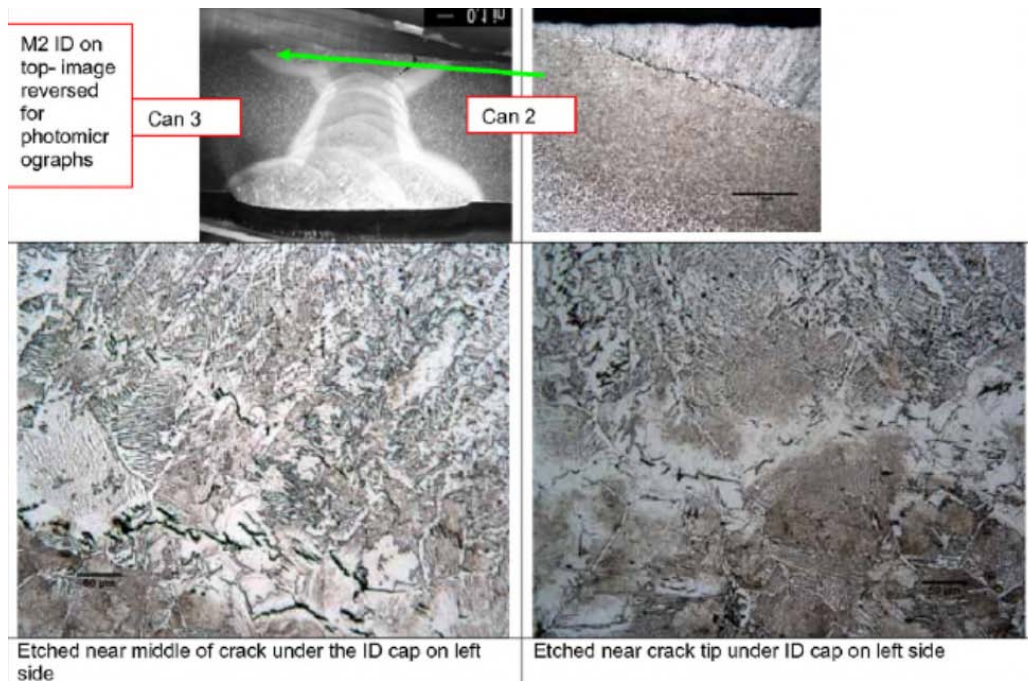
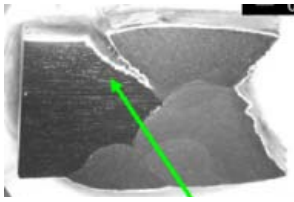
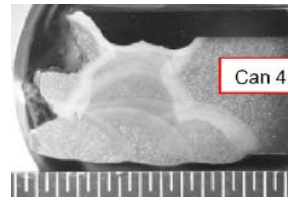


**Figure 17:** Cracks at toe of ID weld pass. Cracking occurs near the fusion line and has decarburization associated with it. Some of these cracks grew into the shell more than ¼ of the thickness (see report 4 fig 16, E-6600E). This figure was taken from report 2, Figure 27.

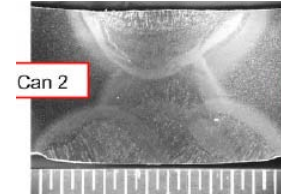
In **Figure 18**, several other examples of cracks at the toe of welds are shown. These examples also show that the failure paths on the E-6600E heat exchanger often ran along the welds, following contours of the multi-pass weld configuration closely.



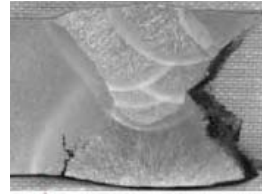
From report 2, Figure 28, LS3 weld, ID top, toe crack left side, fracture right side.



From report 3, Figure 18, CS3 weld, ID top, stainless steel clad right side, fracture left side.



From report 4, Figure 15, LS3-CS3 Tee weld, toe cracks on both sides.



From report 8, Figure 25, LS3, ID bottom, toe crack left side, fracture right side.

**Figure 18:** Examples of toe cracks from LS3, CS3, and the tee between the LS3 and CS3 welds in the E-6600E heat exchanger.

In general, details of the cracking in the E-6600E heat exchanger provide abundant evidence that is consistent with damage from HTHA. For example, in **Figure 19**, intergranular fissures and microcracking typical of HTHA are shown. Here, the damage is in the base metal in the region of the shell where the LS2 and CS3 welds intersect, and decarburization is clearly associated with the fissures at the grain boundaries and interfaces between the ferrite (white matrix) and the pearlite (reddish brown regions) in the steel. As shown in **Figure 20**, macrocracks were also present in this region, which had formed by the linking of fissures. In this example, the macrocrack is extending via an HTHA mechanism. This was a common observation).

The mechanism of HTHA requires that carbon in the microstructure of the steel is dissolved so it can combine with hydrogen diffusing into the steel and form methane at interfaces. It is the formation of methane at the interfaces that initiates the damage to the steel. However, the decarburization of the steel is often quite limited under equilibrium conditions, and does not become easy to identify in the

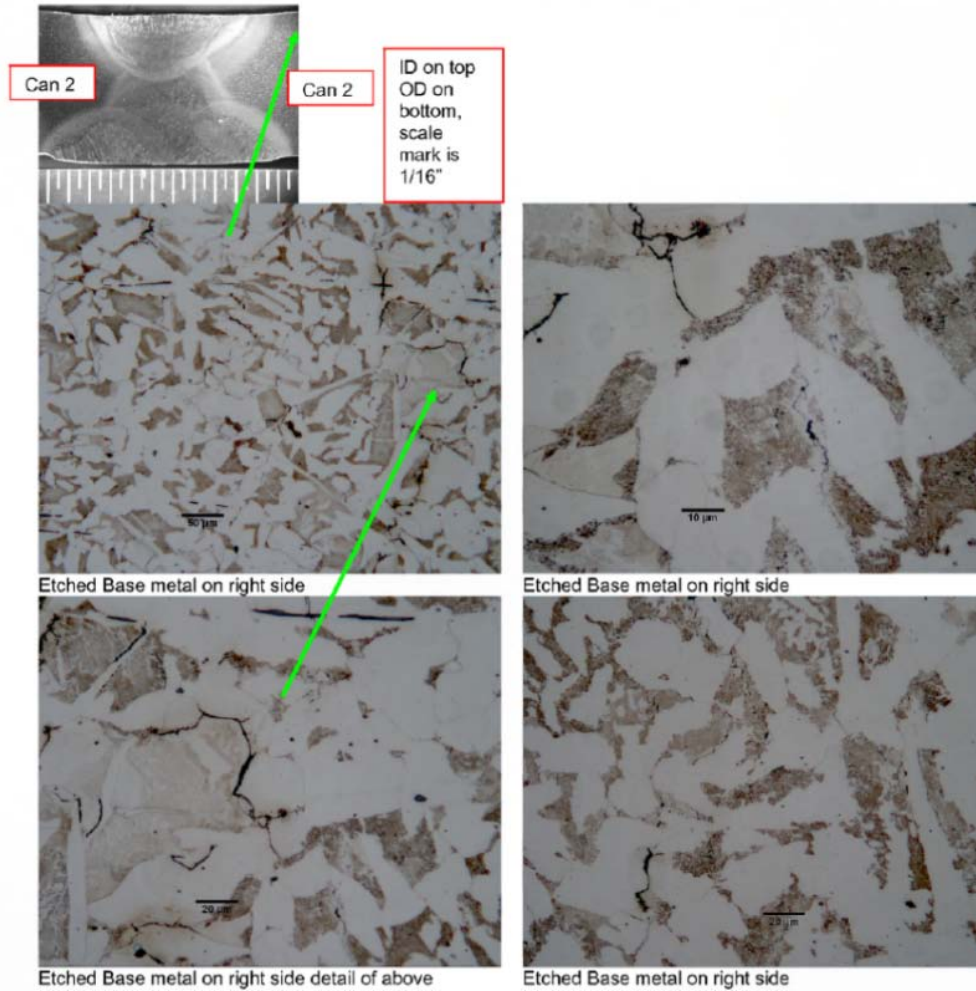


**Figure 19:** Cracking near the surface of the ID in the base metal to right of the weld shows damage morphologies typical of HTHA in carbon steel. Fissures at grain boundaries join to form cracks. The fissures are associated with decarburization of carbides in the steel. Decarburization is apparent here, because the brown pearlite phase is fading in contrast (compared with other pearlite regions) as carbides are dissolved and combined with hydrogen to form methane. This Figure is from report 4, Figure 1, E-6600E.

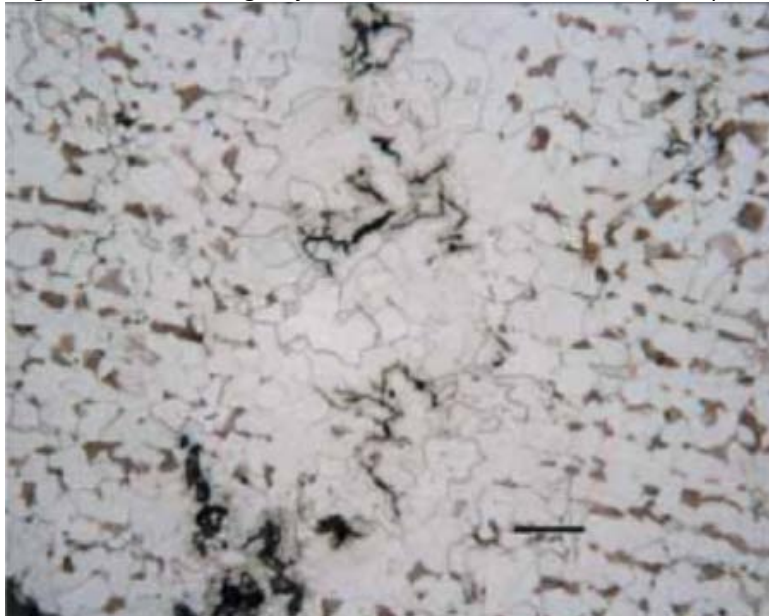


**Figure 20:** A macrocrack in the base metal in the LS2-CS3 Tee region. Details of the macrocrack above are shown below. From report 4, Figure 9, E-6600E.

microstructure until macrocracks are formed that connect the crack to the outside surface of the steel and allow methane to be released from the steel (and change the equilibrium conditions). Under these conditions, decarburization is sometimes more extensive, as shown in **Figure 21**. In this example the cracks are just under the ID surface.



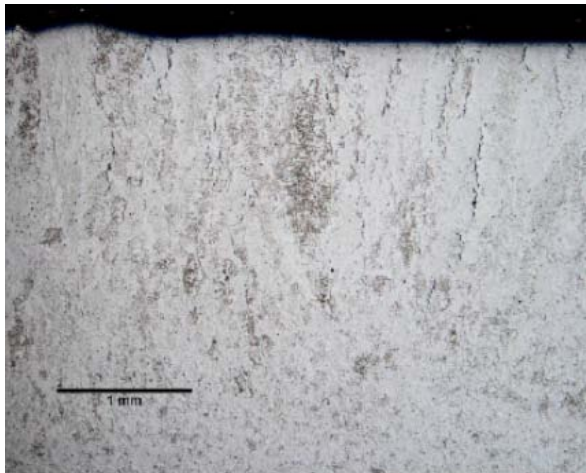
From report 2, Figure 33, LS3 HAZ region just under fracture surface on a plane parallel to ID surface.



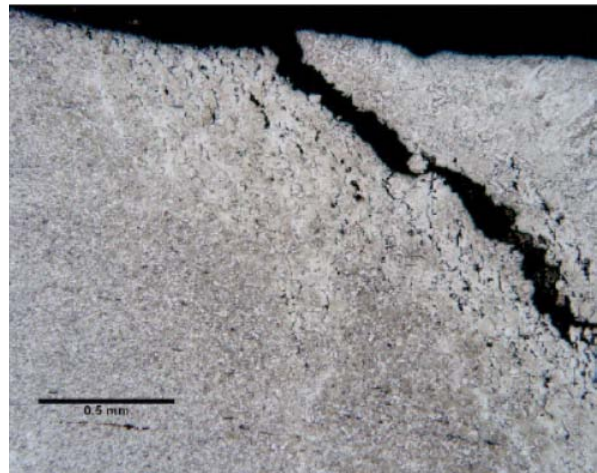
From report 2, Figure 40, base metal region adjacent to CS4 weld/fracture.

**Figure 21:** Showing decarburization adjacent to crack faces that were likely open to the surface of the ID. In the lower micrograph, the decarburized region is made evident because it runs through horizontal bands of ferrite/pearlite in the base metal of the E-6600E heat exchanger and only the white ferrite phase remains in the decarburized region surrounding the cracks.

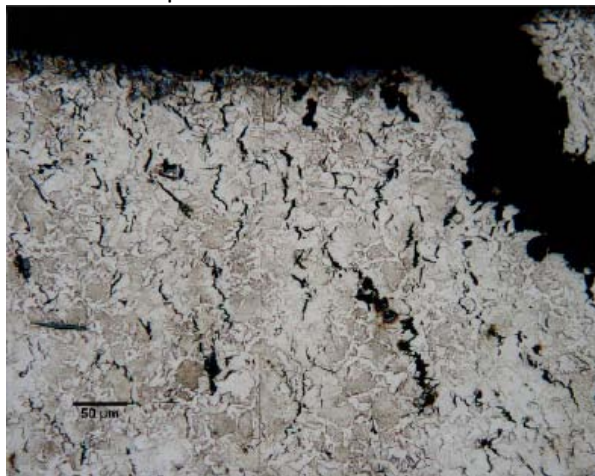
Examples of macrocracks that intersect the surface of the ID at the toe of welds, in the base metal adjacent to welds, and within the welds were each documented in the reports on the E-6600E heat exchanger. A few examples are provided in **Figure 22**. An example of cracking within a weld is provided in **Figure 22a**, where about 10 cracks near the middle portion of the root weld pass are shown to intersect the inside surface of the vessel. In **Figures 22b and c**, details of surface cracking on the surface of the ID adjacent to a toe crack are shown. Much of this cracking is also in weld metal. In **Figure 22d** another example of a macrocrack in the base metal intersecting the surface of the ID is shown (as well as sub-surface cracking). In **Figure 23**, further examples of cracking on the ID surface in the E-6600E heat exchanger are given.



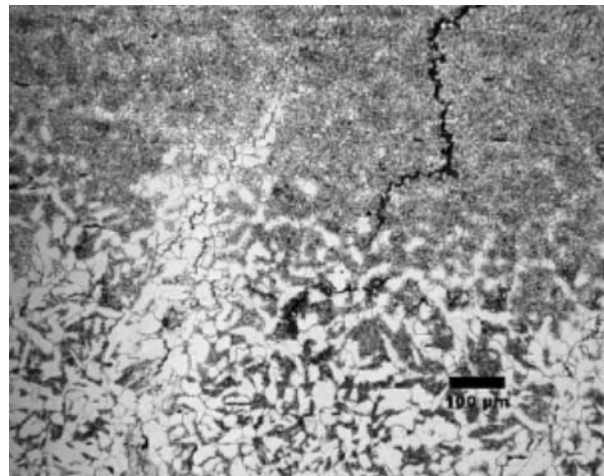
a) Report 4, Figs 10, for LS2-CS3 Tee.  
Surface of ID (top) near middle portion of  
weld pass.



b) Report 4, Figs 13, LS2-CS3 Tee.

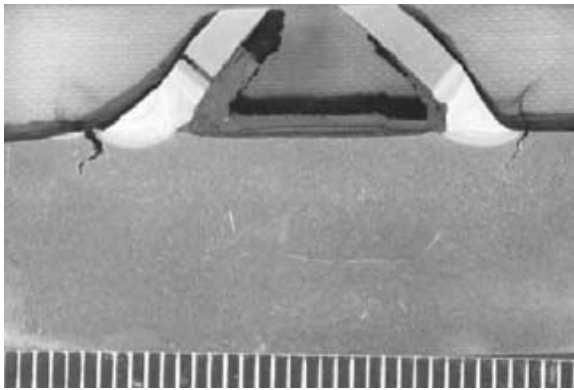


c) Report 5, fig 18, toe crack on right side of  
angle in 18-M2 where fracture intersects  
ID.

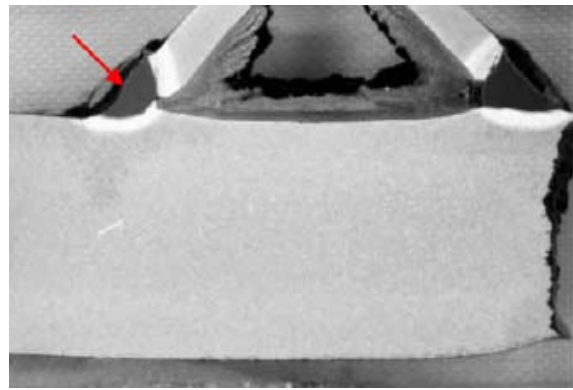


d) Report 4, Figs 14, LS2-CS3 Tee.

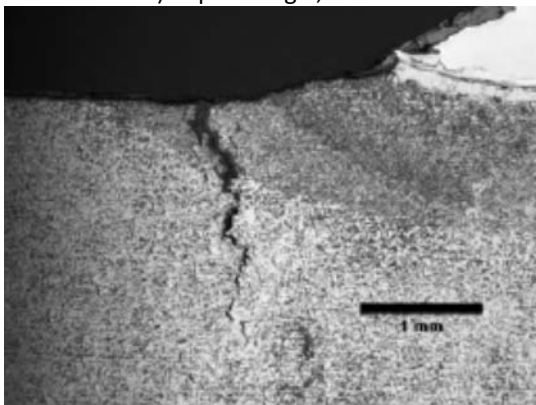
**Figure 22:** Examples of cracks intersecting the ID surface in the E-6600E heat exchanger.



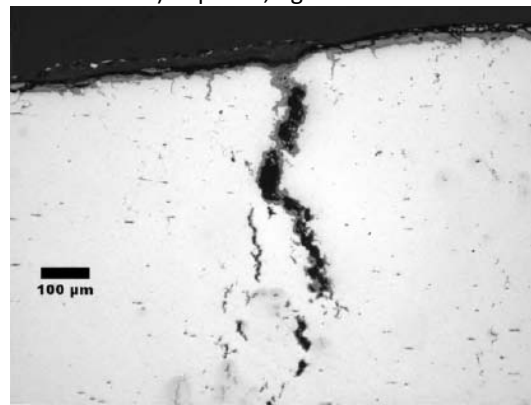
a) Report 5 fig 5, 18-M1



b) Report 5, fig 5 18-M2



(c) Report 5, fig 14, toe crack on left side of angle.



d) Report 5, fig 7, surface cracks to left of toe crack.

**Figure 23:** Extensive cracking in regions surrounding the angle iron welded onto the inside surface of the shell. There is cracking associated with most of the weld regions shown (not all visible) in the angle iron and in the shell of the E-6600E heat exchanger.

The surface cracks shown in **Figure 23** occurred adjacent to welds. In this case, the welds were made to attach an angle iron to the inside surface of the heat exchanger. The cross section in (a) shows toe cracks on both sides of the angle. The cross section in (b) does not show macro toe cracks, but it has a toe crack on the left side of the weld (see c) and the fracture occurred on the right side of the weld where a toe crack might have been present prior to fracture. Details of a smaller surface crack in this region are given in (d). Numerous other cracks intersecting the surface under the angle iron and on the angle iron were also documented in the reports.

As a final example of cracks intersecting the surface of the ID, a cross section through the 48 inch long, 0.3 inch deep crack that was identified in the Phased Array inspections in E-6600B is shown in **Figure 24**. At this particular position we estimate the crack depth is about 0.15 inch. Micrographs were not taken at this particular location. However, there is a crack at this position and the Spectrum Inspection report states that they confirmed the presence of this crack by internal Wet Fluorescent Magnetic Particle inspection.

## LABORATORY REPORT

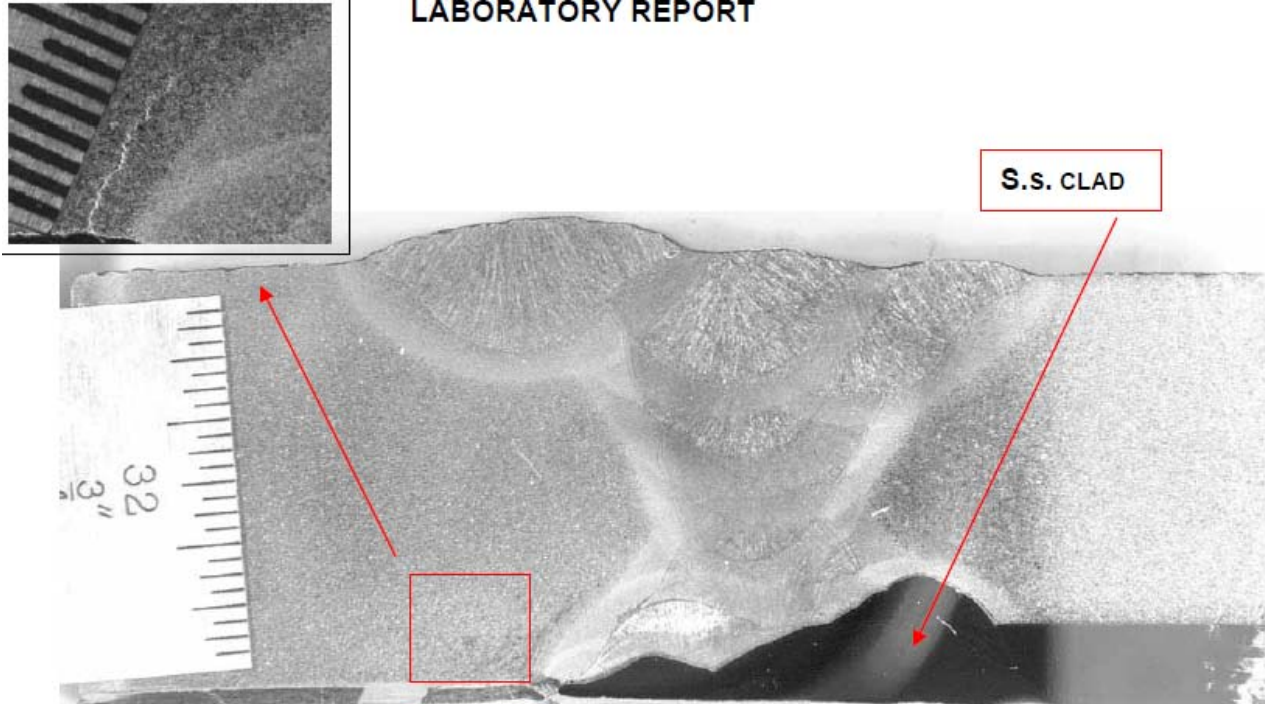


Figure 24: E-6600B exemplar heat exchanger in region where Phased Array inspections showed a 48-inch long, 0.3-inch deep continuous crack that was connected to the ID surface at the CW4 weld. The upper ruler is in 64 inch divisions, indicating a depth of about 0.15 inch for the crack at this position. The crack is barely visible in the larger cross section, but is shown to intersect the surface in the inset macrograph.

### Discussion

Non-destructive evaluations (NDE) of the E-6600E and E-6600B heat exchangers indicated that the shells of both vessels had flaws. The Spectrum Inspection NDE reports identified the locations listed below for further evaluation and testing:

- For E-6600E locations along LW3, CW3, the tee region of CW3 and LW3, and CW4;
- For E-6600B locations along LW3, CW4, and CW5.

Interestingly, the 48-inch long continuous flaw indicated in the NDE inspections at LW3 and the 30-inch long intermittent flaws in the E-6600B heat exchanger were in the same regions that the catastrophic fractures occurred in the E-6600E heat exchanger. These damage regions are in the highest temperature region of the heat exchangers that are not clad with stainless steel – an area where the steel would be most susceptible to HTHA. When samples were removed from the respective heat exchangers and examined (destructively), damage morphologies observed for the two heat exchangers were similar.

The majority of the damage documented for both heat exchangers is best characterized as HTHA, although some details of the damage, discussed below, are not necessarily typical of HTHA. Extensive damage to the shells of both heat exchangers was documented to be present along welds in CANs 3 and 4, which are the regions at the highest operating temperatures and therefore most susceptible to hydrogen damage. Some damage was also documented in CAN2 of E-6600E and CAN5 of E-6600B.

The hot ends of the heat exchangers contained the stainless steel cladding that would be expected to increase the thermal stress during elevated temperature operation, due to the mismatch in coefficient of thermal expansion (C.T.E.) between the stainless steel and carbon steel. The C.T.E. of stainless steel (e.g., 9.0  $\mu\text{in/in-}^\circ\text{F}$  from 32  $^\circ\text{F}$  to 599  $^\circ\text{F}$ ) is significantly higher than that of carbon steel (e.g., 6.5  $\mu\text{in/in-}^\circ\text{F}$  from 60  $^\circ\text{F}$  to 200  $^\circ\text{F}$ ). The stresses developed at this interface could have initiated or driven crack extension by thermal fatigue due to fluctuations in temperature and temperature gradients. In addition, if the interface between the clad weld and the non-clad ID of the heat exchanger has geometric discontinuities, geometric stress concentration at CS4 could develop, which would also help to initiate or extend cracking during thermal cycles. However, damage was dispersed throughout the heat exchangers along welds (clad and unclad), which indicates a general problem rather than a problem at a particular location that resulted in failure. For example, significant amounts of damage in the E-6600E heat exchanger were documented in welded regions of the shell that did not fail in the accident and these regions are not associated with the stainless steel cladding. Extensive damage was also documented in the E-6600B exemplar heat exchanger that would be expected to eventually result in failure of the shell with continued operation (in clad and unclad regions).

In general, the samples removed for evaluation from the failed E-6600E heat exchanger had cracking in the coarse grain HAZ region of the welds. Crack paths were often very near the fusion lines of the welds. This very selective crack path morphology along fusion lines in welds is not the typical cracking morphology associated with HTHA (although general HAZ cracking is typical). This is a crack morphology that is sometimes associated with hydrogen-induced cold cracking in welds, referred to as “underbead cracking” (“toe crack” morphologies can also be a result of hydrogen cold cracking). **Figure 25** shows the typical morphology of hydrogen-induced cold cracks in fillet and butt welds. Note that the morphology of the cold cracks is comparable to some of the damage observed in the heat exchangers. However, details of the damage along the fusion line and in the coarse grain regions adjacent to the fusion lines of the welds examined here often show that fissures are developed and link to form the underbead macro cracks, and that the fissures are often associated with decarburization. These details are not associated with the hydrogen cold-cracking mechanism in welds; they are associated with HTHA.

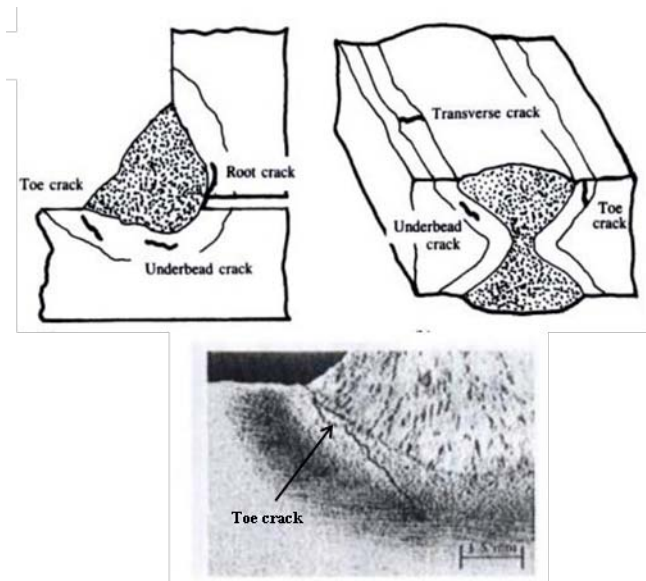


Figure 25: Hydrogen induced cracks in weld HAZs from N. Bailey, et. al., *Welding Steels Without Hydrogen Cracking*, Woodhead Publishing, Cambridge, 2004.

The explanation for the very specific cracking associated with the fusion lines of the welds and the toe cracking is not completely clear and is given further consideration here because a significant portion of the damage to the shells can be attributed to these particular damage morphologies. If hydrogen cold cracking is a possible co-mechanism for this damage, several key factors are necessary: tensile stress, the presence of diffusible hydrogen, and a susceptible microstructure. Clearly, some of the toe cracks and/or underbead cracks could have occurred during the fabrication of the vessel. On the other hand, HTHA cracks documented on the inside surface of the shells near toe cracks could have grown into toe crack morphologies (without the need of a cold cracking mechanism). The fact that no toe cracking was documented at welds on the OD of the shells supports this argument. Tensile stresses are expected to be higher at the OD cap pass than at the toe of ID root weld, so not finding toe cracks on the OD indicates that toe cracking due to fabrication was not likely (HTHA was needed to form the ID toe crack morphologies).

Alternate explanations for underbead cracking might include cold cracking as a possible mechanism or co-mechanism, considering that the heat exchangers have a fusion line microstructure that is predicted to be slightly sensitive to hydrogen embrittlement and that hydrogen was present during normal operation. Simple closed form calculations show that levels of diffusible hydrogen in the exchanger walls could have been as high as 15 ppm or higher during operation at 320 psia hydrogen partial pressure and 550 °F. It is uncertain how much of this hydrogen would remain in the exchanger walls after cooling, since it effuses quite rapidly from steel above approximately 300 °F (150 °C), but several ppm of hydrogen at a crack tip may be sufficient to induce hydrogen cold cracking. The high hardness region in the microstructure is most “sensitive” to hydrogen damage, which may explain the cracking very near the fusion line. However, the particular mechanism(s) in operation are not critical to identify at this time, and when considering specific locations in the microstructure subject to damage it should be kept in mind that predictions of damage from the Nelson Curves are estimates based on average steel properties, and small variations due to steel processing, composition, and welding are known to

cause significant differences in the resistance of particular steel to hydrogen damage. The conservative position is to recognize that a co-mechanism acting with HTHA is one possible explanation for the specific crack paths characteristic of the damage to the heat exchangers.

Regardless of the details for the toe and underbead cracking morphologies, HTHA played a key role in all of the damage documented in the heat exchangers. For typical HTHA cracking, it is expected that methane is formed during the decarburization reaction. Since decarburization was clearly associated with fissures in the heat exchangers, it seems reasonable to assume that methane contributes in some manner to the formation of the fissures, as is the case for classical HTHA. Some attempts were made to identify the initiation mechanism for the damage to the steels and to show that the fissures were due to the classical methane bubble formation mechanism known for HTHA, but the results were limited and did not clearly show methane bubbles to be a characteristic feature for initiation of damage in the steel. If there are differences in the details of HTHA initiation from the typical case, this may support an assumption that the damage was accumulated at lower operation temperatures than typical HTHA as described in the literature (in which methane bubble formation is documented). Details of the initiation of the HTHA damage to the heat exchangers is beyond the scope of the data presented, but data documented on fissures, decarburization, and fissure linking are characteristic of HTHA (for example similar to the damage shown in API Recommended Practice 941 for HTHA, **Figure 3** here).

The ductility measurements made along the fracture paths on the E-6600E heat exchanger show some indications of where fracture was least and most resisted by the shell. All damage observed on the shells of both heat exchangers was associated with welded regions on the shells, and the regions surrounding where the LS3 and CW4 welds intersect appear to have had the least plastic flow associated with the fracture, indicating less resistance to fracture. The lower resistance to fracture in this region is likely due to an increased density in accumulated damage. This does not necessarily identify the fracture initiation region, but it is likely that the catastrophic fracture initiated in a region of high damage.

The Spectrum Inspection report confirmed Phased Array indications of a crack near the fusion boundary in the E-6600B vessel with WFMT along the CS4 weld on the inside surface of the heat exchanger. If one assumes that the cracking on the E-6600B shell is representative of the failed E-6600E shell, as is indicated by the data, it is also reasonable to assume that the heat exchanger that failed (E-6600E) had cracking of a similar morphology and location to the E-6600B shell, but more advanced.

The existing metallurgical data available does not specifically identify the point during the process at which the exchanger failed, and we do not believe additional metallurgical studies will help to further clarify this question. We do know from the existing subcritical cracks found in the E-6600B heat exchanger that it was only a matter of time before one of these cracks would reach a critical size and result in the failure of the vessel. Exactly why this would happen (driving force) and how the critical events would occur (leak, burst, etc.) could vary. The main point is that failure would eventually occur unless the cracking damage was detected and the vessel was removed from service prior to a critical event.

## Appendix I: BETA Laboratory Reports

The BETA reports are arranged here by date and assigned a number accordingly. Table A.1 provides report titles, dates, and the series number assigned for this review. Table A.2 provides a list of additional reports reviewed.

The reports are reviewed here individually. Some summary information on reports is provided and detailed comments on data for the tables and figures of the reports are given. Note: Unless otherwise specified, all identified microcracks in the following analysis appear to be early onset of HTHA.

Table 1: BETA Laboratory reports listed and assigned numbers in this review according to the date that they were written.

Series #	BETA Report Title	Report Date
1	BETA Lab No-M10198 Receipt Inspection (6600-E)	July 29, 2010
2	BETA Lab No-M10198 LS3 Bottom (6600-E)	July 30, 2010
3	BETA Lab No-M10198 CS4-02(6600-E)	August 5, 2010
4	BETA Lab No-M10198 LS2-CS3 Tee Indications (6600-E)	August 13, 2010
5	BETA Lab No-M10198 CS4-01/LS3 Bottom(6600-E)	August 25,2010
6	BETA Lab No-M10198- Mechanical Property Testing (6600-E)	August 27, 2010
7	BETA Lab No-M10198 CS4-01/LS3 Bottom, Rev. 1 (6600-E)	September 20, 2010
8	BETA Lab No-M10198 LS3 Top (6600-E)	September 20, 2010
9	BETA Lab No-M10198 LS3 Bottom Fractography and 19 M-5 Mount (6600-E)	September 23, 2010
10	Beta Lab No-M10198 LS2 and LS2-CS2 Tee (6600-E)	October 13, 2010
11	BETA Lab No-M10198 6600-E Heat Exchanger E, Summary of Results and Part 17 Mounts Evaluation (6600-E)	February 3 2011
12	BETA Lab No-M10198, Rev 1 - Tesoro 6600-E, Summary of the Results	March 7, 2011
13	Beta Laboratory Report No. M10329, 6600-B, Parts 1B, 2B, and 3B,	December 27, 2010
14	Beta Laboratory Report No. M10329-B, E-6600-B, Parts 1B, 4B, and 5B,	March 8, 2011

### Report Number 1

Beta Lab No.M10198 - Receipt Inspection, Part: E-6600E Heat Exchanger Initial Receipt

Date: July 29, 2010

**BACKGROUND:** A truck transported the complete failed E-6600E heat exchanger from the Anacortes Refinery in the state of Washington to Halvorsen Company in Ohio for storage. FirstEnergy BETA Lab was the test laboratory and performed the test protocol.

### RESULTS

On June 5, 2010, the truck arrived at Halvorsen Company's Clinton warehouse in Brooklyn, Ohio. A crane was used to lift the back head and support it on the same wooden rails used for shipping. No hitting, scrapped or damaged was noted during the lifting operations. Inspection of the truck bed after the lift disclosed some debris and a rod. The materials were bagged and logged into evidence for potential examination. The heat exchangers were covered with plastic type sheets and the gates to the fence surrounding the work area within the warehouse were locked.

Figures 1.1 through 1.7 show various images of the bundled exchanger on a flatbed in the as received condition by Beta Laboratory.

## Report Number 2

Beta Lab No. M10198- LS3 Bottom, Part: E-6600E Heat Exchanger LS3 Bottom Part 14

Date: July 30, 2010

### **TESTS PERFORMED:**

The tests on the heat exchanger parts included:

- visual examination,
- chemical analysis via Vacuum Spectrometry [*sic*] and LECO carbon,
- macro and micro-hardness measurements,
- wall thickness measurements (taken 2 inches from fracture edge),
- magnetic and dye penetrant inspection,
- photomicroscopy showing crack morphology and base metal microstructure,
- Scanning Electron Microscopy (SEM) fractography
- Energy Dispersive Analysis of X-rays (EDS).

### **RESULTS**

Part 14, the complete LS 3 bottom fracture and about 20 and 13 inches of the fracture in CS3 and CS4 respectively (approximately 84 inches), were evaluated.

The surface of part 14 was wet fluorescent magnetic particle inspected by others and numerous indications were found (and indicated in figures). Eight locations were selected, by others, for metallurgical mounting. The sample locations on piece 14 and the photos of the etched mounts are shown in Figures 14-16. The mounts were examined in the un-etched and etched conditions and photomicrographs were taken as selected by others. The photomicrographs are shown in Figures 17-51. Selected mounts were examined in the scanning electron microscope. Four locations were selected for SEM fractography but the fracture surfaces were heavily coated with scale/corrosion product. The fracture surfaces of 14-SEM1, SEM2 and SEM3 were cleaned for the evaluations. The T-2 sample was alternately dipped in liquid nitrogen and heated to 180 degrees C for 6 cycles (thermal shock). The results of the chemical cleaning, cathodic cleaning and thermal shock tests were discussed with the signature parties and all SEM work of the oxidized fracture surfaces was placed on hold.

Samples of the CAN 2, CAN 3 and the 10 and 00 crowns of CS2, and LS3 were obtained and chemically analyzed. The CAN is the designation for the rolled plate that has been longitudinally welded to make a cylinder. The various cylinders or cans are then welded together with circumferential welds to make the heat exchanger shell.

Rockwell hardness testing was performed at approximately the mid wall on transverse section for CAN 2 and CAN 3 plate materials. Additionally, microhardness measurements in the 500gm Vickers scale were performed, as directed, on some of the mounts.

### **TABLES**

**Table A2.1:** Shows the types of metallurgical testing and analyses performed.

**Table A2.2:** Shows the chemical analysis of CANs 2 and 3 and CS3 and LS3 weld regions.

**Table A2.3:** Results are reported in the E-6600E summary report.

**Table A2.4:** Reports the wall thickness measurement at the LS3 fracture. Thinning due to the fracture was apparently measured at a distance of 2 inches from the fracture surface. Regions with more wall thinning generally suggests that ductility was higher than locations where less thinning occurred, i.e., where the vessel was more brittle. Locations appear to have been selected based on UT scans of the vessel.

**Table A2.5:** Wall thickness measurements are shown for CS3 and CS4.

**Tables A2.6 through A2.12:** Reports hardness values of various regions. The hardness of the base metal at M5 Fracture Line was quite low at 110 HV – 140 HV.

**Table A2.12:** Summarizes microhardness measurements made during the traverses. These included evaluations of hardness profiles across: CS3, LS3, and CS4.

### **FIGURES**

**Figure A2.1:** Shows heat exchanger, as un-packed.

**Figure A2.2:** Shows position from which the LS3-01 Bottom was removed. This sample contains the fracture surface on the bottom portion of the longitudinal fracture in the exchanger. The sample also contains a portion of the fracture along CS3.

**Figure A2.3:** Shows the fracture surface along CS3 contained in the LS#-01 Bottom specimen.

**Figure A2.4:** Shows fracture surfaces along the length of LS3, from the intersection with CS3. Clearly some portions of the fracture followed the weld profile more closely than others.

**Figure A2.5:** Shows more details along the length of the fracture.

**Figure A2.6:** Shows more details along the length of the fracture.

**Figure A2.7:** Shows more details along the length of the fracture.

**Figure A2.8:** Shows more details along the length of the fracture.

**Figure A2.9:** Shows more details along the length of the fracture, up the CS4 fracture.

**Figure A2.10:** Shows magnetic particle indication location near what appears to be the corner where LS2 and CS4 intersect.

**Figure A2.11:** Shows magnetic particle indication location near what appears to be the corner where LS2 and CS4 intersect.

**Figure A2.12:** Shows magnetic particle indication location near what appears to be the corner where LS2 and CS4 intersect.

**Figure A2.13:** Shows magnetic particle indication location near what appears to be the corner where LS2 and CS4 intersect.

**Figure A2.14:** Shows sample locations for part LS3-bottom 01. M1 and M2 are cross sections of fracture along CS3, and M3 is a cross section of the LS3 weld.

**Figure A2.15:** Shows M4 sample location and orientations. A longitudinal mount was made and a transvers mount was made. Two macro cracks are shown on the longitudinal cross section (polish plane parallel to the ID of the shell).

**Figure A2.16:** Shows location and orientation for M5, M6, and To samples.

**Figure A2.17:** Shows sub-surface cracking near the fusion line of root weld on ID, where CS3 joins to CAN 3 (M1). There is decarburization associated with the cracking at the toe of the weld. Cracking follows the contour of the root pass at the ID. It is referred to as a cap pass, although it is in fact a root pass, and there are multiple passes at the surface.

**Figure A2.18:** Similar cracking damage ID present on the other side of the root weld. The cracking occurs very near the fusion line of the weld (M1 on CS3)

**Figure A2.19:** Micro cracking in the interior of the shell near the fusion line of the CS3 weld (M1). There appears to be decarburization associated with the microcracks.

**Figure A2.21:** This shows good examples of base metal microstructure.

**Figure A2.22:** Cross section of CS3 in M2 specimen showing macro crack at toe of root weld, following contour of fusion line. There is damage in this region out into the HAZ and evidence of decarburization.

**Figure A2.23:** This fracture appears to have initiated in the weld metal. SEM images of micro cracks (fissures) in the HAZ of the M2 specimens near the toe crack at the fusion line. Cracking follows grain boundaries and interfaces between ferrite and pearlite.

**Figure A2.24:** Shows morphology for the tip of the toe crack in M2 (CS3). Tip has excursions to sides that may indicate hydrogen or corrosion damage at base metal inclusion.

**Figure A2.25:** Showing extensive cracking damage in the weld metal adjacent to the toe crack in M2.

**Figure A2.26:** Cracking damage on the other side of the root pass in M2 follows the fusion line closely.

**Figure A2.27:** Details of the cracking in M2 along the fusion line on this side of the weld shows clear evidence of decarburization.

**Figure A2.28:** Secondary crack in M3.

**Figure A2.29:** Secondary crack in M3.

**Figure A2.30:** Secondary crack in M3 and damage adjacent to it at a depth of  $\frac{3}{4}$  inch for ID.

**Figure A2.31:** ID surface are near secondary crack has little cracking.

**Figure A2.32:** Some cracking damage is shown near the mid-thickness of the shell at the fusion line of the weld.

**Figure A2.33:** The cracking on the M4 sample polished parallel to the surface of the ID shows extensive cracking and decarburization. The decarburization adjacent to the cracks here is defined so well, likely because it is so close to the ID surface (due to the orientation of the sample all through the plane of

polish). This finding indicates that these cracks were present on the surface and exposed to the environment of the shell.

**Figure A2.34:** More details of damage in M4.

**Figure A2.35:** More details of damage in M4.

**Figure A2.36:** The M4T cross section of CS3 also shows damage and decarburization.

**Figure A2.37:** The M4T cross section of CS3 also shows damage and decarburization.

**Figure A2.38:** Isolated damage along weld. The morphology of the damage is similar to aqueous pitting but this is unsubstantiated since it could have been induced during the etching of the mount. This mount also appears to be mislabeled as the top being the ID since it seems like this is SS weld metal at the bottom, which would be the ID.

**Figure A2.39:** The M5 cross section shows extensive micro cracking at the surface of the ID near fracture along CS4.

**Figure A2.40:** The decarburization associated with cracking in the base metal is apparent in this figure and it serves as a classic example of HTHA.

**Figure A2.41:** Cracking in M5.

**Figure A2.42:** SEM of micro cracks in M5.

**Figure A2.43:** extensive cracking shown near toe of ID weld in M6 (CS3), in both weld metal and HAZ.

**Figure A2.44:** Cracking at toe on right side of M6 follows the fusion line of the root pass and decarburization is likely.

**Figure A2.45:** Shows tip of toe crack.

**Figure A2.46:** TO specimen showing cracking adjacent to fracture.

**Figure A2.47:** TO specimen showing cracking adjacent to fracture (in weld).

**Figure A2.48:** TO specimen showing some cracking near mid-thickness.

**Figure A2.49:** TO specimen showing significant cracking just under the cap weld at OD.

**Figure A2.50:** TO specimen showing significant cracking just under the cap weld at OD.

**Figure A2.51:** SEM analysis of “product” in cracks.

**Figure A2.52:** Sample selected for SEM.

**Figure A2.53:** Sample selected for SEM.

**Figure A2.54:** Sample selected for SEM.

**Figure A2.55:** Sample selected for SEM.

**Figure A2.56:** SEM 1 showing ductile dimple fracture features typical for ductile fracture in general.

**Figure A2.57:** Cleaning test result.

**Figure A2.58:** Cross section of samples showing location of hardness traces. Locations of the microhardness traverses are shown in Figure A58. One of the traverses used a 10 kg load, whereas the rest used a 500 g load on the indenter. However, data from the 10 kg Vickers traverse was apparently not reported in the table.

## Report 3

Beta Lab No.M10198- CS4-02, Part: E-6600E Heat Exchanger CS4, Part 19 & 20

Date: August 5, 2010

### **TESTS PERFORMED:**

- visual examination,
- chemical analysis via Vacuum Spectrometry [*sic*] and LECO carbon,
- macro and micro-hardness measurements,
- wall thickness measurements,
- liquid penetrant inspection (by others),
- photomicroscopy

### **RESULTS**

Part 19 (CS4-02 East) and part 20 (CS4-02 West) containing about a 6 inch wide of the band of the fracture along CS4 were evaluated. These were given two part numbers because the 360 degree band was into two 180 degree arcs.

The ID surface of part 19 and 20 were liquid penetrant inspected and no reportable indications were found.

Four locations were selected for metallurgical mounting. The mounts were examined in the un-etched and etched conditions.

Samples of the CAN 4 (clad and backing plate) and the ID and OD crowns of CS4 and LS4 were obtained and chemically analyzed.

One location was selected for SEM fractography but fracture surface was very heavily coated with scale/corrosion product, so it was cleaned for the evaluation. (SEM work of the oxidized fracture surfaces was placed on HOLD.)

Rockwell hardness testing was performed at approximately the mid wall on transverse section for CAN 4. Wall thickness measurements were performed about 2 inch away from the fracture surface. Additionally micro-hardness measurements in the 500gm Vickers (HV500) scale were performed, as directed, on some of the mounts.

### **TABLES**

**Table A 3.1:** Shows the types of metallurgical testing and analyses performed.

**Table A 3.2:** Shows the chemical analysis of Can 4 base metal and cladding, and CS4 and LS4 weld regions. The can and cladding meet specified alloying levels. CS4 at the ID surface shows high alloying since it was associated with the cladding layer.

**Table A 3.3:** Results are reported in the E-6600E summary report.

**Table A 3.4:** Reports the wall thickness measurement at the CS4 fracture. Thinning due to the fracture was apparently measured at a distance of 2 inches from the fracture surface. Regions with more wall thinning generally suggests that ductility was higher than locations where less thinning occurred, i.e., where the vessel was more brittle. Locations appear to have been selected based on UT scans of the vessel. Locations 10 and 108 appear to have the least wall thinning, i.e., they may have been the most brittle failure regions.

**Table A 3.5:** Microhardness measurements are shown for CS4.

**Table A 3.6:** Microhardness measurements are shown for LS4.

**Table A 3.7:** Summarizes microhardness measurements made during the traverses reported in **Tables A3.5** and **A3.6**. CAN 3 base metal (141-226), CAN 4 base metal (146-172), HAZ side one (145-218), HAZ side two (138-223), and weld metal (153-242). The location of the microhardness traverses are indicated in the micrographs in **Figure A3.32**.

#### **FIGURES**

**Figure A3.1:** Shows “back head” section of the shell, which contains the fracture surface along the CS4 weld and the intersection of the CS4 and the LS4 welds.

**Figure A3.2:** Shows the 6 inch band cut from the “back head” section. The Zero location is at the nozzle, which is the 12 O’clock position on the shell.

**Figure A3.3:** Shows fracture surface along the CS4 weld. Interpretation of the details on this fracture surface are difficult due to oxidation from the fire, and the complex features that reflect how closely the fracture path followed the shape of the weld. Why some regions of the fracture surface have a reddish oxidation that would be presumed to be from the fire (where oxygen was available) and other regions are darker is not made clear from the fractographs. Darker oxidation regions may indicate cracks that were present before the failure and fire. (Or they may be an artifact of the lighting in these fractographs)

**Figure A3.4:** Additional fractographs are shown.

**Figure A3.5:** Additional fractographs are shown.

**Figure A3.6:** Additional fractographs are shown.

**Figure A3.7:** Additional fractographs are shown.

**Figure A3.8:** Additional fractographs are shown.

**Figure A3.9:** Shows location of M1 and M2 samples and cross section through these samples (through CS4 weld and fracture surface). M1 is taken at 107 inches, near the zero position on the top of the shell.

M2 is taken at 75 inches, which is down the CS4 weld on the side of the shell that ripped open along the longitudinal weld.

**Figure A3.10:** Shows positions of the M3 and M4 samples. M3 is between M1 and M2, at the 81 inch position. M4 is on the back portion of the shell, at 26 inches. Cross sections of the welds at M3 and M4 are also shown. Note the cladding at M3 appears to have a different orientation and must be for region LS4.

**Figure A3.11:** Shows several locations in M1 near the toe of the weld at the SS cladding have subsurface damage adjacent to the fracture path in the shell. Some of this internal damage shows oxidation.

**Figure A3.12:** More regions and damage like Figure A3.11.

**Figure A3.13:** More regions and damage like Figure A3.11.

**Figure A3.14:** More regions and damage like Figure A3.11. More damage here than other regions, and this is near Mid-thickness of the shell.

**Figure A3.15:** More regions like Figure A3.11, but show near OD damage is not present.

**Figure A3.16:** Repeat of series along edge of M1 fracture, but in this series areas are etched.

**Figure A3.17:** Damage is extensive at a position about 2 mm in from the ID surface.

**Figure A3.18:** Damage several mm in is characterized by micro cracks that are associated with grain boundaries and interface regions between ferrite and pearlite.

**Figure A3.19:** Damage further into shell is also shown to follow grain boundaries and some decarburization may be associated with the cracking.

**Figure A3.20:** More details of damage for M1. Looks like decarburization may be associated with the cracking, but details are not clear.

**Figure A3.21:** Details of interface of SS clad are shown. Not clear what the details are, but no cracking is evident.

**Figure A3.22:** Sub-surface cracking shown adjacent to the fracture path in the M2 sample near the SS clad weld. It is likely decarburization is associated with the cracking, but detailed evidence is not provided.

**Figure A3.23:** More evidence of sub-surface cracking further in from ID on M2.

**Figure A3.24:** More evidence of sub-surface cracking further in from ID on M2, but evidence of damage decreases past mid-thickness region of shell.

**Figure A3.25:** More evidence of sub-surface cracking further in from ID on M2, and damage decreasing past mid-thickness region of shell. Details of SS clad interface also shown, no evidence of cracking.

**Figure A3.26:** Cross sections LS4 on M3 sample do not show evidence of OD cracking or other damage.

**Figure A3.27:** Cross section OD CS4 on M3 shows cracking at root weld on SS clad.

**Figure A3.28:** Cracking is shown to continue along the clad root weld and further into the shell along CS3.

**Figure A3.29:** Micro cracking is also shown in the base metal adjacent to the fracture path in the shell. These microcracks are associated with grain boundaries and pearlite/ferrite interfaces, indicating that this is preexisting damage (not random damage for the fracture event). Some evidence of decarburization is associated with the micro cracking.

**Figure A3.30:** More evidence of cracking is shown further into the shell along CS3 and the fracture path. Near mid-plane, damage morphology decreases.

**Figure A3.31:** May be a typo here. From the position shown by the macrograph, this should be the OD not the ID.

**Figure A3.32:** Cross sections of M1, M2, M3, and M4 show position for micro hardness traces.

**Figure A3.33:** Show samples taken for SEM evaluation. Details appear to show a flat, less textured, region that runs the length of the sample and penetrates into the shell thickness about a 1/16 or 1/8 inch. This feature might indicate a preexisting crack on the ID of the shell, but is more likely just the stainless steel sheet that lines CAN4. If it is, it shows that in this location the fracture path went through the stainless steel sheet (haven't seen this in the cross sections of the CS4 welds).

## Report 4

Beta Lab No. M10198-LS2-CS3 Tee Indications, Part: E-6600E Heat Exchanger, LS2-CS3 Tee Indications Part16-1  
Date: August 13, 2010

### ***SAMPLE DESCRIPTION:***

Part 16, LS2 and CS3 refer to longitudinal and circumferential weld seams, respectively, while the part number refers to the chain of custody. This report is the fourth of a series on failed parts of E-6600E heat exchanger.

### ***TESTS PERFORMED:***

- visual examination,
- chemical analysis via Vacuum Spectrometry and LECO carbon,
- macro and micro-hardness measurements,
- wall thickness measurements,
- liquid penetrant inspection (by others),
- photomicroscopy.

## RESULTS

Part 16-1 and 16-2 (LS2-01/CS3-01), containing the field UT indication T2, were evaluated. The parts were given two part numbers because the piece was cut in half for ease of handling and cutting.

The surface of part 16-1 and 2 were magnetic particle inspected and no reportable indications were found. These parts are on the back side of the failed longitudinal weld.

Three locations were selected for metallurgical mounting. The mounts were examined in the un-etched and etched conditions and photomicrographs were taken.

Samples of the CAN 2 and 3, previously removed for a previous report, and crown passes of the CS3 and LS2 welds were taken and chemically analyzed.

Rockwell hardness results, performed for a previous report at approximately the mid wall on transverse section of CAN 2 and 3, are reported in Table 3. Additionally micro-hardness measurements in the 500gm Vickers (HV50o) scale were performed, on some of the mounts.

## TABLES

**Table A 4.1:** Shows the types of metallurgical testing and analyses performed.

**Table A 4.2:** Shows the chemical analysis of CANs 2 and 3 base metal and CS3 and LS2 weld regions. The CAN meets specified alloying levels.

**Table A 4.3:** Results are reported in the E-6600E summary report.

**Table A 4.4:** Reports measurements of microhardness across LS2.

**Table A 4.5:** Summarizes microhardness measurements made during the traverses reported in Table A 4.4. CAN 2 base metal (163-191), HAZ side one (180-229), HAZ side two (175-226), and weld metal (161-196). The location of the microhardness traverses are indicated in the micrograph in **Figure A4.24**.

## FIGURES

**Figure A4.1:** Shows location of Parts 16-1 and 16-2 from the location where UT results indicated flaws on the back side of the shell near the CS3 position. This region is away from where fracture occurred and contains the LS2 weld and where LS2 and CS3 intersect.

**Figure A4.2:** Shows part 16-1 and 16-2 cut out of the shell: 16-1 contains the interstition of CS3 and LS2.



Note T-2 UT indication at CS3 and LS2 TEE

Figure AI.1: Showing location of part on the “back side” of the shell near the CS3 position where the T-2 UT indication of flaws was indicated. The flap opened by the failure event is visible in the top left hand corner of the image.

**Figure A4.3:** Shows labeling of samples on part 16-1 and cross sections of welds. A macro crack is visible in the T2 weld cross section near the fusion line of the root pass on the ID of the shell where the LS2 weld intersects the circumferential weld (CAN 3 side). A macro crack is also visible near the fusion line of the root pass in the T2L sample, and may be cracking on both sides of the root weld.

**Figure A4.4:** Details of the macro crack on the T2 sample show extensive surface and subsurface cracking in this region.

**Figure A4.5:** Further details of this region show multiple areas of cracking where micro cracks are linking to form macro cracks.

**Figure A4.6:** Details adjacent to macro crack show extensive sub critical microcrack networks in the weld metal. The tip of the macro crack is into the base metal. There may be some decarburization associated with the cracking, but the micrographs do not make this detail clear.

**Figure A4.7:** Cracking that appears to be near the fusion line of the weld on the T2 sample (CAN 3 side, mid-shell thickness position) is shown to be in the base metal HAZ. The cracking does not appear to have decarburization associated with it (but slight decarburization may be present), and it typically located at interphases between pearlite and ferrite and along ferrite grain boundaries. The position of this damage in the mid-thickness of the shell along the weld provide a good example of why this type of damage might be interpreted as “lack of fusion flaws” during the UT inspection. However, the morphology of the cracking shows this damage not to be a result of lack of fusion, which is characterized by flat machined surface that were not melted (fused) during the weld process.

**Figure A4.8:** Macro crack at ID surface where LS2 intersects CS3 at CAN 3 (T2 sample) showing sub critical cracks adjacent to the macro crack. Some cracks appear to run along boundaries between weld passes.

**Figure A4.9:** More details of micro cracks in the T2 sample are shown. Here some portions of the cracking are likely associated with decarburization.

**Figure A4.10:** Families of surface cracks on the ID of the shell in the weld metal are shown (T2 sample). The cracks often follow along the elongated grain boundaries in the microstructure of the weld. In this location, approximately 8 cracks are shown to intersect the ID surface of the shell.

**Figure A10:** Shows attack of the weld metal, which appears to be more of the classical case of HTHA than what is seen as atypical, i.e., the HTHA that follows the fusion line.

**Figure A4.11:** Some small defects near the left toe of the weld in the T2C sample are shown.

**Figure A4.12:** Subsurface micro cracks, in early development of linking, are shown near the ID surface of the shell in the root weld pass of a weld.

**Figure A4.13:** Sub critical cracking associated with the macro crack in the HAZ at the root of the LS2 weld (CAN 2 on both sides of weld) on the ID surface of the shell. This is from the T2L sample.

**Figure A4.14:** Details of crack shown in 4.13. The microstructure here has coarsened and has a lot of grain boundary ferrite. Cracking appears to follow interfaces of pearlite and grain boundary ferrite.

**Figure A4.15:** Details of region near the macro crack in Figure A4.14, where there is an area of micro cracking on the ID surface of the shell. This region is at the edge of the HAZ. The microcracks follow the ferrite grain boundaries and interfaces between pearlite and ferrite. There is evidence of decarburization associated with the micro cracking. This is from the T2L sample.

**Figure A4.16:** Details of macro crack at a position further away for the ID of the shell.

**Figure A4.17:** Macro crack along the fusion line of the weld near the mid-thickness of the shell. This is another good example of a flaw region that might be suspected to be due to lack of fusion in a UT inspection...not due to lack of fusion when details of the crack morphology are considered.

**Figure A4.18:** Macro crack on the ID of the shell on the other side of root pass (T2L). In HAZ and cracking follows interfaces in the microstructure.

**Figure A4.19:** Detail on ID surface further away from the root weld (outside of HAZ) show numerous micro cracks are present on the surface of the ID. The crack follows grain boundaries and other interfaces in the microstructure.

**Figure A4.20:** Details of subsurface cracking in this region (Figure A4.19) show clear evidence of decarburization intimately associated with the cracking.

**Figure A4.21:** Another region of cracking on sample T2L, near the root pass of ID. Decarburization may be shown but details are not clear.

**Figure A4.22:** Details of region shown in 4.21. Decarburization is likely associated with this cracking.

**Figure A4.23:** More details of this region (4.21). Decarburization likely associated with cracking.

**Figure A4.24:** Shows the microhardness traverse locations reported in Tables A2.4 and A2.5.

## Report 5

Beta lab M10198-CS4-01/LS3 Bottom, Part: E-6600E Heat Exchanger CS4-01/Bottom Part 18/14

Date: August 25, 2010

### ***SAMPLE DESCRIPTION:***

The pieces labeled 18 containing a part of the weld CS4, as well as a matching small piece labeled 19E from the CAN 4, are subjects of evaluation in this report. The parts are shown in Figures below.

The main fracture is along CS4, but secondary cracking is present perpendicular to CS4 where (it appears) an angle iron is welded onto the ID of the shell. Photographs of the removed part show both sides of the CS4 fracture, and the ID and OD surfaces of the part. The secondary crack follows along the angle iron on the ID and appears to turn again due to a discontinuity on the OD of the shell (adjacent to the number 18 written on the surface).

## ***RESULTS***

### ***TABLES***

**Table A 5.1:** Shows the types of metallurgical testing and analyses performed.

**Table A 5.2:** Shows the chemical analysis of Cans 3 and 4 base metal, Can 4 clad, and CS4 weld regions. The Cans meet specified alloying levels.

**Table A 5.3:** Hardness results of Cans 3 and 4 are reported in the E-6600E summary report.

**Table A 5.4:** Summarizes the spread of measured microhardness values in traverses across CS4.

**Table A 5.5:** Reports the chemistry and microhardness values of weld metal at Can 3. The M2 weld metal contains high alloy levels since it was associated with the cladding. Note that the peak hardness of the M2 weld metal (clad) was reported as being 391 HV. The table indicates hardness traverses are shown in Figures 5.29 and 5.30; however, the regions shown in these micrographs appear to contain the angle iron sections and not the cladding as indicated by the composition.

### **FIGURES**

**Figure A5.1:** Shows whole E-6600E heat exchanger.

**Figure A5.2:** Shows location of part removed for report 5.

**Figure A5.3:** Shows OD and ID surfaces of the part removed from the shell.

**Figure A5.4:** Shows sample locations on the part.

**Figure A5.5:** Shows cross sections of 18-M1 and M2 samples and macro-cracks are apparent on 18-M1.

**Figure A5.6:** Shows fracture path along CS4 in cross section. The fracture path is just outside the heat affected zone of the welds near the ID and near the mid-thickness of the shell, and along the fusion line of the cap weld.

**Figure A5.7:** Shows details of the toe crack in sample 18-M1. Families of microcracks are apparent at the surface of the ID and within a millimeter or so of the ID. The cracks contain oxidation products, suggesting they have been present for a while.

**Figure A5.8:** Details of cracking under the angle iron on sample 18-M1 shows intergranular cracking in ferrite grains with some indications of decarburization.

**Figure A5.9:** Details of surface and subsurface cracking in other locations on the angle iron and the weld regions associated with the angle iron.

**Figure A5.10:** Details of surface and subsurface cracking in other locations on the angle iron and the weld regions associated with the angle iron. Cracking primarily associated with the HAZ. Here isolated micro cracking is shown and linking of isolated damage regions is apparent. Decarburization in damaged regions is likely present, but micrographs don't show this detail too clearly.

**Figure A5.11:** Details of surface and subsurface cracking in other locations on the angle iron and the weld regions associated with the angle iron. Damage from cracking in the shell near the toe regions of the angle iron welds is extensive. Cracks are most advanced at the weld toe, but damage is present regions that macro cracks are not apparent.

**Figure A5.12:** Shows families of micro cracks near one of the macro cracks at the toe of the angle iron welds in HAZ. Decarburization is not shown to be related to cracking in this region.

**Figure A5.13:** Micro cracking is shown at the subsurface region of the ID near where the angle iron is welded to the ID. The micro cracks are clearly intergranular. Decarburization is not apparent and high magnification micrographs are shown.

**Figure A5.14:** Details of macro cracks at weld toe of angle iron welds are shown. There may be decarburization associated with some these crack, but the micrographs do not make this point clear.

**Figure A5.15:** Cracking on the fusion line of the weld in the angle iron (between weld and angle iron... not shell) is shown.

**Figure A5.16:** More sub surface cracking on the ID of the shell is shown near (under) the angle iron.

**Figure A5.17:** Shows extensive micro cracking in base metal of shell and angle iron.

**Figure A5.18:** Shows decarburization associated with micro cracking in HAZ on ID of shell where angle iron is welded.

**Figure A5.18** (there are two figure 18's indicating a typo in the report): Shows extensive subcritical micro cracking associated with the fracture path through the shell in the region where the angle iron was welded to the ID of the shell. (This is figure 19 in revised report)

**Figure A5.19:** Shows a cracking morphology with corrosion products that may indicate delamination associated with base metal inclusions. The features run perpendicular to the fracture surface through the shell in the region under where the angle iron is welded to the ID. (Figure A20 in revised report)

**Figure A5.20:** Shows some subsurface cracking at the OD. (Figure A24 in revised report because new fig added)

**Figure A5.21:** Shows more details of subsurface cracking at OD (not clear if intergranular or if associated with decarburization)

**Figure A5.22:** Shows damaged region near OD along fracture surface.

**Figure A5.23:** Shows details along fracture edge near OD. Shows internal regions (voids) containing oxidation products ... check microstructure here

**Figure A5.24:** Shows extensive decarburization associated with cracking near edge of the fracture path.

**Figure A5.25:** Shows more details like Figure A5.24.

**Figure A5.26:** ID near the SS weld for CS4. Shows subsurface cracking

**Figure A5.27:** Shows crack path along CS4 following bottom portion of cap pass... damage likely due to fracture events.

**Figure A5.29:** Hardness traces are reported near toe of angle iron weld. A decrease in hardness is apparent at the weld HAZ region containing the crack. The removal of carbon by HTHA would result in a decrease in hardness.

**Figure A5.30:** Hardness traces are reported near toe of angle iron weld.

## Report 6

BETA LAB No. M10198 - MECHANICAL PROPERTY TESTING

PART: 6600E HEAT EXCHANGER 17 (LS1- CS2), 16-1 & 2 (LS2- CS3) AND 19 (CS4)

DATE: AUGUST 27, 2010

### **SAMPLE DESCRIPTION:**

This report contains evaluation of heat exchanger 17 (LS1-CS2), 16-1 & 2 (LS2-CS3) and 19 (CS4). Parts 16-1 and 16-2 (LS2-01/CS3-01), shown in Figure A6.2 in this report, are from the side of the heat exchanger opposite the where the shell split open. These parts contain the CS3 weld joining CAN2 and CAN3, and intersection with the LS2 weld. Part 17 (LS1-01/CS2-01) includes the CS2 weld separating CAN1 and CAN2 and the intersection of CS2 and LS1.

Part 19E CS4 appears to be from CAN 4. This part contains a portion of the CS4 weld joining CAN3 and CAN4. This was unclear in the report.

### **TESTS PERFORMED:**

- The surfaces of parts 16-1 & 2 and part 17 were magnetic particle inspected and no reportable indications were found.
- Samples of the CAN 1, CAN 2, and CAN 3, and the ID and OD crowns of CS2, CS3, LS1 and LS2 were sectioned and chemically analyzed.
- Rockwell hardness testing was performed at approximately the mid wall on transverse section for CAN 1, CAN 2 and 3.
- Tensile tests (by Tensile Testing Metallurgical Laboratory )
- Impact tests (by Tensile Testing Metallurgical Laboratory )
- Side bend testing of welds. (by Tensile Testing Metallurgical Laboratory).
- Magnetic Particle Testing (by TEAM Industrial Service Inc. at BETA laboratory 6-15-2010)

## **RESULTS**

### **TABLES**

**Table A 6.1:** Table of test performed.

**Table A 6.2:** Reports chemical analysis for base metal and weld deposits. Cans 1, 2, and 3 meet specifications for the grade SA-515 gr.70 base metal. Weld deposit compositions are shown for LS1, LS2, CS2, and CS3.

**Table A 6.3:** Rockwell (HRB) hardness measurements on plate cross sections from CANS 1, 2, and 3. Results are reported in the E-6600E summary report.

**Table A 6.4:** Reports the base metal Charpy impact toughness of CS4, CS3, LS2, LS1. The table reports that impact tests were on the base metal, but these samples seem like welds.

**Table A 6.5:** Reports weld metal Charpy impact toughness at a single temperature (0 °F). The energies reported at the upper shelf are 30 ft-lb to 40 ft-lb or about 40 joules to 55 joules. The reason 0 °F was selected as the single test temperature is not clear.

**Table A 6.6:** Reports the room temperature tensile test results of base metals in Cans 1, 2, 3, and 4. The test results exceed minimum values for the SA 515 Gr. 70 base metal. Yield strength at CS3 was slightly higher than the other locations.

**Table A 6.7:** Reports tensile test results of weld deposits in CS2, CS3, LS1, and LS2.

**Table A 6.8:** Reports bend test data of CS2, CS3, LS1, and LS2. Bend tests of longitudinal welds (E-6600E) passed ASME acceptance criteria for qualifying welders and welding procedures. Seam welds in Can 2 passed this test, but both seam weld samples in Can 3 failed, indicating the presence of flaws that reduced ductility near the hottest end of the exchanger. While these bend tests provide a good indication of weld ductility, the implication of using such a test in this context is that defects around welds were induced during fabrication of the exchanger, either by the welder, or by the welding process. In the case of these exchangers, defects in the welds were likely a result of HTHA.

#### **FIGURES**

**Figure A6.1:** Showing condition and configuration of un-packaged E-6600E heat exchanger and a diagram of sample locations from the shell. Part 16 is from the back-side of the shell from the opening caused by the failure, and contains the intersection of welds CS3 and LS2. Part 17 is mostly from CAN 1 and contains the intersection of weld CS2 and LS1. Part 19E CS4 appears to be from CAN 4.

**Figure A6.2:** Shows details for removal of Parts 16-1 and 16-2 from the shell.

**Figure A6.3:** Shows details for removal of Part 17 from the shell.

**Figure A6.4:** Shows orientations of mechanical tests sample with respect to Parts 16-1 and 16-2 and the rolling direction of the steel. Plans indicate from the CS3 region of 16-1 above LS2 – 20 BM Charpy (notch with RD), 2 WM Charpy, 2 bend specimens, 2 BM tensiles (trans to RD), and 2 dog bone specimens from weld... from the CS3 region of 16-1 below LS2 – 20 BM Charpy (notch in RD), 2 bend specimens, 2 BM tensile (transverse to RD), and 2 dog bone specimens. From the Part 16-2 near weld LS2 the plan was for 20 BM Charpy (notched in RD), 3 WM Charpy, 2 bend specimens, 2 BM tensile (transverse to RD), 2 dog bone specimens.

**Figure A6.5:** Shows orientations of mechanical tests sample with respect to Part 17 and the rolling direction of the steel. Plans indicate from LS1 region - 20 BM Charpys, 2 WM Charpys, 2 BM tensile, 2 dog bone tensile of weld 2 bend specimens, from CS2 region – 2 dog bone tensile of weld, 2 bend specimens, and 3 WM Charpy.

**Figure A6.6:** Impact energy and lateral expansion results (plots) for BM specimens.

**Figure A6.7:** Percent shear of BM specimens.

**Figure A6.8:** Impact energy and lateral expansion results (plots) for weld specimens at 0 F.

**Figure A6.9:** Percent shear for weld specimens.

**Figure A6.10:** Tensile data for BM and WM.... Note when tensile under 70ksi in weld metal, elongation also low...may indicate a flaw was present.

#### **ATTACHMENTS**

**Attachment 3:** Result of Magnetic particle inspections state that 6 plates with welds were inspected. Of these, 3 plates (LS3-01 bottom, LS3-01 top, and CS4-01) were found to be conforming to linear indications (using procedure MT ASME N2, acceptance criteria ASME Section III). The other 3 plate specimens were found to be conforming (LS1-01 CS2-01 TEE, LS2-01 CS3-01) The BETA Laboratory reports states that ID surface of part 16-1 and 2 and Part 17 were inspected (by others) and no reportable indications were found. The ASME acceptance criteria for welds indicates that any linear indication interpreted to be a cracks, lack of fusion, or incomplete penetration are unacceptable regardless of length. Other linear indications are unacceptable dependent on length and amplitude. We see in report 7 that one of these non-conforming samples LS3-01 top has secondary cracking that was likely the result of the failure. It is not clear if this is true in general.

**Attachment 4:** Tensile test results including stress-strain data, yield strength, tensile strength, elongation and area reduction are reported. The test reports from TTML indicate that ASME Section IX was the test standard used for weld metal tensile testing of CS2, LS1, LS2, and CS3. The tests were apparently conducted on flat tensile specimens with rectangular cross-sections. CS2 failed in the base metal under ductile mode. LS1 failed in weld metal and HAZ under ductile mode. LS2 failed in the weld and HAZ. CS3 failed in the weld metal under ductile mode. The plots appear to show stress versus displacement instead of stress versus strain. It is invalid to calculate tensile properties (elongation and yield strength) from displacement of the crosshead. The only useful data from these tests is breaking load and failure location. The test reports from TTML indicate that ASTM A370-09a was the test standard used for base metal tensile testing of LS1. Those were apparently round specimens, and they failed in the base metal under ductile mode. Stress-strain data are shown for those tests although it is difficult to determine which stress-strain curve belongs to which physical test.

### **Report 7**

BETA LAB No. M10198 - CS4-01/LS3 bottom (Rev 1)  
PART: 6600-E HEAT EXCHANGER CS4-01 Bottom Part 18/14  
September 20, 2010

**NOTE:** This report is a revision of report 5 here. It is the revised fifth in the series, but by date it is the seventh report.

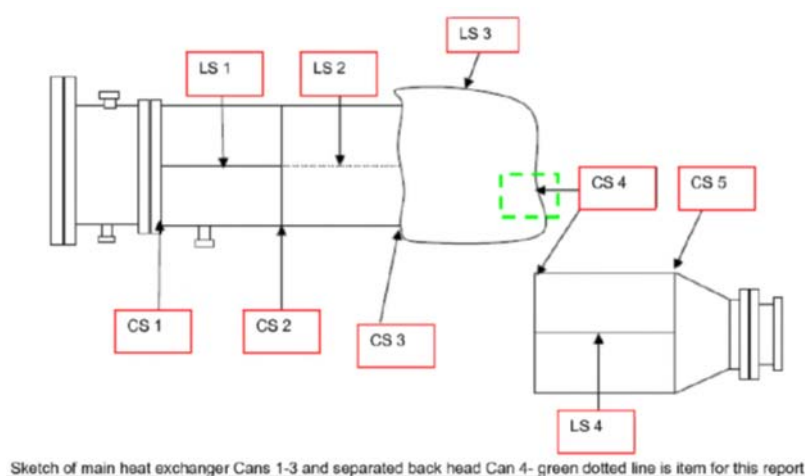


Figure AI.2: Showing sample location in green.

THE FOLLOWING CHANGES/ADDITIONS ARE MADE IN THIS REPORT (with reference to report 5):

1. Added source references to the Tables 2, 3 and 4
2. Changed Table 1
3. Added the results of the bundle guides angle evaluation - chemistry, Rockwell hardness, and microphotographs (Figures 21 through 23).

Here, only revised items are covered. See Report 5 for redundant details.

## **RESULT**

### **TABLES**

**Table A 7.1:** Reference to Fractography with EDS, Liquid Penetrant Testing (Fluorescent Dye) by TEAM Industrial Service, and wall thickness measurements by BETA were removed from the table. There were no results for then fluorescent dye evaluation given in the report, so this was likely a typographical error that was corrected by the revision. It is not clear why the references to the other data were removed from the table.

**Table A 7.2:** Added "(The data are from previous report M10198-LS3 bottom finding, July 30, 2010)"

**Table A 7.3:** Added "(The data are from previous report M10198-LS3 bottom finding, July 30, 2010)"

**Table A 7.4:** Added "(The data are from previous report M10198-LS3 bottom finding, July 30, 2010)". The spread of microhardness measurements of CAN 3 and CAN 4 show that CAN 4 may have lower hardness than CAN 3. Table 5 indicates that the hardness of the cladding is significantly higher than the steel weld metal. This is unexpected and explanation of where these hardness/compositions were measured should have been provided to explain this behavior.

**FIGURES**

**Figure A7.21:** Shows cracking associated with a weld on the angle iron welded onto the ID of the shell (Sample 18-M2, Angle). There is extensive cracking near the fusion line of the weld and some cracking in the HAZ region.

**Figure A7.22:** Showing more cracking in Sample 18-M2- Angle. This crack is in the base metal of the angle iron. This cracking is not associated with the weld (directly).

**Figure A7.23:** Showing the cracking in the HAZ and base metal region of the angle etched. The cracking is likely associated with interface regions of pearlite and ferrite in the microstructure.

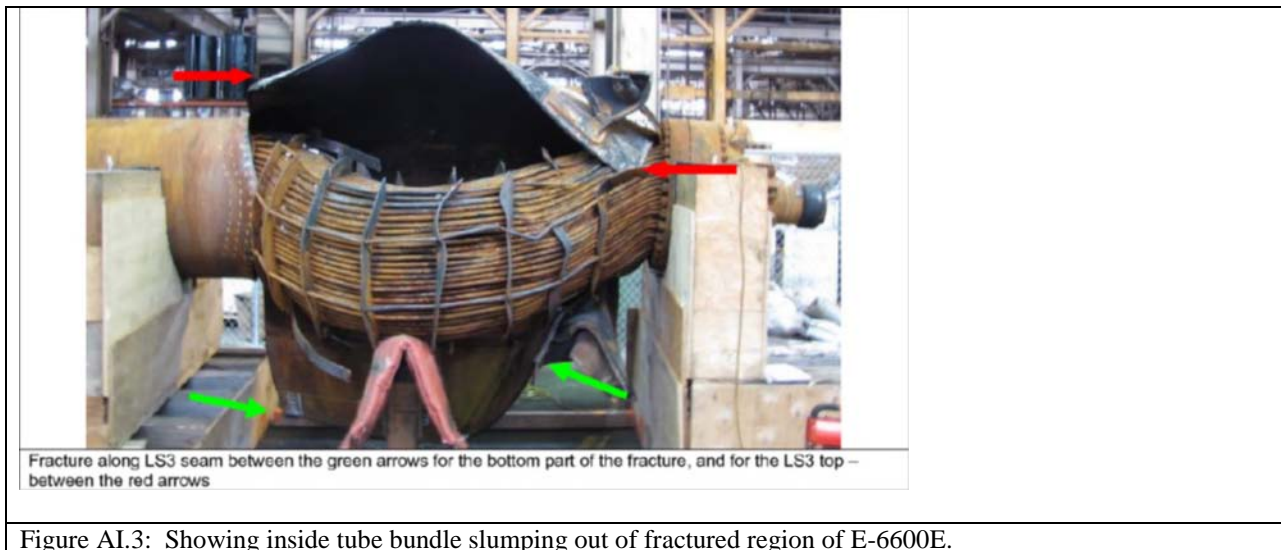
**Figure A7.34:** Indicates that the crack is associated with a drop in hardness. This is not unexpected since carbon depletion surrounding a crack results in a ferrite zone. The absence of the cementite phase (Fe<sub>3</sub>C) would tend to reduce strength and hardness. The figure also indicates that the angle bracket weld metal has significantly higher hardness than the exchanger wall. The same appears to be true in Figure A7.35 as well.

**Report 8**

BETA LAB No. M10198- LS3 Top, PART: 6600-E HEAT EXCHANGER LS3 Top, PART 15  
SEPTEMBER 20, 2010

**SAMPLE DESCRIPTION:**

Three mounts from Part 15 (from the top portion of the LS3 fracture) which are matching parts to the mounts from part 14 (bottom fracture of LS3) that were evaluated in a previous report (M10198-LS3 Bottom Findings July30, 2010). Part 15 is a six inch wide section of the top portion of the LS3 fracture between the CS3 and CS4 welds.



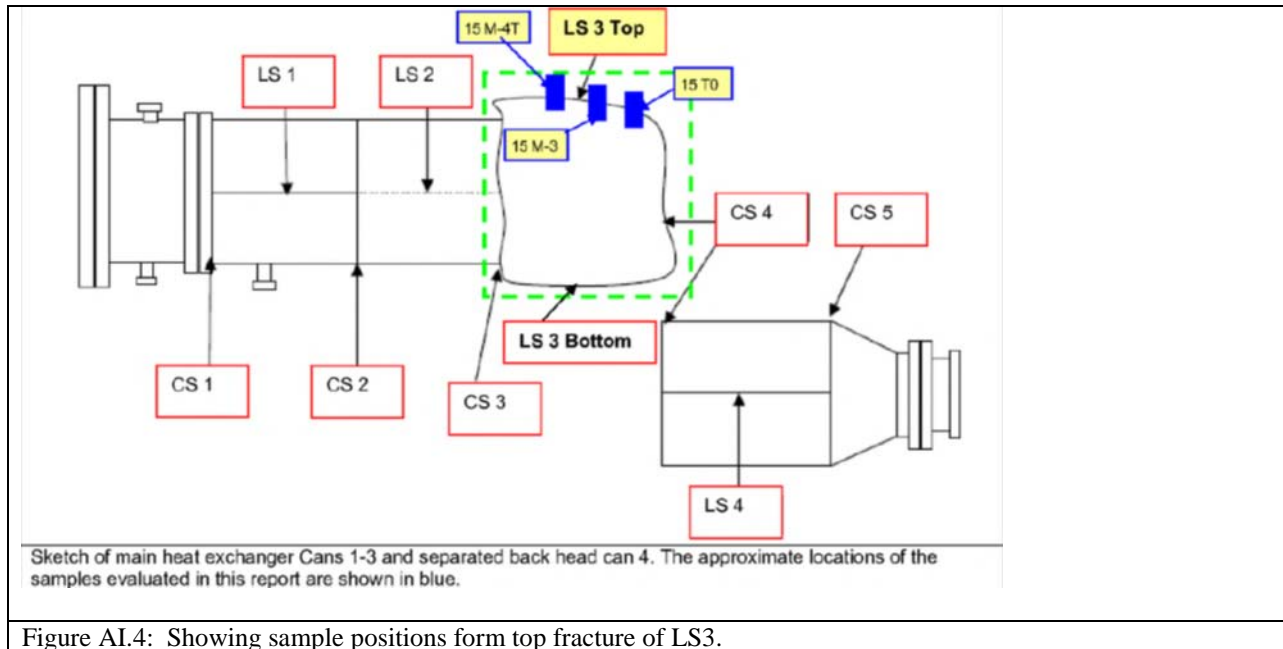


Figure AI.4: Showing sample positions form top fracture of LS3.

### TESTS PERFORMED:

The tests on the LS3 Top part of the exchanger included:

- Visual examination,
- thickness measurements,
- fracture surfaces recording,
- magnetic particle inspection and
- photo-microscopy.

### RESULTS

#### TABLES

**Table A 8.1:** Table of test performed.

**Table A 8.2:** Chemical analysis data from previous report M10198-LS3 Bottom Finding July 30, 2010. Shows that carbon contents in CAN 3 seam welds have carbon contents that are approximately 50 % to 70 % below those found in the base metal.

**Table A 8.3:** Hardness data for base metal from previous report M10198-LS3 Bottom Finding July 30, 2010. Hardness values of Can 3 (in Tables 3 and 4) are from a previous report: M10198-LS3 Bottom.

**Table A 8.4:** Summary of micro-hardness data from report M10198-LS3 Bottom Finding July 30, 2010. Hardness values of 14 TO LS3 base metal (VHN 129-149) and weld metal (VHN 134-147) reported in Table A 4 are significantly lower than other regions.

**Table A 8.5:** Wall thickness measurements along fractures following LS3, CS3, and CS4. The measurements are all taken at position 2 inches in from the fracture surface. The measurements wer

taken along LS3 measurement range between 0.884 and 0.851 inches (difference of about 1/32 inch), in a fairly random manner. This shows uniform “necking” near the fracture which indicates that the conditions along the LS3 weld from CS3 to CS4 were likely similar. For example, if there were significant differences in the size and density of crack-like flaws along the LS3 weld, more variation in the “necking” associated with the fracture might be expected. Wall thickness near LS3 along the CS3 weld was measured at 0.83 inches. It is not made clear if this thickness is for CAN2 or CAN3, but we assume it is for CAN3 and should compare directly to the LS3 measurements made on CAN3. If this is the case, the extent of “necking” is slightly more along the CS3 weld. Differences in plate orientation (LS3 perpendicular to rolling direction of plate and CS3 is parallel to the rolling direction) do not explain the differences in necking. Wall thickness CS4 is near 0.85 inches, which is near the low range of the necking measured for LS3. Here we also assume the measurements are relative to the thickness on the CAN3 side of the circumferential weld (the CAN4 side would be thicker due to the SS clad). No nominal thickness for CAN3 is given for comparison.

### **FIGURES**

**Figure A8.1:** Shows the un-packed condition of the heat exchanger and the sample locations.

**Figure A8.2:** Shows photograph of failed section along LS3 where a 6 inch wide sample along the fracture was removed between CS3 and CS4 for evaluation (the top portion of LS3).

**Figure A8.3:** Shows Part 15 with the LS3 fracture running between CS3 and CS4.

**Figure A8.4:** Shows fracture surface of CS4.

**Figure A8.5:** Shows fracture surfaces of location H1 to H8 along the LS3 weld. Clearly the fracture path through the thickness of the plate is following the weld passes (fusion line regions). The LS3 weld passes are visible on fracture surfaces indicating that the fracture follows a certain region of the weld, e.g., see Figure A5 Location H3 through H8. Location H2 may show some of the HTHA at the bottom of the fracture. Similar transitions are observed in other images of the fracture.

**Figure A8.6:** Shows fracture surfaces of location H9 to H16 along the LS3 weld. There may be some indication of preexisting crack at the ID on these fracture surfaces. The features are planar, flat regions adjacent to the ID that do not have the same texture as the fracture surface.

**Figure A8.7:** Shows fracture surfaces of location H17 to H22 along the LS3 weld.

**Figure A8.8:** Shows fracture surfaces along the CS4 weld. Here the weld bead morphology is not too apparent.

**Figure A8.9:** Shows magnetic particle inspection regions at location 1-4, near intersection of LS3 (Top) and CS3. Cracks are apparent, but it is not clear if these cracks were preexisting or are a result of the fracture. Cracks in LS3 appear detectable by eye. Magnetic particle was used to find indications, but these are clearly detectable by a postmortem visual inspection. The deformation induced by the explosion may have opened these cracks to their postmortem extent.

**Figure A8.10:** Magnetic particle inspection regions at location 5-8, showing some secondary cracking associated with the fracture surface.

**Figure A8.11:** Magnetic particle inspection regions at location 9-12, showing some secondary cracking associated with the fracture surface.

**Figure A8.12:** Magnetic particle inspection regions at location 13-16, showing some secondary cracking associated with the fracture surface.

**Figure A8.13:** Magnetic particle inspection regions at location 17-19, showing some secondary cracking associated with the fracture surface.

**Figure A8.14:** Macrographs of mounts 15 M-3, 15 M-4T, and 15 TO, and matching mounts from Part 14 (other side of the LS3 fracture) that were reported on in a previous report. Typical fracture paths follow the contour of the weld passes.

**Figure A8.15:** Showing some isolated cracking at the ID on mount 15 M-3. Details are not clear.

**Figure A8.16:** Showing cracking at the ID on mount 15 M-3. Details are not clear.

**Figure A8.17:** Showing cracking adjacent to the fracture for mount 15 M-3. This cracking is likely preexisting to the fracture and the etched micrographs shows microcracks are associated with grain boundaries in the steel (not random paths).

**Figure A8.18:** Showing region near mid-thickness on mount 15 M-3. Details are not clear.

**Figure A8.19:** Showing region in cap weld for mount 15 M-3. Details are not too clear, but some cracking along grain boundaries is apparent adjacent to the fracture path through the cap weld (at OD). Much of the LS3 fracture failed in shear mode as evident by the fracture planes oriented 45 degrees from the axis of the exchanger plate (Figure A19).

**Figure A8.20:** Showing some isolated cracking at the ID on mount 15 M-4T. Some isolated cracking is apparent in the HAZ and base metal of this sample. The largest crack is near the fusion line of the root pass of the weld (ID).

**Figure A8.21:** Showing details of the cracking in the base metal near the ID for mount 15 M-4T. Details are not too clear, but some micro cracking appears to follow grain boundaries.

**Figure A8.22:** Showing macro crack along the fusion region of the root pass at the ID on mount 15 M-4T. Secondary cracking and isolated micro cracks are apparent along the fracture.

**Figure A8.23:** Showing cracking in region near the tip of the macro crack on mount 15 M-4T. Secondary cracking and isolated micro cracks are apparent along the fracture.

**Figure A8.24:** Showing more cracking associated with the macro crack on mount 15 M-4T. There is extensive damage in some regions near the macro crack.

**Figure A8.25:** Showing region in weld metal near the macro crack on mount 15 M-4T. Some damage is apparent, but details not clear.

**Figure A8.26:** Showing region in weld metal near the macro crack on mount 15 M-4T. Details of the damage show damage regions linking to form cracks in the weld metal. One crack is linked to the

surface of the ID. Again, the main damage associated with this region is cracks associated with the fusion lines of the welds.

**Figure A8.27:** Showing region adjacent to fracture path on mount 15 M-4T. Isolated damage adjacent to the fracture is apparent.

**Figure A8.28:** Showing region adjacent to the fracture path for mount 15 TO.

**Figure A8.29:** Showing regions near ID at the fusion line, in the weld metal, and in the HAZ region for mount 15 TO. Cracking along the fusion line region is apparent. Some cracking in the weld and HAZ is also likely, but details not clear.

**Figure A8.30:** Showing details of cracking near the toe of the weld near the ID in mount 15 TO. Cracking shown here is in the coarse grained HAZ near the fusion line of the root weld. The cracking is closely associated with the grain boundaries in this region.

**Figure A8.31:** Showing details of cracking weld metal near the ID in mount 15 TO.

**Figure A8.32:** Showing details of cracking in coarse grain HAZ at fusion line in mount 15 TO. The cracking is associated with grain boundaries and other interfaces in this region.

**Figure A8.32:** Showing cracking associated with HAZ and fusion line regions near the mid-thickness of the shell adjacent to the fracture path through the plate in mount 15 TO.

**Figure A8.33:** Shows mount 15 T0.

## Report 9

Beta Lab No. M1 0198- LS3 Bottom - Fractography And 19 M-5 Mount  
6600-E Heat Exchanger, Fractography of Sem2 Sample, LS3 Bottom Part 14, And M-5 Mount From CS4, Part 19  
September 23, 2010

### ***SAMPLE DESCRIPTION:***

- All from the LS3 bottom portion of the fracture, between CS3 and CS4.
- Part 19, CS4 weld, marked M-5 (match to the sample CS4 M-5 from part 14 reported in M10198-LS3 Bottom Findings, July 30, 2010.)
- Fracture surface in the SEM of the sample SEM2 from LS3, with a service crack which had been opened in the Laboratory (location near mount 14-M3 from M10198-LS3 Bottom Findings, July 30, 2010).

### ***TESTS PERFORMED:***

The tests in this report include:

- visual examination,
- SEM evaluation of a fracture surface of the crack opened in the Laboratory, and
- photo-microscopy of the sample M5 from the part 19,

## RESULTS

The extensiveness of the HTHA near the cladding (Figure A3) supports an argument of increased thermal stresses due to thermal expansion coefficient mismatch causing an exacerbation of cracking.

### TABLES

**Table A 9.1:** Table of tests performed.

**Table A 9.3:** Hardness results are reported in the E-6600E summary report.

**Table A 9.3:** Shows the chemical analysis of CANs 3 and 4 base metal and CAN 4 cladding, CS4 and LS4 weld regions, and CS3 and LS3 weld regions. The CAN and cladding meet specified alloying levels. CS4 and LS4 at the ID surface shows high alloying since it was associated with the cladding layer.

### FIGURES

**Figure A9.1:** Shows un-packed condition of the heat exchanger and the term used for naming welds.

**Figure A9.2:** Show top and bottom sections of the fracture along LS3.

**Figure A9.3:** Macrograph of Part 19, mount M-5 (and mate). The fracture path follows the HAZ region of the root pass at the ID. The stainless steel cladding is black and the weld that joins it to the shell is also black.

**Figure A9.4:** Shows isolated non-critical (did not form a crack that resulted in failure) cracking adjacent to the fracture in the mount M-5 specimen.

**Figure A9.5:** Shows some cracking associated with the clad weld near the fracture (maybe result to fracture event).

**Figure A9.6:** Shows the cracking associated with the clad weld.

**Figure A9.7:** Shows cracking further in to the thickness of the shell, associated with HAZ region adjacent to the fracture path. Cracking is extensive in this region was likely pre-existing to the fracture event.

**Figure A9.8:** Shows details of several crack features shown in Figure A9.7. Cracking is associated with interface regions in the microstructure (not random paths). It is unclear if there is any decarburization associated with the cracking.

**Figure A9.9:** Shows cracking a bit further in to the thickness of the shell, almost to the mid-thickness region. Again extensive non-critical cracking is apparent in this HAZ/fusion line region.

**Figure A9.10:** Shows cracking further in to the thickness of the shell.

**Figure A9.11:** Shows the location where the SEM 2 specimen was taken from the bottom section of the LS3 fracture.

**Figure A9.12:** Shows macrographs of the SEM 2 specimen, which indicated the depth of the existing cracking that will be broken open in the laboratory for examination.

**Figure A9.13:** Shows scanning electron fractographs of SEM 2. Features typical of quasicleavage (little ductility) are shown, as might be expected for the steel when fractured at the lower shelf of the Charpy

impact toughness curve. Area 1 shows microcracks in the specimen region near the leading edge of the existing macrocrack in in SEM 2. The microcracks are likely associated with grain boundaries or other interfaces in the microstructure.

**Figure A9.14:** Shows details on the surface of the fracture specimen in Area 3. The features are void-like (spherical and cylindrical) shapes that may be positioned along a grain boundary. It is difficult to draw conclusions from this one micrograph.

## Report 10

Beta Lab No. M10198, 6600-E Heat Exchanger, Tesoro LS2 And LS2/CS2 Tee Findings

Part: LS2 22 In, 36.5 in Mounts, LS2 T2L Sem Fractography and Part 22 LS2-CS2 Tee Findings (Parts 16-1 And 22) 10\13\ 2010

### *Sample Description*

- Sample from the LS3 weld at location of about 22 inches from CS3
- Sample from the LS3 weld at location of about 36 ½ inches from CS3
- Sample (Part 22) on LS3 weld about 84 inches from CS3, at intersection of LS2 and CS2
- LS2 T2L SEM sample was evaluated in SEM, cross section through LS2 near CS3.

### *Test Performed:*

- Visual
- Metallography
- SEM

## *Results*

### *Tables*

**Table A10.1:** Test performed.

**Table A10.2:** Rockwell hardness results (from previous reports).

**Table A10.3:** Micro hardness results (from previous reports).

**Table A10.4:** Micro hardness results on CS2 sample.

**Table A10.5:** Summary of micro hardness results from Tables 3 and 4.

**Table A10.6:** Compositions of base metal and weld metal (from previous results).

### *Figures*

**Figure A10.1:** Sample locations.

**Figure A10.2:** Fracture along LS2.

**Figure A10.3:** Skipped

**Figure A10.4:** Locations of samples from Part 16-1 and cross section of LS2 weld at 22 and 36.5 inch locations. It appears that there is cracking under the root pass in the 36.5 inch cross section, but later

figures show only microcracking. This location is well away from the fractured region (36.5 inches from CS3) and the cracks appear to intersect the ID surface.

Figure **A10.5**: Showing base metal near the CS2 specimen at the 22 inch location unetched.

Figure **A10.6**: Showing cracking in the fusion line region of CS2 specimen at the 22 inch location. Cracks intersect the ID surface.

Figure **A10.7**: Showing details of the fusion line region of CS2 specimen at the 22 inch location. Fissures are likely present.

Figure **A10.8**: Showing more details of the fusion line region of CS2 specimen at the 22 inch location.

Figure **A10.9**: Showing details of the fusion line region of CS2 specimen at the 22 inch location. Here base metal inclusions are shown and blistering is not apparent. Decarburization is associated with cracking in the HAZ near the fusion line of the weld (root pass at ID).

Figure **A10.10**: Showing microstructure of the fusion line region on the other side of the CS2 cross section at the 22 inch location. Some isolated carbides are present near the ID surface, but this is an isolated occurrence. Base metal inclusion may show onset of blistering, but may be polishing artifact.

Figure **A10.11**: Showing cracking near the fusion line region on the other side of the CS2 cross section at the 22 inch location.

Figure **A10.12**: Showing cracking near the fusion line region on the other side of the CS2 cross section at the 22 inch location.

Figure **A10.13**: Showing cracking near the fusion line region on the other side of the CS2 cross section at the 22 inch location.

Figure **A10.14**: Showing cross section of CS2 from the sample taken at 36.5 inches from CS3. The macro of this cross section has dark linear features that follow the shape of the fusion line region of the root pass and look like cracks. However, the micrographs do not show macrocracks, only small isolated microcracks.

Figure **A10.15**: Showing more details of isolated micro cracks on cross section of CS2 from the sample taken at 36.5 inches from CS3.

Figure **A10.16**: Showing more details of isolated micro cracks on cross section of CS2 from the sample taken at 36.5 inches from CS3.

Figure **A10.17**: Showing SEM sample location in Part 61-1.

Figure **A10.18**: Showing T2L SEM sample prior to break that created fracture surfaces.

Figure **A10.19**: Fracture surface of T2L sample.

Figure **A10.20**: Fracture surface of T2L sample.

Figure **A10.21**: The fracture surface shows brittle, low deformation features as expected of a fracture (in laboratory) at low temperature. We assume the fracture experiment was conducted to identify and isolate methane bubble initiation at boundaries in the steel. Some spherical “holes” are shown aligned

along one boundary, but the holes are on the same size scale as the spherical inclusions in the steel and this isolated example is not too convincing.

Figure **A10.22**: Shows location of Part 22 at the intersection of the LS2 and CS2 welds.

Figure **A10.23**: Shows location of samples taken from Part 22 at the intersection of the LS2 and CS2 welds.

Figure **A10.24**: Macrographs of the LS2 and CS2 cross section (no apparent cracking).

Figure **A10.25**: Micrographs of the LS2 weld shows micro cracks along fusion line region of root pass at ID.

Figure **A10.26**: Micrographs of the LS2 weld shows micro cracks along fusion line region of root pass at ID.

Figure **A10.27**: Micrographs of the LS2 weld shows micro cracks in HAZ region of root pass at ID.

Figure **A10.28**: Micrographs of the LS2 weld shows micro cracks in HAZ region of root pass at ID.

Figure **A10.29**: Micrographs of the LS2 weld shows micro cracks in HAZ region of root pass at ID.

Figure **A10.30**: Micrographs of the LS2 weld shows micro cracks in HAZ region of root pass at ID. Also shows figure stating that no damage was found on the cross section of the CS2 weld evaluated (CS2-A).

Figure **A10.31**: Microhardness plots across the CS2 weld showing peak hardness in HAZ near 240 HV500 for OD and ID welds.

Figure **A10.32**: Macrograph of LS2 cross section (T2L mount) showing location of hardness profiles. The macrograph shows a long crack on this cross section.

## **Report 11**

BETA Lab No-M10198 6600-E Heat Exchanger E,

Summary of Results and Part 17 Mounts Evaluation (6600-E),

February 3 2011

A revised draft of this report was reviewed, Beta Laboratory Report No. M10198, Revision1. This is Report 12 in this appendix.

## **Report 12**

Beta Laboratory Report No. M10198, Revision1

Tesoro exchanger E-6600-E Heat Exchanger "E" Summary of Results

March 7 2011

BETA Laboratory examined the Tesoro exchanger E-6600E as the test laboratory and prepared a report titled Tesoro exchanger E-6600E Heat Exchanger "E" Summary of Results. This report summarized the finding of 10 previous reports. The protocol for the work was supplied to BETA Laboratory by agreement between signatory parties.

## Discussion of Chemical and Mechanical Properties

### Hardness Traverses

The hardness traverse indicates a single root pass as evident in microstructure. This *is not* shown for specimen LS1. Hardness traverses across LS1 would likely indicate multiple weld passes in the root. It is unclear why this is so. This seems to be a *significant* discrepancy. The root pass weld is symmetric about the centerline although the hardness traverse indicates a significantly wider HAZ on the right side of the weld. It may just be that the location of the HAZ/BM boundary is not indicated correctly.

### Chemical Analysis

Chemical analysis apparently shows some cladding compositions although no text was given to discuss the location of the cladding. The OSHA report (DNV) mentions that the cladding material was 316. Cladding introduces a whole new set of weldability issues (carbon migration is possible as mentioned previously). More information is required to assess this aspect of the component vessel. Other reports did not seem to discuss the pertinence of this information.

### Bend Tests

Table 8 shows bend testing results of welded joints. Two circumferential seam weld (CS3) specimens failed during bend testing. This could be from fabrication- or service-related defects. No information was provided on the failure mode other than the apparent observation that cracks were perpendicular to the bending. Upon request, images of tested bend specimens were provided to the reviewers however no significant new information could be obtained by observing the failed welds, except that it is likely that the bars contained flaws in the region near the fusion line of the root passes of the welds (ID). SEM evaluation would have given more insight into cause of cracking during bend testing.

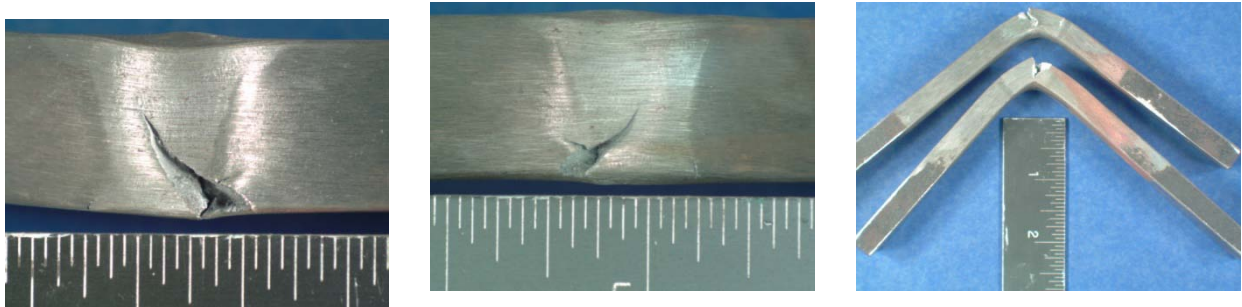


Figure A1.5: Showing two bend specimens that cracked during testing. It is difficult to clearly see the weld position in the figures, but it appears that the failures of both specimens initiated near or at the toe of the root pass in the welds (ID). Both fractures then propagated into the weld metal, where the stress of the bend bar is expected to be highest.

### Discussion of Macrographs and Micrographs

Figure A3 shows cross-sections of welds LS1 and 17-LS1. They are taken close to each other and it is not clear why the two cross sections have different pass configurations (17-LS1 has single ID pass and LS1 has multiple ID passes). Considering the sample location and orientation in Figure A2 we would expect very similar weld pass configuration. This point aside, the weld passes show typical HAZ sizes.

Figure A4 shows the ID region of LS1 weld. There may be a few small flaws present, but the resolution of the micrographs is not sufficient to determine this. Decarburization is not apparent.

Figure A5 shows also shows the toe region of the LS1 at the ID. Again there may be a few small flaws, but resolution is too low to be sure. Decarburization is not apparent. Detail here shows a region at the fusion line (some base metal (BM) some weld metal). The sample preparation (polish) is good but the contrast in the unetched micrograph makes it difficult to determine if there is fissuring. Some of the BM inclusions are seen to be filling the shapes; others are too dark to distinguish between a fissure and just an inclusion. At a little higher magnification in the etched sample we do see BM inclusions (grey features on the micrographs which could likely be Mn stringers) that appear to be present with no signs of fissuring. If fissuring is present here it is just initiating and has not yet resulted in significant damage.

Figure A6 shows 17-LS1 ID region. No flaws or decarburization are apparent.

Table A11 Figures:

- Part 19W, macrographs of the CS4 19w-m1 and CS4 19w-m2 welds/fractures showing fusion line fractures on CAN 4 (between cans 3 and 4). Fracture follows the fusion line closely from about mid-thickness to the OD, but not so much at ID. The fractures are near the clad weld.
- Part 19W, macrograph of LS4 19W-m3 showing the cladding at the ID.
- Part 19E, macrograph of CS4 19E-m4 (same orientation as CS4 19w-m2). The fracture follows the fusion line closely. Again, the fracture is near cladding weld.
- Part 19E, macrograph of SC4 19e-M5/14-M5 (same orientation as CS4 19w-m2).
- Part 19W, macrograph of the CS4 Weld, sample 19W-m1, showing that the fracture profile does not follow the fusion line exactly, but fairly close. There is a small damage region at the toe of angle iron welded onto the ID surface that may or may not be a resulting damage from the fracture process.
- Part 19W, macrograph of CS4 Weld, sample 19W-m2, showing that the fracture profile follows the fusion line at the cap weld but not through the whole cross section. Fracture likely initiated at the toe of the weld, which is a higher stress region. This is a typical fracture location of weld hydrogen induced cracking, a process that occurs at low temperature and a short period of time after weld fabrication.
- Part 19W, macrograph of the LS4 Weld, sample 19W-m3, showing no fracture.
- Part 19E, macrograph of CS4 Weld, sample 19E-m4, showing that the fracture follows the fusion line closely. Again this was near the clad weld.
- Part 19E, macrograph of CS4 Weld, sample 19E-m5. Fracture follows fusion line fairly closely and near root of clad. Fracture profile is much like 19E-m4. Detailed features are not clear. This one could have been investigated more closely to compare microstructures. Also, note the damage locations are all about same distance from fracture surface. This might indicate the damage is a result of plastic flow during fracture rather than pre-existing damage. This sample was sectioned from nearly the same position as 19E-m4.

- Part 19E, macrograph of CS4, sample 19E, exact location unclear, showing fracture following the fusion line near clad.
- Part 18, macrograph of CS4 18-m1, showing cracking at the fillet weld toes on what appears to be a section of angle iron welded onto the shell ID.
- Part 18, macrograph of CS4 18-m2, showing toe cracks at the fillet weld on the angle iron welded to shell (this was not exactly clear to the reviewers).
- Part 14, macrograph of CS3 14-m1. No fracture is apparent.
- Part 14, macrograph of CS3 14-m2, showing a crack at the toe of the ID weld on the fusion line.
- Part 14, macrograph of 14-m3/15-m3, showing a large crack at the toe of the ID weld and a fracture path along the fusion line on the other side of ID weld. The fracture apparently propagated into the weld in OD region.
- Part 14, macrograph of 14-m4T/15m4T, showing a large crack at the toe of ID weld and a fracture path along the fusion line on other side of ID. The fracture path went into the weld region near the OD (not on the fusion line).
- Part 14, macrograph of 14-TO/15-TO, showing the fracture did not follow along the fusion line at the toe of the ID weld, but did appear to follow the fusion line throughout most of the thickness.
- Part 14, macrograph of 14-m6 showing that the fracture path likely initiated at the fusion line on the ID (fusion line ID crack at other toe), but the fracture path was not along the fusion line for much of thickness.
- Part 16-1, macrograph of LS2 and CS3 combination region (LS2-CS3 Tee region) showing no damage.
- Part 16-1, macrograph of CS3 T-2C showing weld cross-section with no fracture. No damage is evident to reviewers, but damage in the HAZ is indicated in the table.
- Part 16-1, macrograph of LS2 T-2L showing weld cross section with no fracture. Damage is indicated for this macrograph; on the fusion line and in the base metal, but the reviewers found difficulty in resolving this in the micrograph.
- Part 16-2, macrograph of LS2-22 inch showing no fracture. Damage is indicated for this macrograph, on the fusion line and in the HAZ, but the reviewers found difficulty in resolving this in the micrograph.
- Part 16-2, macrograph of LS2-36 inch showing no fracture. Damage is indicated for this macrograph, on the fusion line (left side) and indicated. No decarburization is apparent in the region.
- Part 22 (LS2-CS2 Tee), macrograph of LS2-A showing no fracture. Damage on the fusion line and in the HAZ is indicated in the table, and the fusion line is likely visible, but the reviewers found difficulty in resolving this in the micrograph. No decarburization is apparent in the region.

- Part 22 (LS2-CS2 Tee), macrograph of CS2-A showing no fracture. Damage on the HAZ is indicated in the table but the reviewers found difficulty in resolving this in the micrograph. No decarburization is apparent in the region.
- Part 17, macrograph of LS-1 showing no fracture. No damage is indicated in the table (NA).
- Part 17, macrograph of 17-LS1 showing no fracture. No damage is indicated in the table (NA).

Figure A10 macrograph and micrographs of CS4 weld (sample 19W-m1) show details along the fracture path. On the unetched cross section some voids very near the fracture surface are shown. These features are often present for numerous ductile failure modes. What the reviewers did not see were fissures in the more general region here, away from the edge of the fracture path where there had been extensive deformation during the fracture event. On the etch cross-section the same voids are shown and the reviewers noted absolutely no indication of decarburization associated with them or the general region.

Figure A11 macrograph and micrographs of the CS4 weld (sample 19W-m2) show details along the fracture path. Like Figure 10, some voids are present very near the fracture surface, but this is not an uncommon feature for ductile fracture. Fissures were not noted in the general region here, and decarburization was not evident.

Figure A12 macrograph and micrographs of the LS4 weld (sample 19W-m3) in HAZ region with clad weld. The damage depth indicated in the table below for this region is zero, so apparently there was not thought to be flaws in this region. There are dark contrasting features in the micrographs.

Figure A13 macro and micrographs of CS4 weld (sample 19E-m4) showing features along the fracture path. The fracture path here was more in the base metal adjacent to the HAZ of the clad. Voids in this region are further away from the edge of the fracture and some have micro crack or fissure-like morphologies. No evidence of decarburization is present and no indication of blistering at base metal inclusions.

Figure A14 macro and micrograph of CS4 weld (sample 19E-m5/15-m5) showing features along the fracture path. Several small microcrack-like features within 0.5 mm of the fracture surface (on the 19E-m5) are shown. There is no decarburization associated with the features. A flaw, not associated with the fracture path, is shown on the 14-m5 sample, but again, no decarburization is associated with this flaw (and it is basically an isolated flaw).

Figure A15 macro and micrograph of CS4 weld (sample 19E-18-m3/18-m3) showing features along the fracture path. There are some microcrack-like features (in two isolated regions, not general features) adjacent to the fracture path in this location that may have some decarburization associated with them.

Figure A16 macrograph and micrographs showing regions on sample 18-m1 where angle-iron is welded onto the surface of the shell (at ID). The unetched cross sections show general microcrack-like regions. No decarburization was apparent.

Figure A17 macrograph and micrographs showing the CS4 welded region (sample 18-m2) under where an angle-iron was welded onto the ID of the exchanger. The region under the right fillet weld shows some micro-crack-like features in a region away from the edge of the fracture path. A box highlights a base metal inclusion but the resolution is not adequate to determine what is being shown (void, blister,

etc.). Under the left fillet weld there is clear evidence of microcracking that is forming cracks radiating into the thickness of the shell. This region was not etched so it is not known if there was any decarburization associated with the region. However, there was no decarburization associated with the region under the other weld, where fracture occurred.

Figure A18 macrograph and micrograph showing CS3 weld (sample 14-m1). The interpass region between the root pass at the ID and the welding pass above it has a long crack (maybe 4 or 5 mm). The region adjacent to the crack shows evidence of decarburization. The micrographs show the decarburization is likely not limited to the crack flanks, and that some of the surrounding region may also be decarburized. It is difficult to tell just how general and extensive the decarburization might be from the figure.

Figure A19 macrograph and micrographs showing a cross section of the CS3 weld (sample 14-m1). Similar cracking is identified on the right side of the CS3 weld at this location. It appears that this region is extensively decarburized, but the contrast between the interpass HAZ and the weld in the micrographs makes it difficult to be sure. Details of the microstructure are not resolved in the figure.

Figure A20 macrograph and micrographs of the CS3 weld (sample 14-m2) showing details at the tip of a crack at the toe of the weld on the fusion line of the root pass at the ID. At the tip of the toe crack there is no apparent decarburization, but on the left side of the weld there is microcracking and decarburization along the root interpass region.

Figure A21 micrographs from LS3 (sample 14-m3/15-m3) showing isolated microcrack along the fusion line region left of the weld. No decarburization is evident in these regions. Isolated details to the right of the weld are too close to the oxidized fracture surface to indicate anything clearly.

Figure A22 micrographs of a LS3 weld cross section (sample 14-m4T/15-m4T) showing a few isolated microcrack-like features; several in the weld metal and several in the base metal are shown. No evidence of decarburization is in these regions.

Figure A23 micrographs of the LS3 weld (samples 14-TO/15-TO) showing an isolated microcrack near the fusion line on the side opposite to the fracture side of the weld and details along the fracture path on the right side of the weld. No decarburization is apparent in these regions.

Figure A24 micrograph of LS3 weld (sample 14-TO/15-TO) showing details along the fracture path near the ID. A series of microcracks are likely present along the fusion line of the root pass. There may be some decarburization of the weld metal (although it was difficult to tell) but no decarburization of the HAZ region near the fusion line is apparent.

Figure A25 micrograph of CS3 weld (sample 14-m6) showing details along the fracture path (left side of weld) and details near the tip of a toe crack on the ID of the root pass on the right side of the weld. There is a region near the fracture path that likely has significant microcracking. The details of the toe crack show a morphology that is not consistent with numerous ductile fracture modes.

Figure A26 micrographs of a mixed region of the LS2 and CS2 welds (sample T-2) showing a region of microcracking. There is no apparent decarburization associated with the cracking.

Figure A27 micrographs of the CS3 weld (part 16-1, sample T-2C) showing a series of microcracks in the HAZ region under a cap weld on the OD of the shell.

Figure A28 micrographs of LS2 weld (part 16-1, sample T-2L) showing a series of microcracks that are joining to form a crack along the fusion line of a weld pass near the ID of the shell. There may be some decarburization associated with the fusion line cracking, although it was difficult to tell. No decarburization is apparent at isolated microcracks on the right side of the weld.

Figure A29 micrographs of the LS2 weld (part 16-2, sample 22) showing isolated microcracks near the fusion line of the weld.

Figure A30 micrographs of the LS2 weld (sample 36 inches from CS3) showing what we assume are several isolated cracks along the fusion line (perpendicular to it) on the left side of the weld (it is difficult to determine if this is actually a crack in this micrograph). The cracks are clearly associated with the grain boundaries, run along the interface between the pro-eutectic ferrite at the boundaries and the finer structures within the grains. The long crack-like feature shown on the right side of the weld is difficult to interpret. It is likely a long inclusion stringer.

Figure A31 micrographs of LS2 (part 22, LS2-CS2-T and LS2-A) showing isolated microcracks along the fusion line of the root pass at the ID. The cracks are perpendicular to the fusion line and are associated with grain boundaries.

Figure A32 micrographs of the CS2 weld (part 22, LS2-CS2-T and CS2-A) showing one small microcrack, although this could be a flaw or artifact.

Figure A33 micrograph of the LS1 weld (part 17, sample LS1) showing a few isolated microcracks, flaws or artifacts. (No damage depth was indicated in the table.)

Figure A34 micrograph of LS1 (part 17, sample LS1) showing a few isolated microcracks, flaws or artifacts. (No damage depth was indicated in the table.)

Figure A35 micrographs of the LS1 weld (part 17, sample 17-LS1) showing no damage.

### *Section Summary*

The strongest evidence supporting HTHA was presented in Figures 15, 17, 18, 19, 20, 21, and 28. These figures use samples from welds CS4, CS3, and LS2 and LS3, as shown in the schematic of the failed exchanger. Figure A18 and Figure A19 may show the clearest evidence that decarburization has taken place. However, higher magnifications would have been able to really confirm this. It's interesting that this decarburization follows the fusion boundary just in the CGHAZ.

Toe cracks were often observed at the ID of weld root passes. However, the geometrical stress concentration would likely be greater at the OD weld toe, so if toe cracks occurred during fabrication due to cold cracking, it might be expected to find toe cracking at the cap welds on the OD also. This is not the case, so the observation of ID toe cracking only likely supports HTHA not cold cracking, as the cause of the toe cracks. (The ID is exposed to the vessel environment and more susceptible to HTHA.)

Many inclusions in BM and weld metal were observed. Fissuring in BM was not apparent and no apparent linking damage between inclusions was observed. Weld micrographs show some features that could be small isolated fissures albeit with no linking.

## Report 13

Beta Laboratory Report No. M10329, 6600-B  
Parts 1B, 2B, and 3B  
12/27/2010

BETA Laboratory examined the Tesoro exchanger E-6600B as the test laboratory. The protocol for the work was supplied to BETA Laboratory by agreement between signatory parties. This report evaluates specimens from the following locations:

- Part 1B, on CW4 weld
- Part 2B, on LW3 weld
- Part 3B, near the intersection of LW3 and CW3

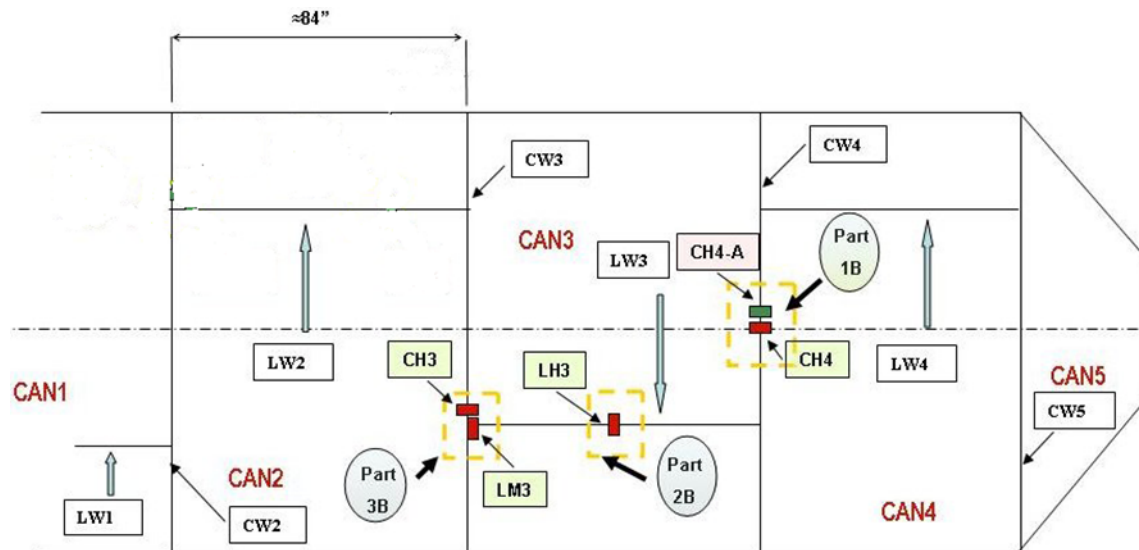


Figure AI.6: Showing part and sample locations in E-6600B.

The tests of the heat exchanger parts included:

- Visual examination,
- chemical analysis of the base and weld metal,
- macro and semi-micro hardness measurements,
- wall thickness measurements,
- liquid Penetrant (PT) non-destructive testing (done by others),
- photo microscopy (metallography),
- depth of the damage ,
- damage location and width of the Coarse Grain HAZ and Fine Grain HAZ measured,

- fractography by Scanning Electron Microscopy (SEM),
- tensile testing of the welded joints (done by others).

### *Tensile*

The tensile measurements (Table 10) show that when full thickness specimens were tested, the ultimate tensile strength was substantially lower than when reduced thickness specimens were tested. This finding is not developed further in the report, however, it is assumed that pre-existing flaws in the ID regions of the shell thickness resulted in the lower tensile properties of the full sized samples. However, the failure location for the full thickness specimens is listed as base metal in Table 10, which would not correlate with the characteristic locations of microcracks in the shells (fusion line region of root weld at ID). So, this detail is left unexamined in the report (no fractography of the full thickness specimens, only the reduced thickness fractograph shown in Figure A53).

### *Chemistry*

The chemical evaluations show that the base metal is within specification for SA-515 Grade 70 steel. The weld metal chemistries (CW4, CW3, LW3) show differences, but all are within expectations for carbon steel filler metals. The composition does not show Ti, Nb, or N contents, which would have made it more complete.

### *As-received Condition (Visual inspection)*

In Figures 1-10 documentation of the as-received condition of the shell and tube bundle are given.

### *Sample Locations*

In Figures 11-19 documentation of sample locations are given.

### *Cracking (Visual inspection)*

Figure A15 shows the crack identified on surface of ID of Part 1B adjacent to the stainless steel clad along the CW4 weld. We note that dye penetrant results on this crack are indicated to be documented in Appendix 3, but there are no Appendices in the report we reviewed.

### *Discussion of Macrographs and Micrographs*

In Figures 20 and 21 macrographs of the weld cross sections are shown. In Figure A20 the cross section of CW4 weld (part 1B) shows a deep crack that intersects the ID surface very near to the end of the cladding (about 1-2 mm away). A macrograph of weld LW3 is also shown (part 2B). In Figure A21 two cross sections from welds in Part 3B are shown: CW3 and LW3.

In Figure A22, three micrographs are used to define abbreviations and terminology used in the report.

Micrographs documenting details of parts 1B, 2B, and 3B are given in Figures 23-40.

Part 1B, which is a cross section of weld CW4, has a deep crack at the ID of the shell.

- Figure A23 shows the length of the crack into the base metal is about 8 mm. The crack path curves to follow the contour of the HAZ. Damage depth measurements by BETA (Table A 12) estimate the depth of this crack from the surface of the ID to be about 5 mm, which is near 24 % of the thickness.
- Figure A24 shows microcracking at another location on the surface of the ID.

- Figure A25 shows details of the cracking damage and the microstructural changes associated with the deep cracking. The microcracking or fissuring is apparent on this cross section, and linking of these microcracks extend a macrocrack into the shell. Decarburization of the pearlite colonies surrounding the microcracks is shown to some extent, but extensive decarburization is not apparent.
- Figure A26 shows additional details of the deep cracking in part 1B. Part 2B is a cross section of weld LW3. In Figures 26-31 details of internal cracking associated with the fusion line region of root pass (ID) are shown.
- In Figure A27 extensive microcracking is shown at the ID associated with fusion line/HAZ region of the root pass.
- Microcracking is apparent in this region from the surface of the ID to near mid-thickness of the shell (Figure A28). Some isolated microcracking is also shown past mid-thickness associated with the fusion line HAZ region of other weld passes in the cross section.
- Microcracking is also shown at the ID on the other side of the weld (Figure A30) and details of the microcracking show it is occurring at interphases between the pro-eutectic ferrite at grain boundaries and the pearlitic matrix.
- Microcracking is also occurring around pearlite packet boundaries
- (Figure A31). Some decarburization appears to be associated with the microcracking, but the extent of decarburization is not clear.

Part 3B contains two welds, CW3 and LW3.

- Figure A32 shows very clear decarburization on a cross section of CW3. The decarburized region follows the contour of the fusion line of the weld very closely, perhaps just in the HAZ. This is in a region near the left toe of the weld at ID. A network of microcracks is associated with the decarburized region.
- Again, the microcracks are shown to be associated with various boundaries in the microstructure of the steel (Figures 33 and 34).
- Figure A35 shows similar decarburization on the right side of the CW3 weld in part 3B. Microcracking in this location follows the curvature of the fusion line closely, just in the HAZ. Microcracks appear to have morphology similar to the pro-eutectic ferrite paths at the grain boundaries, but crack paths inside the grain are also apparent (likely around pearlite-ferrite boundaries).
- Further details of the microcracking and decarburization are shown in Figure A36 and 37.
- In Figure A38-40 a cross section of the LW3 weld is shown. Microcracking is apparent in the near the fusion line and in the HAZ of the root pass (Figure A38). Details of isolated microcracks are shown in Figures 39 and 40.

*Scanning electron micrographs of specimens failed in the laboratory.*

Two locations were selected for fractography in the SEM. The two samples (sample CS4 with weld CW4 from Part 1B, and sample LS3 with weld LW3 from Part 2B) were V-shape cut from the O.D. to decrease the cross section but leaving untouched the damaged area, submerged in the liquid nitrogen for over half an hour and then impact failed to expose fracture surface (see Figure A41). The fracture surfaces then were examined in Scanning Electron Microscope and the results introduced on Figures 42 through 45.

- In Figure A42 cleavage is the dominant feature of the fracture, as expected for a fracture at liquid nitrogen temperature of this steel. The box likely indicates the position of a microcrack at a grain boundary in the sample. However, the general fracture has regions of quasi-cleavage and it is difficult to be sure of what we are looking at here.
- Figure A43 shows details in another region of the CS4 sample. The more ductile void-like regions in the box are likely suspected to be voids formed by methane formation along a grain boundary, however, again it is difficult to be sure of what these features represent. Comparisons with a weld fracture from this vessel that contained no micro cracks might have been helpful in the interpretation here.
- In Figure A44 the ID portion of the fracture for the LW3 weld is shown. Likely what is shown here is the depth of pre-existing surface cracks at the ID (oxidized).
- In Figure A45, another region of the LW3 sample is shown. Here a region from the bottom of the v-cut is compared with a region near the middle of the fracture surface. The region near the v-cut has a smaller grain or packet size (located in the weld metal), but not knowing the underlying microstructure of the middle region (maybe HAZ), we are not sure of the point of this comparison.

Overall the SEM data does not add too much to what optical microscopy has shown. Microcracking in the regions tested was evidently limited (isolated damage) and surface cracks at the ID of the shell are present.

#### *Hardness Traverses*

Hardness traverses of the weld samples are shown in Figures 46-48. For the CW4 weld the hardness of the weld metal adjacent to the fusion line and near the ID is near 88 HRB, the highest. For the LW3 weld the fusion line region near the ID is 94HRB, which is also high compared with other regions (on the HAZ side). Although the highest hardness overall in this weld was the fusion line region (HAZ) near the OD of the specimen (hardness of 100HRB). The hardest region of the CW3 weld is also the fusion region near the OD. In this weld the hardness near the ID was non-symmetrical and highest in the HAZ on the left side of the weld.

#### *Tensile specimen locations, test records, and fractures*

The tensile specimens were all cut from the OD portion of the shell.

- The CW4 T4-1 sample failed with 11 % elongation. The failure mode was recorded as brittle.
- The CW4 T4-2 sample failed with 9.5 % elongation in a ductile failure mode.

- In Figure A53 the fracture paths for both specimens are shown to follow the fusion line curves of the cap welds for a distance about 1/3 the thickness of the specimen and the remaining fracture occurred in the base metal.

It is likely that the fracture initiated near the fusion line of the cap welds and final fracture occurred in the base metal, but information is not available to determine this (fracture surface evaluations). In any case, the fusion line/HAZ region of the cap weld is a preferred fracture path in the CW4 weld.

## Report 14

Beta Laboratory Report No. M10329-B, E-6600-B  
Parts 1B, 4B, and 5B  
3\8\2011

BETA Laboratory examined the Tesoro exchanger E-6600B as the test laboratory. The protocol for the work was supplied to BETA Laboratory by agreement between signatory parties. This report contains evaluations of specimens from the following locations:

- CW4
- LW2
- CW2

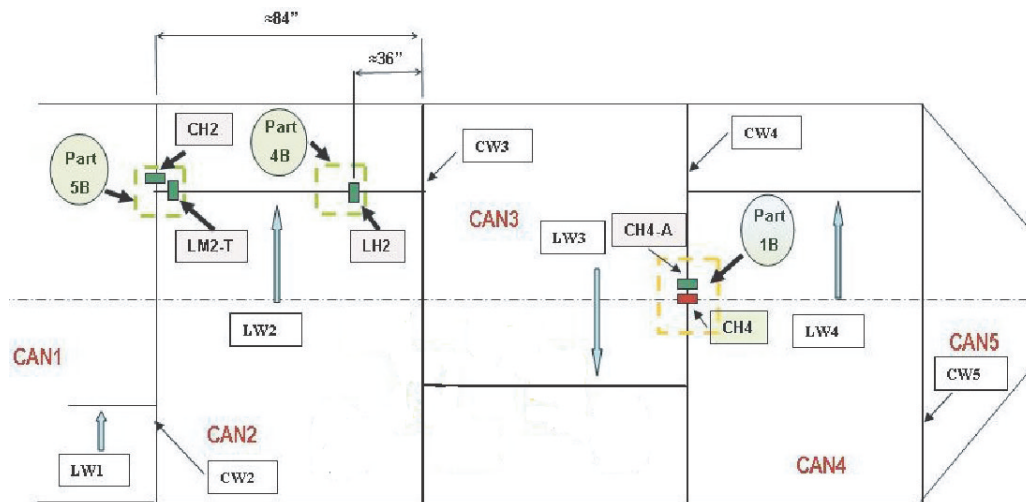


Figure AI.7: From the BETA laboratory report No. M10329-B showing the locations of the specimens examined.

## Hardness

Part 1B CAN 3 base metal HRB=82 to 86

Part 1B CAN 4 base metal HRB=76

Part 1B Figure A20 shows hardness profile of the CW2 weld. The hardness in the fusion line region is typically high in comparison with the weld metal or base metal.

Part 4B CAN 2 base metal HRB=87 to 88

Figure A19 shows hardness profile of the LW2 weld. Again the fusion line and HAZ regions typically have higher hardness than the base metal or the weld metal.

In regards to the circumferential weld CW4, hardness traverses were not provided for the SS clad weld regions. It may have been noteworthy to perform such traverses and for the reviewers to see this data. Carbon migration may occur at dissimilar weld interfaces such as between stainless cladding and carbon steel. This is due to a carbon activity gradient where chemical potential of carbon is lower in austenitic stainless steel than in carbon steel. This establishes a driving force for diffusion from carbon steel to the stainless steel. However, the diffusivity of carbon is significantly lower in austenitic stainless steel than in carbon steel. A high hardness region might be expected at or very near to the clad interface due to a carbon pileup phenomenon, which may have occurred during the welding procedure or even at the highest operating temperatures of the pressure vessel (after long periods of time).

## *Chemistry*

Part 1B

- Circumferential weld CW2: C=0.09 to 0.11, Mn=1.14 to 1.28, S=0.02
- Base metal: C=0.26, Mn=0.62, S=0.02
- T-joint of LW2 and CW2 C=0.27, Mn=0.62, 0.02
- Longitudinal weld LW2: C=0.08 to 0.13, Mn=1.14 to 1.08, S=0.02

## *Specimen locations*

Figures 5-9 show details of specimen locations.

## *Discussion of Macrographs and Micrographs*

Table 9 provided macrographs of the cross sections evaluated and measurements on the depth and location of damage. Damage is typically associated with fusion line of welds. A cross section of CW4 is included in Table 9, but unlike other specimens, further details are not presented in the figure that follows.

Figure A10 shows macrographs of welds CW4 and LW2 (CH4-A and LH2) and the HAZ region of the ID pass for LW2. The longitudinal weld is larger than the circumferential CW4 weld. The CW4 weld includes the edge of the stainless steel cladding that covers CAN 4.

Figures 11 shows macrographs of welds LW2 and CW2 (at T with CW2 and at T with LW2 respectively). The HAZ of the ID pass on the LW2 longitudinal weld is larger than on circumferential CW2 weld.

Figure A12 shows a crack near the toe of the weld at the ID on a cross section of CW4 (CH4-A). The crack has oxidation on its crack faces but does not show evidence of decarburization even very near the crack faces. The crack is in the base metal near the toe of the cladding weld.

In Figure A13 higher magnifications are shown and the crack has a morphology that might be consistent with numerous mechanisms. The crack path appears to be transgranular and at the highest

magnification shown (and 400% blow-up) dissolution of the carbides is not evident. On the unetched surfaces, it does appear that the microcracking is closely associated with interphase boundaries in the microstructure.

Figure A14 may indicate some damage to the microstructure, but it is very hard to tell.

Figure A15 (4B LH2 weld LW2) shows a small crack at the fusion line. No decarburization is apparent in this region.

Figure A16 (4B LH2 weld LH2) shows 2 small cracks very near the fusion line. Again, there is no decarburization apparent in this region.

Figure A17 (CH2 on weld CW2 at tee with LW2) showing no damage.

Figure A18 LM2-T of weld LW2 at tee with CW2) showing no damage.

## Appendix II:

Table 2: Additional reports for review.

Author	Report Title	Report Date
Spectrum Inspection	Spectrum Inspection Engineering report	May 20 2010
Spectrum Inspection	Spectrum Inspection Engineering report	June 24 2010

### Spectrum Inspection Engineering report, May 20 2010

The Spectrum Inspection Engineering report, dated May 20 2010, documented the inspection of the Tesoro Anacortes Refinery Heat Exchanger E-6600E. Spectrum Inspection Engineering inspected the Exchanger E-6600E prior to the destructive testing that was done on the unit. They used Advanced Ultrasonic Backscattering Techniques (AUBT) to check for High Temperature Hydrogen damage and a Phased Array to perform cracking inspections. The scope of the work was stated to be “Phased Array and Hydrogen Attack AUBT inspection on exchanger E-6600E fracture surface weld, HAZ and Base Metal.

The AUBT backscattering mode was used for detection of defects and was followed by frequency spectrum analysis and velocity ratio for defect confirmation. The transducers used were as follows: 10 MHz/0.5” L-wave straight beam, 5 MHz/0.5” L-wave straight beam, 5 MHz/0.5” 0 degree S-wave straight beam, 10 MHz 45 degree angle beam, and a 5 MHz phased Array 32 element transducer.

In retrospect, the reviewers find that this inspection was a good starting point to gather information on how to proceed with sampling and the techniques used were appropriate. Based on post-inspection destructive evaluations microcrack flaw sizes were detected in the initial inspections.

#### *The phased array and AUBT inspection located cracks in the following locations:*

- (1) both sides of the Long Seam Weld LS (region labeled T0)
- (2) along the circumferential weld C-3 (region labeled T1)
- (3) the T-joint of C3 and L2
- (4) on the long seam LS-3 (label as T3)
- (5) on the fracture surface of weld/HAZ using AUBT (labeled as T4)

The report did not specifically say, but it appears that all cracking, with the exception of the T1 region, are sub-surface (do not connect to surface). Cracks were either associated with the fusion lines of welds or closely associated with a fractured region.

The scope indicates that the whole vessel was inspected, so we assume that the cracking reported by represents all of the cracking detectable in the vessel.

### Spectrum Inspection Engineering report, June 24 2010

Another report by Spectrum Inspection, dated June 24 2010, documented the evaluation of the Tesoro Anacortes Refinery, Exchanger E-6600B. In this report Spectrum Inspection Engineering performed Advanced Ultrasonic Backscattering Techniques (AUBT), Phased Array weld inspection, Material identification, and hardness testing. Wet fluorescent magnetic particle testing (WFMT) was also performed on the inside of the shell. The scope of this work was to perform the following tasks:

- (1) 100 % Phase Array inspection on welds,
- (2) AUBT inspection on circumferential welds C3 and CW4, and longitudinal weld LW3,
- (3) Material identification (PMI) on all longitudinal welds, circumferential welds, and base metal,
- (4) Brinell Hardness on all longitudinal weld, circumferential weld and HAZ

*The Phased Array evaluations found the following:*

- (1) ID connected 48 inch crack-like flaw 0.3 inch deep at edge of stainless cladding on CW4.
- (2) 30 inch long intermittent mid-wall flaw in longitudinal weld LW3
- (3) ID connected flaw in CW5 that was 4 inches long and 0.17 inches deep
- (4) ID connected flaw in longitudinal weld LW5

WFMT confirmed the presence of the 48 inch long crack in CW4. This crack extended over 50 % of the length of the CW4 weld (48" long on the ID surface) between the stainless steel cladding and carbon steel shell.

This crack and others in exchanger E-6600B were characterized as lack of fusion (LOF) flaws by the inspector. No reason for this characterization is given in the report, and it is assumed that the characterization is because the flaws are associated very closely with the fusion lines of the welds. Lack of fusion would be one logical possibility for this flaw geometry and location.

The other welds on exchanger E-6600B were reported to be in good conditions (CW1, CW2, CW3, LW1, LW2, and LW4). No cracking was identified in the base metal.

Material identification confirmed E-6600B is carbon steel, but no details were given. The hardness of base metal was estimated to be between 114 and 146 BHN. The hardness of the HAZ and welds were estimated at 120 to 157 BHN and 130 to 159 BHN respectively. The HAZ of the LW4 weld was the hardest region (> 150 BHN) tested. The inspector indicated that locations for some of the linear

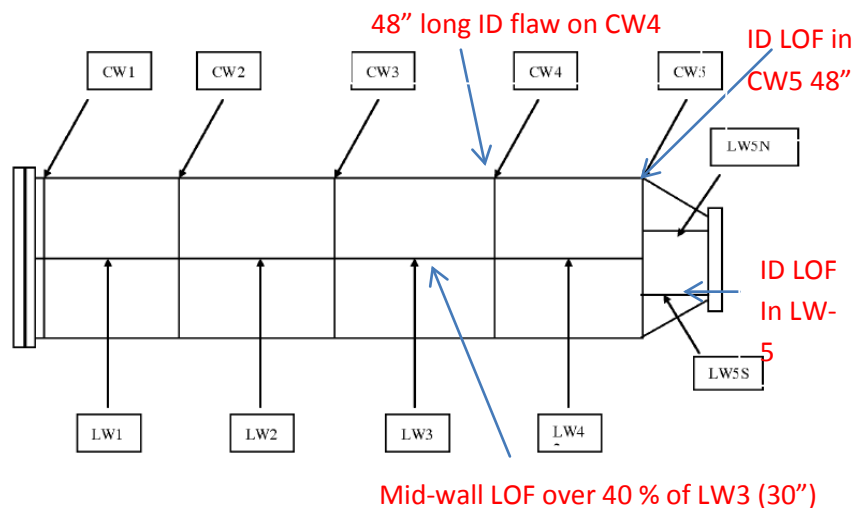


Figure AII. 1: Showing the weld identification notation used and the locations of the flaws identified in the report on the E-6600B heat exchanger.

discontinuities were in similar locations of those on the failed E-6600E exchanger.

This inspection, like the inspection of exchanger E-6600E, located relevant regions for metallurgical samples.